IRE Transactions

on ANTENNAS and PROPAGATION

VOLUME AP-3 | OCTOBER 1955 | NUMBER 4

Published Quarterly

Paul Weaver

PUBLISHED BY THE

Professional Group on Antennas and Propagation

IRE TRANSACTIONS PGAP IS A QUARTERLY PUBLICATION DEVOTED TO EXPERIMENTAL AND THEORETICAL PAPERS ON ANTENNAS AND WIRELESS PROPAGATION OF ELECTROMAGNETIC WAVES

MANUSCRIPTS should be submitted to John B. Smyth, Editor, SRA, 3930 4th Avenue, San Diego 3, California. Manuscripts should be original typewritten copy, double spaced, plus one carbon copy. References should appear as footnotes and include author's name, title, journal, volume, initial and final page numbers, and date. Each paper must have an abstract of not more than 200 words. News items concerning PGAP members and group activities should be sent to the News Editor, Mr. H. A. Finke, Polytechnic Research and Development Company, 55 Johnson Street, Brooklyn, New York.

ILLUSTRATIONS should be submitted as follows: All line drawings (graphs, charts, block diagrams, cutaways, etc.) should be inked uniformly and ready for reproduction. If commercially printed grids are used in graph drawings, author should be sure printer's ink is of a color that will reproduce. All half-tone illustrations (photographs, wash, airbrush, or pencil renderings, etc.) should be clean and ready to reproduce. Photographs should be glossy prints. Call-outs or labels should be marked on a registered tissue overlay, not on the illustration itself. No illustration should be larger than 8 x 10 inches.

Copies can be purchased from
THE INSTITUTE OF RADIO ENGINEERS
1 East 79 St., New York 21, N.Y.

PRICE PER COPY: members of the Professional Group on Antennas and Propagation, $2.10; members of the IRE, $3.15; nonmembers, $6.30.

ANNUAL SUBSCRIPTION PRICE: IRE members, $8.50; Colleges and public libraries, $10.00; nonmembers, $17.00.

Entered as second-class matter, at the post office at Menasha, Wisconsin, under the act of August 24, 1912. Acceptance for mailing at a special rate of postage is provided for in the act of February 28, 1925, embodied in Paragraph 4, Section 412, P. L. & R., authorized October 26, 1927.

news and views

Administrative Committee

Henry Booker and John Smyth have been re-elected to the Administrative Committee of the PGAP, and J. I. Bohnert and D. D. King have been elected. These are for three year terms beginning June 1, 1955. Henry Booker has also been elected Vice-Chairman for the coming year.

PGAP Sponsorship and Participation in National Technical Symposia

The Administrative Committee, under the effective jurisdiction of Mr. Bolljahn, is evolving a policy for PGAP's role in symposia. It has been agreed that we plan to take a very positive active part in the symposia of which we consider ourselves co-sponsor, and that in other meetings where we take a subordinate role and assist only by such things as contacting our membership and other minor promotional activities, we should consider ourselves as only participants, and not be classified as a co-sponsor.

As a tentative program for the coming year, it has been agreed that we should take an active part in the IRE National Convention in New York. We would also plan to sponsor sessions at the National Electronics Convention and the WESCON. Plans for this are already well under way. It has also been planned that, subject to acceptance by the appropriate URSI Commissions, we should take part as co-sponsor in the Spring and Fall National URSI Meetings. In addition to these, we should sponsor other national meetings where our group would have a definite, positive contribution to make.

We have received an invitation from W. W. Mumford, Chairman of PGMTT, inviting us to participate and co-sponsor a technical symposium in Philadelphia on February 2 and 3, 1956. The theme of this session is to be Microwave Techniques. It has been agreed that we will accept this invitation and some PGAP representatives will be named to help prepare the arrangements and program.

Mr. Bolljahn has requested suggestions for interesting session titles. Roy Spencer has suggested "Fourier and Information Theory Techniques Applied to Antenna Scanning." Please forward your suggestions to Mr. Bolljahn.

For the National Convention, it has been suggested that the general format for the contributed paper sessions be changed to accommodate more papers. The general feeling is that, when necessary, authors could reduce the length of their papers without sacrificing pertinent details, and that discussion could be reduced to a minimum. The general plan is to allow 15 minutes for each paper with no discussion following the paper. However, the authors would be requested to remain and written questions could be submitted to the chairman who would address them to the appropriate author during the general discussion period at the end of the session. The papers of general interest, such as new applications, would be emphasized and the authors of more scientific papers of significance would be encouraged to submit their papers for the URSI Sessions. D. C. Ports is advising the Convention Committee of our plans in this regard.

PGAP News

An annual index to the 1955 volume of IRE Transactions on Antennas and Propagation will appear in the January, 1956 issue in order that it may include the Proceedings of the URSI-Michigan Symposium, which will be published shortly.

—The Editor

The July issue of Transactions contained abstracts of the papers presented at the IRE-URSI Symposium held May 2–5, 1955, in Washington D. C. The PGAP,

as co-sponsor of the USA URSI Meetings, will henceforth publish in the July issue of the TRANSACTIONS abstracts of the papers presented, thus providing a means of distributing this information to those who did not attend the sessions. This will serve as a permanent reference.

The Washington Chapter of PGAP is quite active and has formulated an ambitious plan for a technical symposium on "Communication by Scatted Techniques," November 14 and 15, 1955. It is being co-sponsored by the Professional Group on Communication Systems and George Washington University, who will provide the auditorium and other meeting facilities. The general theme is on application rather than theoretical aspects.

CHAPTER NEWS

Washington, D. C.—At its May 23, 1955 meeting, the following officers were elected for the coming year:

Chairman	Coleman Goatley
Vice-Chairman	Clarence H. Stewart
Secretary	William W. Balwanz

A paper entitled "Behavior of Ferrites in Microwave Components" was presented by John C. Cacheris.

Los Angeles—The summer meeting of the Los Angeles Chapter of the PGAP, held on August 11 at the I.A.S. Building, 7660 Beverly Boulevard, featured two outstanding speakers in the antenna field: V. H. Rumsey of the University of Illinois and L. C. Van Atta of Hughes Aircraft Company. The dinner before the meeting was held as usual at the Encore Restaurant, 806 N. La Cienega, with 54 members attending. A total of 106 members and guests were present at the general meeting.

Professor Rumsey, who is spending the summer at the Lockheed Missile Systems Division in Van Nuys, gave a highly stimulating talk on "Some Recent Developments in Antennas" which included some very useful ideas in the design of antennas. Configurations specified only by angles were shown to have infinite bandwidth and some practical approximations were discussed. One interesting topic was the 60 Pi antenna resulting from a configuration having a Babinet complement identical to the antenna itself and having always an input impedance of 60 Pi regardless of shape.

Dr. Van Atta presented a summary of developments in surface wave antennas including two dimensional arrays of slots, printed dipoles, leaky waveguides, and wave trapping surfaces. Some experimental data were presented which showed the excellent beam shaping that can be obtained with corrugated surface wave antennas.

CALENDAR OF COMING EVENTS

The National Electronics Conference, Hotel Sherman, Chicago, Ill., Oct. 3–5.

AIEE Fall General Meeting, Morrison Hotel, Chicago, Ill., Oct. 3–7.

AIEE Aircraft Electronic Equipment Conference, Los Angeles, Calif., Oct. 11–13.

IRE East Coast Conference on Aeronautical & Navigational Electronics, Lord Baltimore Hotel, Baltimore, Md., Oct. 31–Nov. 1.

World Symposium on Applied Solar Energy, Conducted under leadership of Standford Research Institute, Phoenix, Arizona, Oct. 31–Nov. 4.

Nuclear Congress and Atomic Exposition, sponsored by the Engineers Joint Council, Cleveland, Ohio, Dec. 12–17.

AIEE Winter General Meeting, Statler Hotel, New York, N. Y., Jan. 30–Feb. 3, 1956.

Symposium on Microwave Theory and Techniques, University of Pennsylvania, Philadelphia, Penna, Feb. 2–3, 1956.

The 34th Annual Convention of the National Association of Radio and Television Broadcasters, Conrad Hilton Hotel, Chicago, Ill., April 15–19, 1956.

National Aeronautical and Navigational Electronics Conference, Dayton, Ohio, May 14–16, 1956.

contributions

Prediction of Oceanic Duct Propagation from Climatological Data*

L. J. ANDERSON† AND E. E. GOSSARD†

Summary—Techniques are described for predicting the effect of the "oceanic duct" in increasing the coverage of low-sited microwave radars. Prediction is made on a monthly basis using statistical data on sea temperature, air temperature, humidity, and wind speed. A large area in the northwest Pacific is used to illustrate the methods used. The basic prediction approach is to deduce refractive index profiles from available data parameters and to use Schelkunoff's ducting criteria to predict radar propagation effects. Monthly contours are then drawn over the area for each radar band showing the probability of extended coverage.

Introduction

THE EVENTUAL goal of all tropospheric propagation research is the prediction of field strengths, at frequencies above 50 mc, from routine meteorological data. For most situations where such predictions are desired the problem is sufficiently complex that predictions require careful analysis by experienced personnel. It should be stated parenthetically that such predictions can be made and in fact have been made and verified on several occasions with surprising accuracy. In such cases, however, semi-empirical methods must be employed and cookbook routines cannot be specified.

There is one important case, however, where a routine method has been developed which has greatly simplified the mechanics of preparing the predictions. This is the case of predicting the coverage of low-sited microwave radars as affected by the oceanic duct. The meteorological parameters used are routine shipboard observations of sea temperature, air temperature, and humidity at bridge height, and wind speed. The purpose of this paper is to outline the method of reducing these data to statistical radar coverage prediction charts for a large area of the northwest Pacific.

* Original manuscript received by the PGAP, February 18, 1955; revised manuscript received, May 6, 1955.

† U. S. Navy Electronics Lab., San Diego 52, Calif.

Background

In order to assess the effect of the meteorological conditions upon propagation, one must work with vertical profiles of refractive index. Therefore, the first step in the prediction process is to deduce these profiles from the routine meteorological parameters enumerated above. Having the shape of the profile, one then must determine its effect upon the propagation of radar energy of a given wavelength.

Details of these two steps are discussed in a previous paper[1] and will be outlined only briefly here. The temperature and humidity data allow one to compute the refractive index difference ΔM_b between the sea surface and bridge height. Using the work of E. L. Deacon,[2] one can then deduce the shape of the profile using a profile index β which can be obtained from the air-sea temperature difference and wind data. The wind data also enables one to pick a value for Z_0, a length parameter characteristic of the roughness of the sea surface. Thus from the four simple observables listed in the introduction, the profile is determined. Detailed profiles[3] have been found to agree with those computed by the foregoing method. To assess the effect of a given profile upon

[1] L. J. Anderson and E. E. Gossard, "The effect of the oceanic duct on microwave propagation," *Trans. Amer. Geophys. Union*, vol. 34, p. 695; October, 1953.

[2] E. L. Deacon, "Vertical diffusion in the lowest layers of the atmosphere," *Quart. Jour. R. Met. Soc.*, vol. 75, p. 89; January, 1949.

[3] L. J. Anderson and E. E. Gossard, "The Oceanic Duct and its Effect on Microwave Propagation," U. S. Navy Electronics Lab., Rep. No. 305; August, 1952.

radar energy we use the approximate method of S. A. Schelkunoff.[4]

Practical experience has shown that as trapping conditions are approached for a given wavelength, radar coverage is extended two to five times normal, whereas normal coverage is obtained from standard to almost trapping. The best one can predict seems to be whether radar coverage will be normal or extended two to five times. The gamut between these extremes is run with very slight changes in meteorological conditions. Inasmuch as measured M profiles exhibit wide changes in both time and space one must work with time or space averages of the profiles to arrive at reliable results. Hence, one is hardly justified in attempting to refine the method to predict anything beyond the simple yes-no answer. When conditions are borderline between trapping and no trapping, they are so variable with time that further refinement would be unusable even if one could achieve it.

With this philosophy in mind, one can solve for a minimum ΔM_b required to just trap a given wavelength.[1] This yields:

$$\Delta M_b \text{ (min)} = \left[\frac{.060[3770\lambda^2(3-\beta)/\beta]^{\beta/3}}{\frac{3-\beta}{2-\beta}\,\frac{\beta-1}{b^{1-\beta}-Z_0^{1-\beta}}} \right] + 0.8,$$

where b is the bridge height in feet and λ is the wavelength in cm. This expression is the criterion used for predicting whether or not extended coverage should be experienced. It should also be stated that inherent in the method is the assumption that both the radar and the target are located within the oceanic duct, usually within 50 feet of the sea surface. This condition is met in the case of surface ship targets, but most shipboard radars are mounted as high as possible and only in the case of surfaced submarines is this below 50 feet. Furthermore, oceanic duct intensities normally encountered limit the wavelengths which are affected to 10 cm and shorter. On rare occasions 25 cm radars should also be affected.

Prediction Procedure

Routine surface meteorological observations over the sea have been taken for many years and have been compiled as monthly averages for 5 degree latitude and longitude squares in the "Atlas of Climatic Charts of the Oceans."[5] Three such parameters that we need; namely, sea surface temperature, air temperature, and wet bulb depression have been tabulated and plotted in this way. In the case of wind speed, we have the percentage of observations where the wind is Beaufort Force 3 (9 knots) or less. This is sufficient for determining the value of Z_0 to use.

These average values are not sufficient to determine the percentage of time extended coverage should be encountered since they tell us nothing about the frequency distribution over a given month of β and ΔM_b; all we get are monthly average values. In order to determine such distributions we must go to the individual ship observations and determine β and ΔM_b for each set and plot a histogram of a hundred or more such values. Figs. 1 and 2 are histograms of β and ΔM_b respectively for the Far East area in December. Plotting similar data for July and for the north and south extremes of the area shows that the shapes of the histograms are similar and are merely shifted along the abscissa. In Fig. 2 the histograms are shown for both the stable ($\beta < 1$) (solid curve) and the unstable ($\beta > 1$) (dashed curve) cases and are seen to have virtually the same shapes.

Using this fact we assume that since we know the average values of β and ΔM_b for each month and each 5 degrees square, we can simply shift the histogram curves along the abscissae until the average coincides with the monthly average and we will then have the required histograms for the particular month and square.

From the criterion equation we can draw curves, for each wavelength of interest, of ΔM_b (min) vs β. We must actually draw two such curves; one for the smooth sea case ($Z_0 = 0.00005$ feet) and one for the rough sea case ($Z_0 = 0.02$ feet). Furthermore, if the correlation between ΔM_b and β is not significant we can obtain the probability of ΔM_b min (as given by the β vs ΔM_b min curves) being exceeded for a given wavelength. There is actually some correlation between β and ΔM_b, but this has been partially taken into account by computing the probabilities separately for stable and unstable conditions.

Fig. 3 illustrates the procedure. The numbers across the top of the figure are the percentages of observations of ΔM_b in unstable air that fall in the class intervals shown along the bottom; the row of numbers across the middle of the figure (along the $\beta = 1.00$ line) are similar percentages for stable air. The numbers just outside the left border are percentages of β observations in the class intervals indicated at the far left. One now multiplies each β percentage with each ΔM_b percentage along its horizontal row and obtains a cross probability product. Starting at the right end of each row and working toward the left, adding the incremental cross probabilities as one proceeds, yields the numbers typed in the body of the grid. For the unstable cases (top half of the figure) one uses the ΔM_b percentages at the top of the figure; for the lower half one uses those across the middle of the figure. Shifting histograms in this way gives a slight discontinuity in the vertical columns which is

[4] S. A. Schelkunoff, "Microwave Transmission in a Non-Homogeneous Atmosphere," Bell Tel. Lab. Rep. MM-44-110-53; July, 1944.

[5] "Atlas of Climatic Charts of the Oceans," U. S. Weather Bureau W. B. No. 1247, U. S. Gov't. Printing Office; 1938.

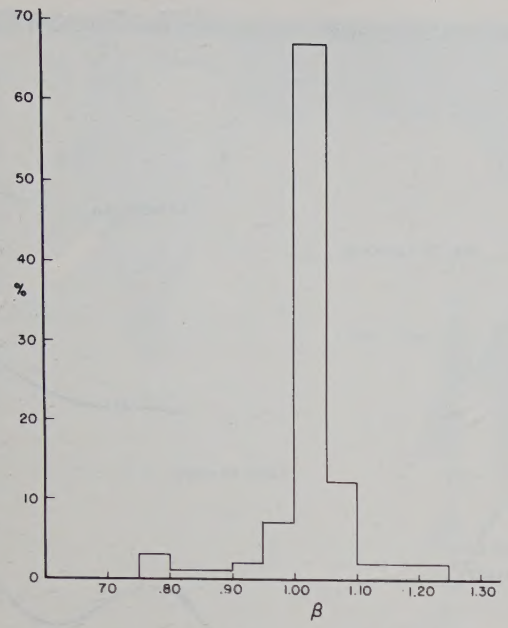

Fig. 1—Distribution histogram of β, Far East, December.

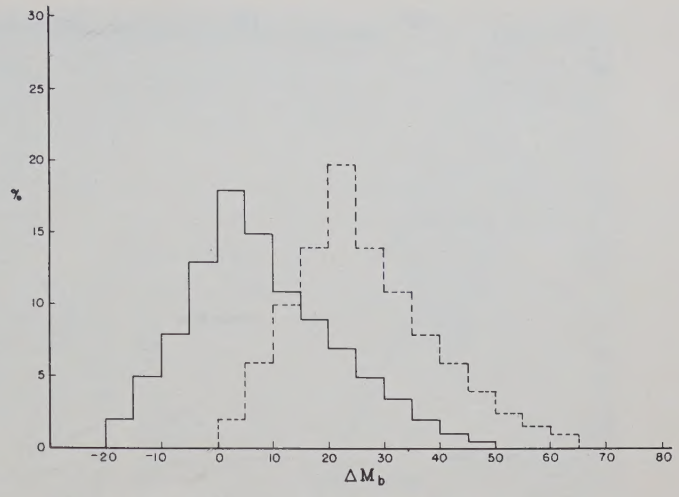

Fig. 2—Distribution histogram of ΔM_b, Far East, December: solid curve, stable case; dashed curve, unstable case.

smoothed by computing the first row above and below the discontinuity both ways and taking an average value. In this case the differences were at most a few per cent.

The arrows shown indicate the average β value and the average ΔM_b for the whole set of ΔM_b values (both stable and unstable) used in plotting the histograms of Figs. 1 and 2.

The criterion curves are now plotted as an underlay on the same coordinate axes. The curves shown are both

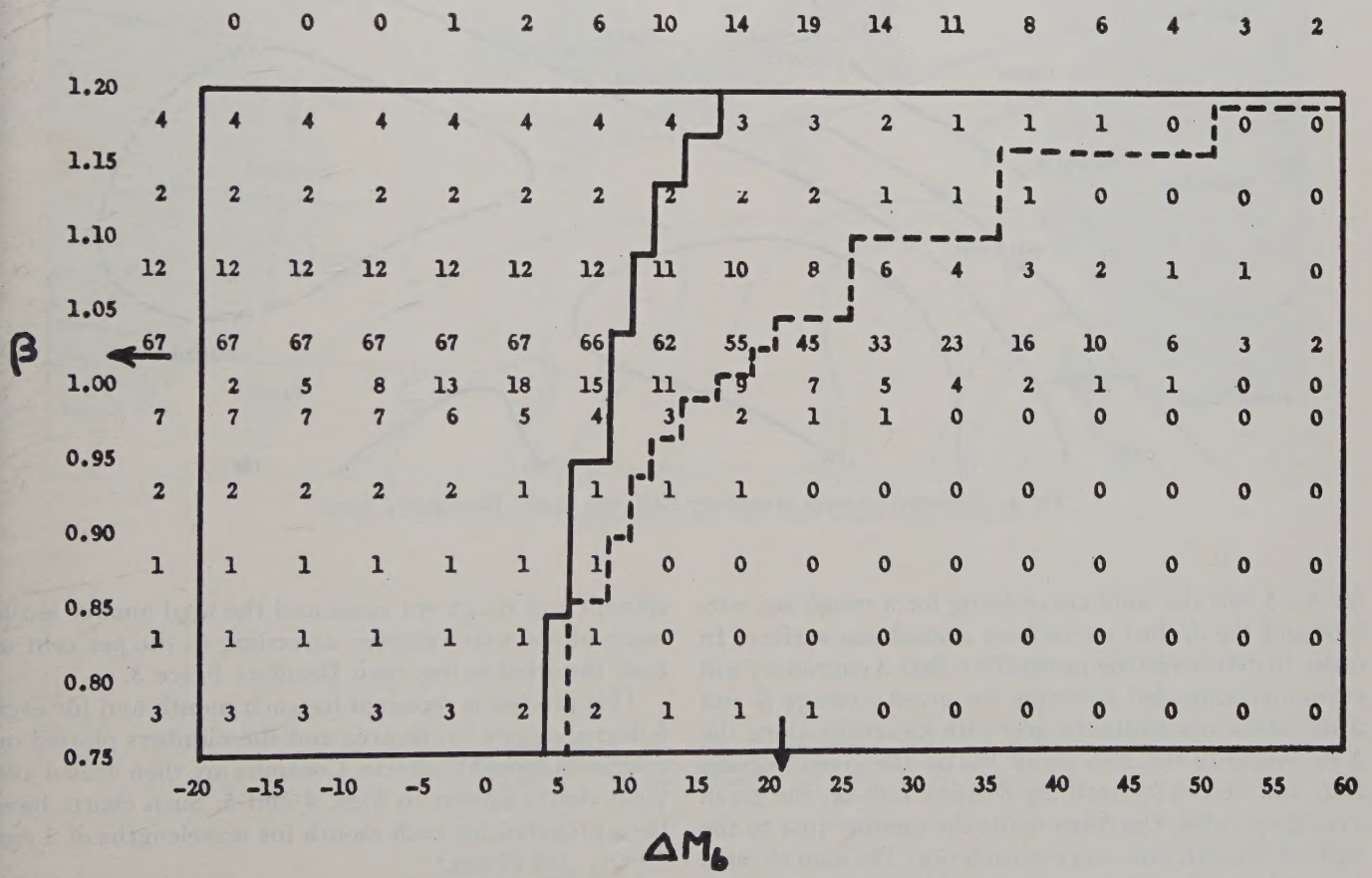

Fig. 3—Cumulative probability product and X-band criteria, Far East, December.

Fig. 4—Extended coverage expectancy East Asia Coast, December X-band.

for $\lambda = 3$ cm; the solid curve being for a rough sea surface and the dashed curve for a smooth sea surface. In order to determine the probability that 3 cm radars will encounter extended coverage for given average β and ΔM_b values, one shifts the grid with its arrows along the ΔM_b axis until the ΔM_b arrow lies on the given average ΔM_b and vertically until the β arrow falls on the given average β value. One then reads the number just to the right of the criterion curve in each row. The sum of these nine values gives the required probability in per cent. In practice these probabilities are read for both the smooth and rough sea cases and the final answer is the mean of the two weighted according to the per cent of time the wind is less than Beaufort Force 3.

This process is repeated for each month and for each 5 degree square in the area and the numbers plotted on a series of monthly charts. Contours are then drawn and yield charts similar to Figs. 4 and 5. Such charts have been prepared for each month for wavelengths of 3 cm, 10 cm, and 25 cm.[6]

[6] "Far East Radio-Radar Propagation Conditions for Fleet Units," U. S. Navy Electronics Rep. No. 319; July, 1952.

Fig. 5—Extended coverage expectancy East Asia Coast, July *X*-band.

The Curved Passive Reflector*

E. BEDROSIAN†

Summary—**The curved passive reflector is analyzed theoretically by the aperture-field method and the results are presented in the form of gain characteristics and radiation patterns. It is seen that curving the reflector produces a focusing effect in addition to the basic diffraction phenomenon, thereby providing increased gain as compared with the flat reflector. The limiting value for the flat reflector gain is 6 db while the gain of the curved reflector increases continually with reflector size when properly illuminated. Radiation patterns are computed and it is shown that the effect of reducing tower height is to widen the main lobe and to move the side lobes outward and depress them. It is concluded that, in general, the curved reflector causes lower side lobes than the flat reflector. The dish illumination is shown to be relatively unimportant with respect to the total antenna gain but the side lobe levels are reduced when the dish illumination is made more uniform.**

Introduction

EARLY microwave radio-relay systems employed antenna pairs mounted atop suitable towers which provided the terrain clearance between relay points. The relatively large tower heights required to allow reasonable path lengths made the placing of receiving and transmitting equipment at the top of a tower difficult and expensive while the base location led to inefficiencies because of transmission-line losses. The solution employed in modern microwave systems is the use of a vertically directed antenna at the base illuminating a passive reflector mounted at the top of the tower.

The reflector is usually a flat elliptical sheet of conducting material mounted at a 45-degree angle and illuminated by a parabolic dish. Such a reflector has been the subject of a number of recent articles. Unger[1] assumed a typical illumination of the dish aperture and performed the diffraction analysis graphically. Jakes[2] performed essentially the same analysis using analog computation techniques assuming a 10 db-tapered parabolic dish illumination. His work was verified experimentally by Drexler.[3] Greenquist and Orlando[4] reported a theoretical and experimental analysis of a rectangular reflector based on a method of applying successive corrections to the far-field approximation assuming a dish illumination of the form $(1-\rho^2)^{1/2}$. Finally, Crosby[5] analyzed the flat reflector using an approximate graphical procedure with a 10 db-tapered parabolic illumination. These works are in excellent agreement and show that the flat reflector can yield an increase in the far-field signal strength over that due to the parent antenna alone.

The curved reflector is a natural outgrowth of its flat predecessor. The flat reflector yields an increased far-field signal strength because of the Fresnel-ring type of interference obtained by illuminating properly shaped apertures. The preceding analyses show the limiting increase for such a system to be 6 db. The curved reflector utilizes not only the diffraction effect but also its natural focussing ability to yield an additional increase.

The Diffraction Problem

A comprehensive treatment of the methods available for computing the diffracted field is given by Silver.[6] The current-distribution method used by Crosby assumes a current distribution on the reflector surface such that the incident field which would appear at the reflector surface in its absence is properly terminated. The current distribution is then used to compute the reradiated field. The aperture-field method used by the others assumes that the reflector may be replaced by the aperture formed by its projection in the principal direction of reflection. The aperture is then considered to be illuminated by the field obtained by simple geometrical reflection from the reflector.

The concept of gain is introduced as a means of evaluating the reflector performance. Unger and Crosby defined the gain as the ratio of the distant field intensities obtained with and without the reflector in the system when serving as a transmitting antenna. Jakes considered a receiving system and defined the gain (indirectly) as the ratio of the received signal powers obtained in the two cases. The reciprocal properties of antenna systems make these definitions equivalent. The analysis to follow uses the aperture-field method and assumes a transmitting system.

Mathematical Analysis

The curved reflector is assumed to be a segment of a very large paraboloid of revolution whose focus lies at the center of the illuminating dish throat and whose axis is directed toward the distant receiving point. A typical system is illustrated in Fig. 1 from which it is seen that the practical reflector is only slightly curved and resembles a flat ellipse mounted directly above the dish at a 45-degree angle.

The aperture system is shown in Fig. 2(a). The feed aperture is taken as the dish throat which is circular of

* Original manuscript received by the PGAP, February 23, 1955.
† Motorola Inc., Riverside, Calif.

[1] H. G. Unger, "Ebene spiegel zur strahlumlenkung bei richtantenen," *Frequenz*, vol. 6, pp. 272–278; September, 1952.

[2] W. C. Jakes, Jr., "A theoretical study of an antenna-reflector problem," PROC. IRE, vol. 41, pp. 272–274; February, 1953.

[3] J. Drexler, "An experimental study of a microwave periscope," PROC. IRE, vol. 42, p. 1022; June, 1954.

[4] R. E. Greenquist and A. J. Orlando, "An analysis of passive reflector antenna systems," PROC. IRE, vol. 42, pp. 1173–1178; July, 1954.

[5] D. R. Crosby, "Theoretical Gain of Flat Microwave Reflector," 1954 IRE CONVENTION RECORD, Part 1, "Antennas and Propagation," pp. 71–75.

[6] S. Silver, "Microwave Antenna Theory and Design," Rad. Lab. Series, vol. 12, McGraw-Hill Book Co., Inc., New York, N. Y., chaps. 3–6; 1949.

radius P. It is separated by a distance h, corresponding roughly to the tower height, from the reflector aperture which is taken as the projection (assumed circular of radius R) in the direction of the path. While the reflector aperture itself is flat it appears curved to the signal rays because of the reflector curvature. Since the reflector is a segment of a paraboloid it is seen that its aperture is a segment of a sphere of radius h. The far-field geometry is shown in Fig. 2(b), where the true reflector aperture is shown in relationship to an arbitrary point in space.

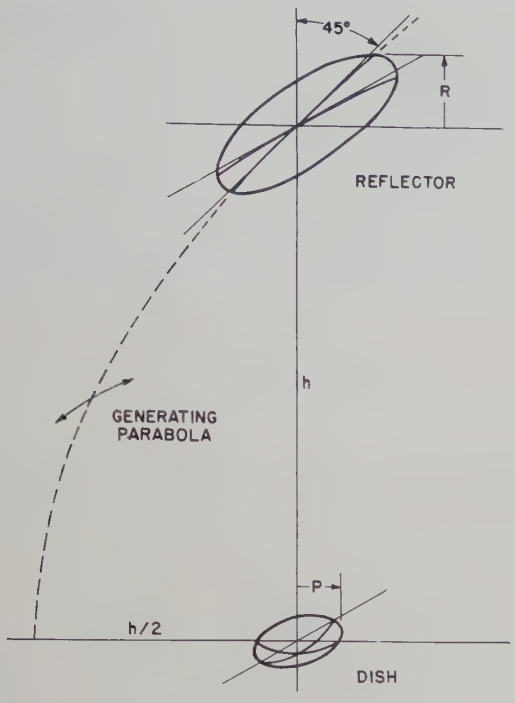

Fig. 1—Typical passive-reflector antenna system.

By the Kirchoff-Huygens approximation, the diffraction field $E(x, y, z)$ at an arbitrary point in space due to radiation from a surface S on which the field is described by $E'(\xi, \eta, \zeta)$ where (ξ, η, ζ) are coordinates of the surface is given by

$$E(x, y, z) = j\frac{1}{\lambda}\int_S E'(\xi, \eta, \zeta)\,\frac{e^{-j\beta l}}{l}\,dS, \quad \beta = \frac{2\pi}{\lambda}. \tag{1}$$

where l is the distance from the point (ξ, η, ζ) to the point (x, y, z), λ is the wavelength and β is the phase constant. In general, both E and E' are complex quantities. The approximations involved are that the dimensions and the radii of curvature of the reflector are large compared to a wavelength and that the point (x, y, z) does not depart greatly from the axis.

The dish illumination is assumed herein to be given by the parabolic function

$$E_P(x) = 1 - kx^2, \tag{2}$$

where k is an adjustable parameter and x is the normalized radius variable. When $k=0$, the illumination is uniform, when $k=1.0$, it is completely tapered to zero at the edge. The case $k=0.684$ gives the common 10 db taper (i.e., 10 db down at the edge). The phase at the dish aperture is assumed constant.

The distance l between points on the apertures is well approximated by

$$l = h + \frac{\rho^2 - 2r\rho\cos\psi}{2h}, \tag{3}$$

where h is the average dish-to-reflector spacing, ψ is the angular spacing between the arbitrary points and ρ and r are the dish and reflector variables, respectively. Taking dish aperture as surface and (3) for l leads, upon substitution into (1), to reflector-aperture illumination

$$E_R(r) = j\frac{\beta}{h}e^{-j\beta h}\int_0^P E_P(\rho/P)J_0\left(\frac{\beta r\rho}{h}\right)e^{-j\beta\rho^2/2h}\rho\,d\rho, \tag{4}$$

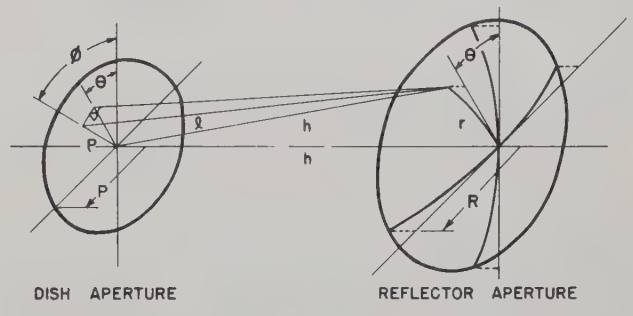

(a) DISH-REFLECTOR GEOMETRY

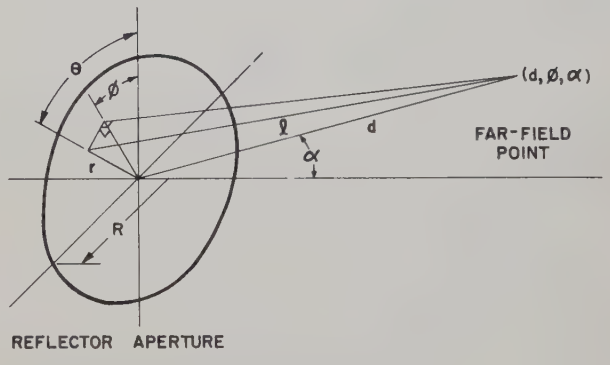

(b) REFLECTOR-FAR-FIELD GEOMETRY

Fig. 2—Aperture configuration for curved-reflector system.

where E_P is the dish illumination. Making the changes of variables

$$x = \frac{\rho}{P}, \quad y = \frac{r}{R}, \quad p = \frac{\beta P^2}{h}, \quad q = \frac{R}{P} \tag{5}$$

and using the dish illumination of (2) the reflector illumination becomes, upon integration,

$$E_R(y) = je^{-j\beta h}e^{-jp/2}f(y), \tag{6}$$

where

$$f(y) = [U_1 + jU_2] - 2\frac{k}{p}[U_2 + jU_3] + kq^2y^2[U_3 + jU_4] \tag{7}$$

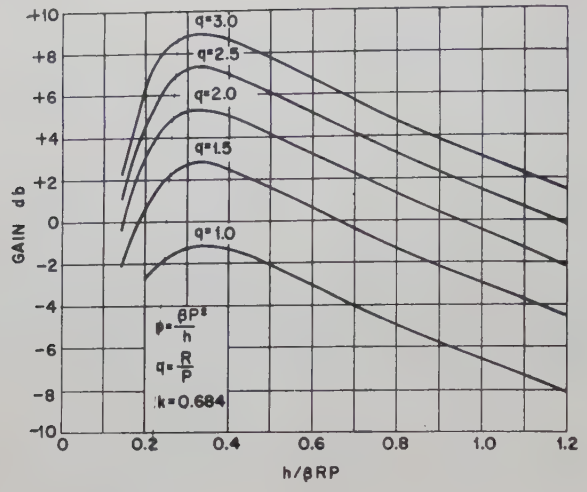

Fig. 3—Gain characteristics of curved reflector.

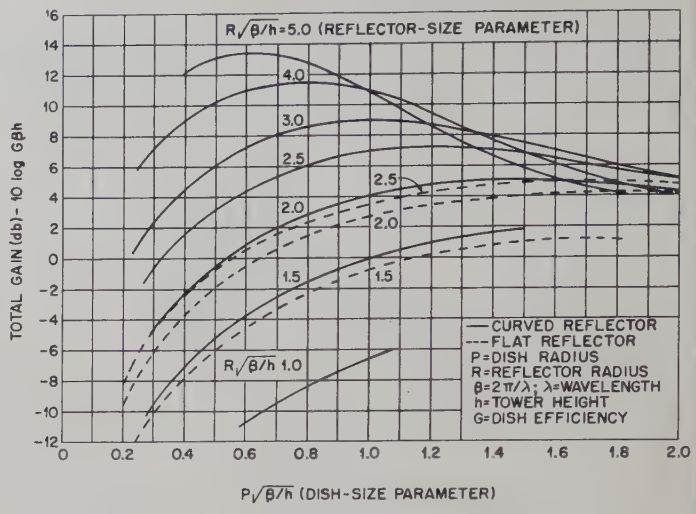

Fig. 4—Total gain characteristics of curved and flat reflector systems.

and $U_n \equiv U_n(p,pqy)$ are Lommel's functions[7] of two variables defined by

$$U_n(w, z) = \sum_{m=0}^{\infty} (-1)^m \left(\frac{w}{z}\right)^{n+2m} J_{n+2m}(z). \tag{8}$$

The radiated field at a distant point is found by applying the procedure again using the reflector aperture as the radiating surface and (6) for the illumination. Referring to Fig. 2(b), the distance l from a point (r, θ) on the reflector aperture to the point (d, ϕ, α) is seen to be approximated by

$$l = d - r \cos \psi \sin \alpha, \tag{9}$$

where d is the distance from the center of the reflector aperture, ψ is the angular spacing between the points and α is the angle off the axis. Performing these substitutions and integrating leads to the distant field

$$E = -\frac{\beta R^2}{d} e^{-j\beta(h+d)} e^{-jp/2} \int_0^1 f(y) J_0(by)\, y\, dy, \tag{10}$$

where

$$b = \beta R \sin \alpha. \tag{11}$$

The distant on-axis field which would appear if the dish alone were used is obtained simply as

$$E' = j\frac{\beta P^2}{d} e^{-j\beta d}\left(\frac{2-k}{4}\right), \tag{12}$$

while the distant on-axis field from the reflector is obtained from (10) by setting α to zero. The power gain is then the square of the magnitude of the ratio of these fields and is given by

$$G = \left| \frac{4q^2}{(2-k)} \int_0^1 f(y)\, y\, dy \right|^2. \tag{13}$$

[7] G. N. Watson, "A Treatise on the Theory of Bessel Functions," 2nd ed., Cambridge Univ. Press, London, England, pp. 537–550; 1952.

The radiation pattern of the reflector is the square of the magnitude of the ratio of the far-field E as given by (10) to its on-axis value. Thus

$$P = \left| \frac{\int_0^1 f(y) J_0(by)\, y\, dy}{\int_0^1 f(y)\, y\, dy} \right|^2. \tag{14}$$

The solutions to the various integrals appearing in (13) and (14) are summarized in the Appendix.

Gain Characteristics

The gain characteristics of the curved reflector are presented in Fig. 3 as a function of $h/\beta RP$ for various values of R/P, the reflector-dish radii ratio. The dish illumination has been taken as 10 db-tapered to conform with illuminations actually observed. Each curve has a maximum corresponding to the point representing the best compromise between the amount of power intercepted by the reflector and the uniformity of the intercepted illumination. Also, the curves rise without limit as R/P is increased reflecting the focusing ability of the curved reflector.

Of more practical interest to the systems engineer than the gain of the reflector over that of the dish is the total gain of the tower, i.e., the gain of the reflector-dish combination. The dish gain over an isotropic radiator can be expressed as

$$G_P = \mathcal{G}(\beta P)^2 = \mathcal{G}\beta h(P\sqrt{\beta/h})^2, \tag{15}$$

where $\mathcal{G}$ is the dish efficiency. If the reflector gain is expressed as a function of $P\sqrt{\beta/h}$ then the total gain in decibels can be written

$$G_T - 10 \log \mathcal{G}\beta h = G_R(P\sqrt{\beta/h}) + 20 \log P\sqrt{\beta/h}. \tag{16}$$

Fig. 4 is a plot of total gain with $R\sqrt{\beta/h}$ as a parameter.

Since the operating frequency is normally specified and the tower height is determined on the basis of providing proper terrain clearance, it is apparent that the curves amount to a plot of total gain per tower versus dish size for various reflector sizes. The optimum reflector-dish combination may be readily selected from Fig. 4. The smaller reflectors are seen to be relatively insensitive to dish size while the larger reflectors yield significant increases in total gain and require but small dishes.

The total gain characteristics of the flat reflector were computed from Jakes' curves and are shown on Fig. 4 for comparison. Though not shown, the curve for $R\sqrt{\beta/h}=1.0$ probably falls only slightly below the corresponding curve for the curved reflector while curves for larger values of $R\sqrt{\beta/h}$ fall below that for 2.5. The curved-reflector system is clearly at an advantage when large reflectors are used with small dishes.

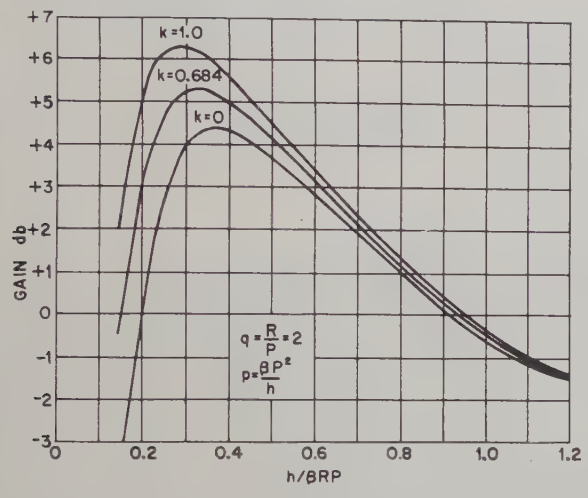

Fig. 5—Effect of dish illumination on reflector gain.

The effect of dish illumination is illustrated in Fig. 5 where the reflector gain has been plotted for a fixed value of R/P and the values of k corresponding to complete taper, 10 db taper and uniform dish illuminations. These curves show optimum dish and reflector gains to be incompatible since optimizing dish gain by making its illumination uniform results in a sharper feed beam which causes the reflector illumination and gain to deteriorate. In the vicinity of the optimum, the variations in dish gain are comparable to the compensating variations in reflector gain making the total gain relatively insensitive to dish illumination.

Radiation Patterns

Radiation patterns were computed for the curved reflector for various values of $\beta P^2/h$ and are presented in Fig. 6 as a function of b, the angle parameter. The reflector-dish radii ratio was chosen as 2 and the dish illumination assumed uniform for simplicity. It is seen that as the tower height is reduced the main lobe widens and the side lobes become depressed and move outward. At very low tower heights the main lobe begins to split and display a shallow minimum in the forward direction. The effect of dish illumination is illustrated in Fig. 7 which is the radiation pattern at a fixed value of $\beta P^2/h$ and R/P. The principal effect of making the dish illumination more uniform is to reduce the side lobe levels.

While radiation patterns for the flat reflector are not available in order to permit a direct comparison with the curved reflector it is possible to draw general conclusions from the fact that the principal difference between the two lies in the phase distribution of their aperture illuminations. The curved reflector obtains its increased gain by presented equi-phase wavefronts to its aperture thus minimizing phase error. The flat reflector, on the other hand, produces a phase error at its aperture as it reflects the curved wavefront it encounters. Silver[8] points out that the effect of a quadratic phase error such as that displayed by the flat reflector is to increase the side-lobe level.

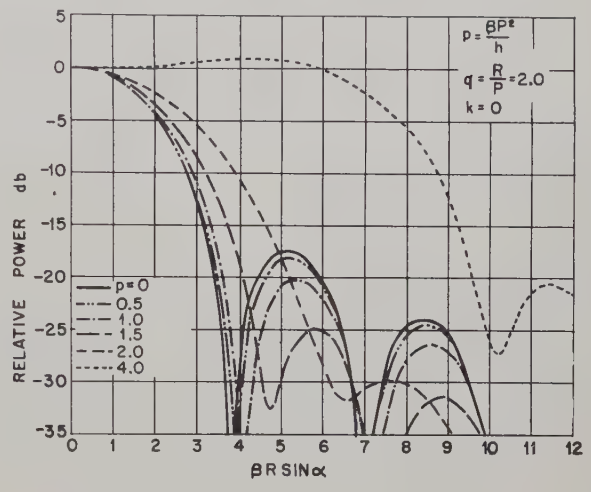

Fig. 6—Typical curved-reflector radiation patterns.

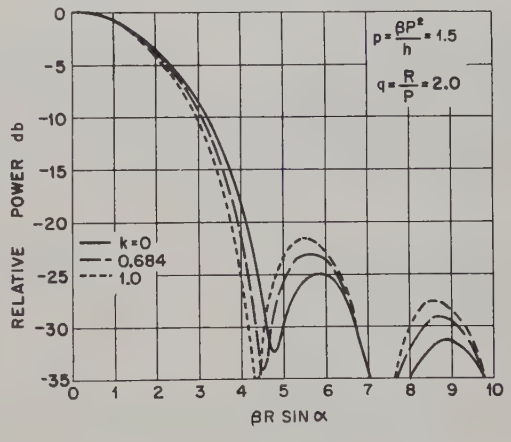

Fig. 7—Effect of dish illumination on radiation pattern.

At very large tower heights both reflectors may be considered uniformly illuminated thus giving identical patterns similar to that for $p=0$ in Fig. 6. As tower height is initially reduced neither reflector experiences much illumination taper but the flat reflector has an

[8] Silver, *op. cit.*, p. 189.

appreciable phase error even at large tower heights so that its side lobes increase in amplitude. At lower tower heights the illumination taper probably predominates over the phase error thereby permitting the side lobes to recede. The radiation patterns of Fig. 6 show that the side lobe levels for the curved reflector decrease continually as tower height is reduced, the decrease being due principally to the tapering of its illumination since phase errors are corrected except at very low tower heights. It may be assumed from the foregoing that the curved reflector will generally have a lower side-lobe structure than the flat reflector in the range of practical tower heights.

Conclusion

The curved reflector offers increased gain as compared with the flat reflector under all practical conditions; values of from 2 to 4 db more gain per tower being typical. Furthermore, for a given reflector the optimum dish size is smaller enabling a reduction in cost. Dish illumination is relatively unimportant with respect to the total antenna gain but the side-lobe levels are reduced when the dish illumination is made more uniform. In general, the curved reflector has lower side-lobe levels than the flat reflector thereby reducing stray radiation and providing greater immunity to interference.

Practical curved reflectors are formed by indenting flat reflectors at several points; the most modern types being continually adjustable. The value of curving has been demonstrated repeatedly in the field by erecting such reflectors when flat, aligning the system for maximum gain and then adjusting the curvature for a new maximum. The system gain invariably increases by this procedure. Rough gain measurements on systems which employ curved reflectors are in good agreement with the theoretical results thus tending to confirm the approximations made in the analysis. However, actual reflectors exhibit greater beam splitting and side lobe formation at very lower tower heights than predicted herein. It is felt this may be attributed to the nonperfect curvature.

Appendix

The integrals in (13) and (14) are all represented by the following general forms:

$$\begin{aligned}
&\text{(a)} \quad \int_0^1 U_\nu(p, pqy)\,y\,dy && \nu = 1, 2, 3\\
&\text{(b)} \quad \int_0^1 U_\nu(p, pqy)\,y^3\,dy && \nu = 3, 4\\
&\text{(c)} \quad \int_0^1 U_\nu(p, pqy)J_0(by)\,y\,dy && \nu = 1, 2, 3\\
&\text{(d)} \quad \int_0^1 U_\nu(p, pqy)J_0(by)\,y^3\,dy && \nu = 3, 4.
\end{aligned} \tag{17}$$

Type (a) is evaluated as

$$\int_0^1 U_\nu(p, pqy)\,y\,dy = \frac{1}{pq^2}\left[U_{\nu-1}(p, 0) - U_{\nu-1}(p, pq)\right], \tag{18}$$

where

$$U_0(p, 0) = \cos\frac{p}{2}, \qquad U_1(p, 0) = \sin\frac{p}{2},$$

$$U_2(p, 0) = 1 - \cos\frac{p}{2}. \tag{19}$$

Type (b) is given by

$$\int_0^1 U_\nu(p, pqy)\,y^3\,dy = -\frac{1}{pq^2}\left\{U_{\nu-1}(p, pq) + \frac{2}{pq^2}\left[U_{\nu-2}(p, pq) - U_{\nu-2}(p, 0)\right]\right\}. \tag{20}$$

Types (c) and (d) are cases of the general form

$$\int_0^1 U_\nu(p, pqy)J_n(by)\,y^{n+1}\,dy \tag{21}$$

since

$$\begin{aligned}
\int_0^1 U_\nu(p, pqy)J_0(by)\,y^3\,dy &= \frac{2}{b}\int_0^1 U_\nu(p, pqy)J_1(by)\,y^2\,dy\\
&\quad - \int_0^1 U_\nu(p, pqy)J_2(by)\,y^3\,dy.
\end{aligned} \tag{22}$$

Integrating by parts gives

$$\int_0^1 U_\nu(p, pqy)J_n(by)\,y^{n+1}\,dy = \frac{1}{b}\sum_{m=0}^{\infty}\left(\frac{pq^2}{b}\right)^m U_{\nu+m}(p, pq)J_{n+1+m}(b) \tag{23}$$

which, for convenience of computation, may also be expressed as

$$\int_0^1 U_\nu(p, pqy)J_n(by)\,y^{n+1}\,dy = \sum_{m=0}^{\infty}\frac{b^n}{2^{n+1}(n+1+m)!}\left(\frac{pq^2}{2}\right)^m U_{\nu+m}(p, pq)\Lambda_{n+1+m}(b) \tag{24}$$

where

$$\Lambda_n(x) = \frac{2^n n!}{x^n}J_n(x). \tag{25}$$

For the case of uniform illumination ($k=0$) these integrals become

$$\int_0^1 f(y)\,y\,dy = \frac{1}{pq^2}\left\{\left[\cos\frac{p}{2} - U_0(p, pq)\right]\right.$$

$$+ j\left[\sin\frac{b}{2} - U_1(p, pq)\right]\Big\} \tag{26}$$

$$\int_0^1 f(y)J_0(by)\,y\,dy$$

$$= \sum_{m=0}^{\infty} \frac{\left(\frac{pq^2}{2}\right)^m}{2(m+1)!}\left[U_{m+1}(p, pq) + jU_{m+2}(p, pq)\right]\Lambda_{m+1}(\beta R \sin\alpha).$$

At an infinite tower height ($p=0$) the limiting form of the radiation pattern is simply

$$P = \left(\frac{J_1(b)}{b}\right)^2. \tag{27}$$

Acknowledgment

The helpful criticisms and suggestions of H. Magnuski are gratefully acknowledged. Credit is also due Paul Cunliffe who performed the bulk of the mathematical computations.

A Multiple Telemetering Antenna System for Supersonic Aircraft*

R. E. ANDERSON,† C. J. DORRENBACHER,‡ R. KRAUSZ,† AND D. L. MARGERUM†

Summary—**The existing angle-of-attack indicator spike and ram-pressure tubes on a high-speed aircraft are modified to permit their use as telemetering antenna elements. The antenna system utilizing these elements provides for operation of three airborne telemetering transmitters. Operation of each transmitter and its antenna is independent of damage to or malfunction of the other components in the system, and no multiplexing loss is suffered in the antenna system. Since current flow on the fuselage is limited to the vicinity of the antenna elements, antenna performance would be little affected by variations in configuration of aircraft with similar basic design, and direct adaptation of this system to other aircraft of this type, therefore, is relatively straightforward.**

Introduction

THE OBJECTIVE of the work described in this paper was the development of an antenna system suitable for the transmission of telemetered intelligence from supersonic aircraft. The antennas developed provided for the radiation of energy from three independent airborne transmitters operating in the 216 to 235 megacycle telemetering band.

The antenna system discussed here utilizes existing ram-pressure tubes and the Angle-of-Attack Indicator, which were modified to permit use for the desired antenna functions. A pair of dummy ram-pressure tubes were added to serve as the antenna for the third transmitter.

Angle-of-Attack Indicator Antenna

The Angle-of-Attack Indicator, or spike, normally protruding from the nose of a supersonic test vehicle offers obvious possibilities for antenna purposes. Since this protrusion is about $\lambda/4$ in length the impedance match is easily obtained over the telemetering band. The problems in adapting such an installation are: (1) excitation of the spike as an antenna with provisions for carrying the wiring from the Angle-of-Attack Indicator across the feed gap, and (2) realization of a satisfactory radiation pattern in the forward direction.

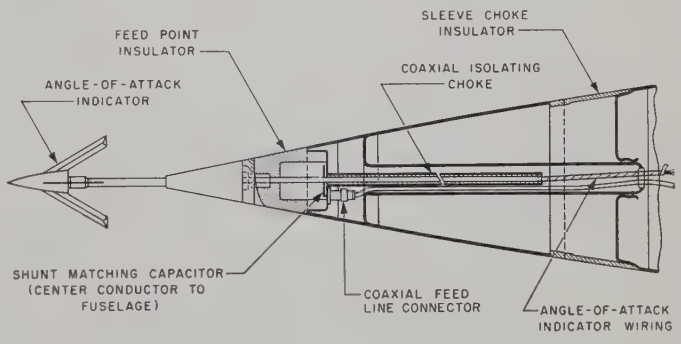

Fig. 1—Angle-of-Attack Indicator antenna installation.

Feedpoints for the Angle-of-Attack Indicator antenna were provided by replacing a short section of the nose casting with a Fiberglas structure located about a quarter-wavelength from the end of the spike, as shown in Fig. 1. The spike is connected to the center conductor of the coaxial feed cable through a shunt matching capacitor, the outer conductor being bonded to the fuselage. The Angle-of-Attack Indicator wiring is brought across the isolated section through the center conductor

* Original manuscript received by the PGAP, November 10, 1954; revised manuscript received, April 1, 1955.
† Stanford Res. Inst., Mount Lee Lab., Los Angeles, Calif.
‡ Douglas Aircraft Co., Inc., Santa Monica, Calif.

which is isolated by a coaxial quarter-wave choke and, therefore, does not disturb the feedpoint impedance. Leakage of the signal into the fuselage interior is also prevented.

The radiation pattern of a stub in the nose of a thin aircraft fuselage longer than a quarter-wavelength becomes directive in the aft direction. Since this type of pattern has insufficient coverage forward for most telemetering applications, steps were taken to prevent currents from flowing on the fuselage aft of a quarter-wavelength from the feed point. This was accomplished by incorporating a coaxial quarter-wave choke into the nose section of the aircraft as shown in Fig. 1. Attempts were made to use a choke whose inner conductor was only slightly smaller than the skin of the nose section; however, it was found that such configurations were ineffective in preventing current flow on the remainder of

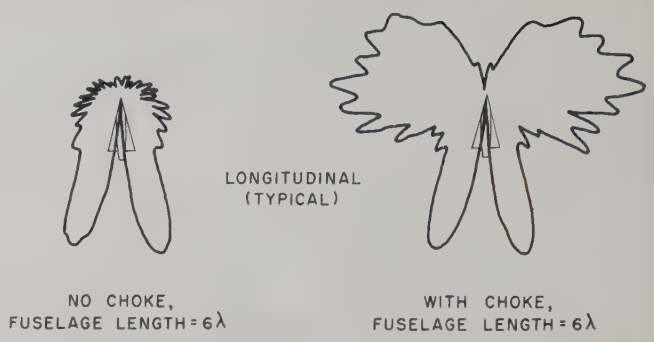

Fig. 2—Radiation patterns of Angle-of-Attack Indicator antenna for circularly polarized receiving antenna.

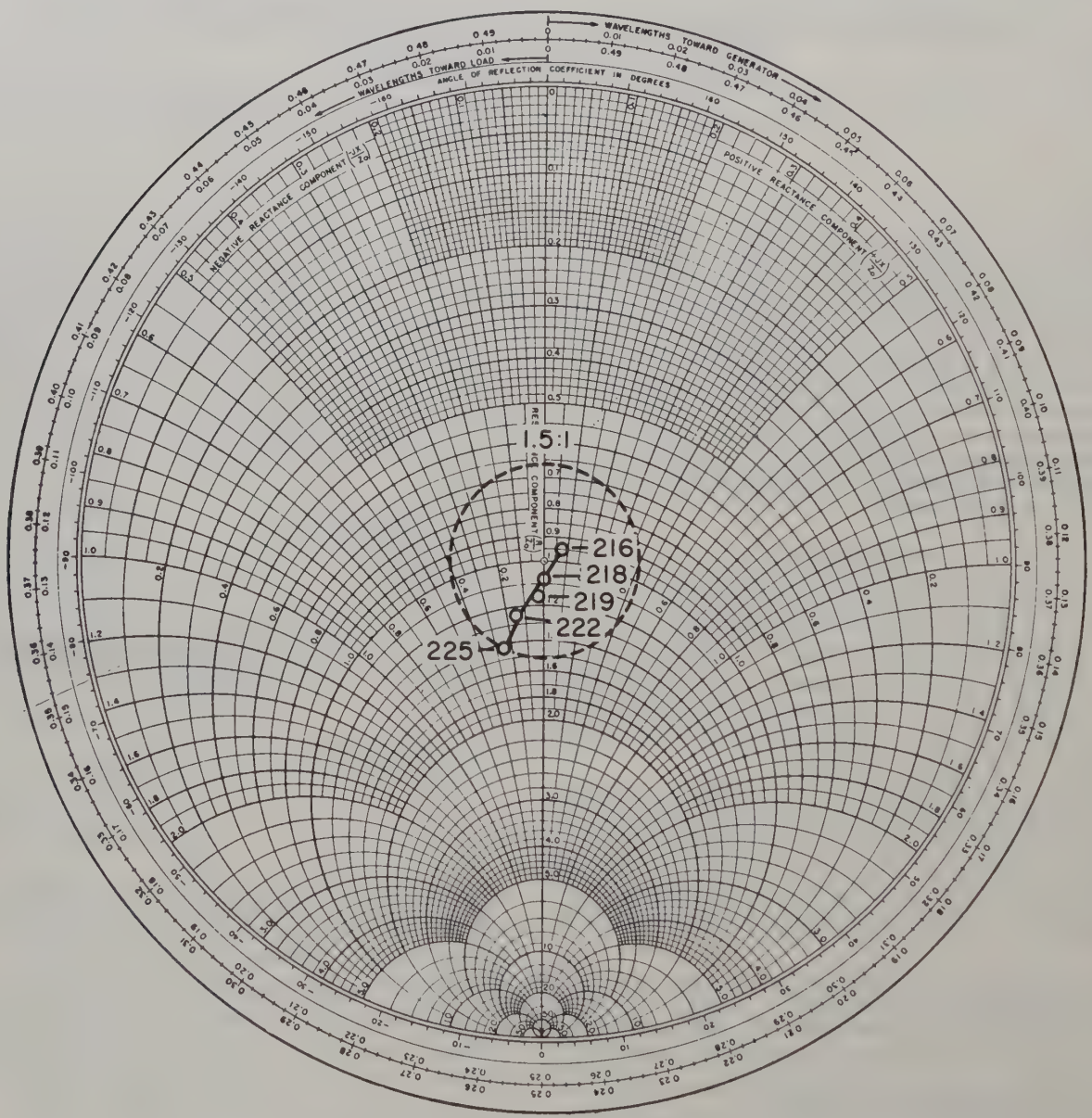

Fig. 3—Impedance plot of tuned AAI antenna.

the fuselage. The lack of effectiveness was attributed to the large fringe capacity across the input to the choke and the low characteristic impedance of the coaxial section, which, in the presence of even small losses, will result in a lowered impedance at the input to the choke. By reducing the center conductor of the choke section so that the characteristic impedance was about 100 ohms, the desired performance was obtained. The results of this choking action can be seen in the radiation patterns shown in Fig. 2, on the previous page.

The tuning capacitor consisted of a brass plate (connecting the center conductor of the feed line to the spike) spaced from the fuselage bulkhead by a Teflon gasket (see Fig. 1). The excursion of impedance with frequency about the design frequency after tuning is shown in Fig. 3, on the previous page.

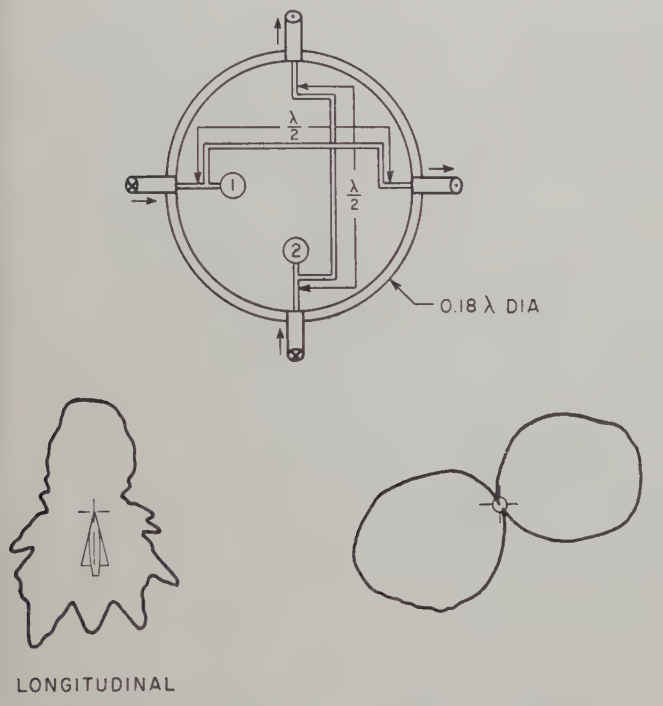

Fig. 4—Radiation patterns of two opposite out-of-phase ram-pressure-tube antenna elements for circularly polarized receiving antenna.

Ram-Pressure-Tube Antenna

Other protruding elements offering possibilities for adaptation to antenna functions on supersonic test vehicles are the ram-pressure pickup tubes. The ram-pressure-tube installation on the airframe considered consisted of two *L*-shaped stainless steel pickups located 180 degrees apart on the nose section of the fuselage. These elements were increased in size to permit impedance matching, and additional dummy tubes were added between the existing two to make a total of four elements spaced 90 degrees apart about the periphery of the nose. These four elements were to act as antennas for two independent telemetering transmitters.

Exciting opposite antenna elements out of phase cancels the longitudinal currents on the fuselage; consequently, each element operates as a bent stub in a ground plane rather than as a feed for exciting long-wire currents on the fuselage. Choosing the relative lengths of the transverse and longitudinal portions of these stubs allowed amplitude control of the relative radiation in the E_θ and E_ϕ polarizations. Fig. 4 shows a longitudinal pattern which is entirely satisfactory; the transverse pattern, however, does have two deep nulls with this antenna arrangement. It should be pointed out that both E_θ and E_ϕ components of the field are present in these directions, and to ground stations antennas having polarizations other than circular, the maximum reduction in signal may occur at slightly different aspects of the aircraft with the depths of the nulls also modified.

General Discussion

Inherent in the system is the isolation between pairs of antennas, as can be seen from consideration of the diagram in Fig. 4. The radial currents on one pair are perpendicular to the elements in the opposite pair and thus induce no currents, and the longitudinal currents in one pair are phased so that no net current is induced in the longitudinal portions of the elements in the opposite pair. Measured decoupling between any two of the three telemetering antenna systems was in excess of 33 db.

A drawing of the ram-pressure-tube antenna installation is shown in Fig. 5. Impedance matching of these antennas was accomplished by choosing the distance from the external antenna feedpoint to the feedline input and controlling the length of a coaxial shunt stub built into the antenna mount. A Smith Chart plot of the impedance of a pair of ram-pressure-tube antennas is shown in Fig. 6 (next page).

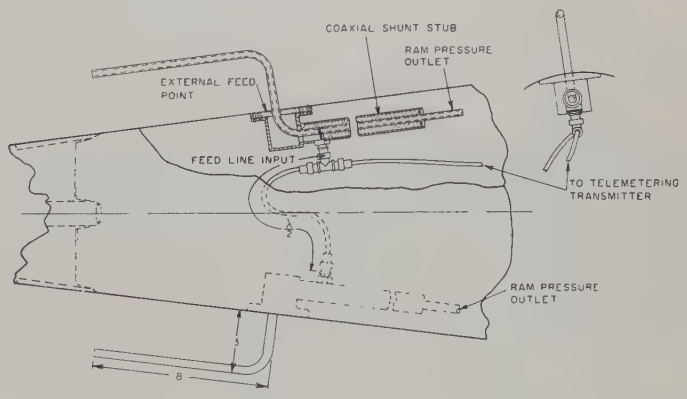

Fig. 5—Ram-pressure-tube antenna installation.

Conclusion

The antenna system described in this paper provides for transmission from three airborne transmitters in the 217 to 235 megacycle frequency range. All of the antennas are located in the nose section of the aircraft. The electrical performance of the antenna system, although

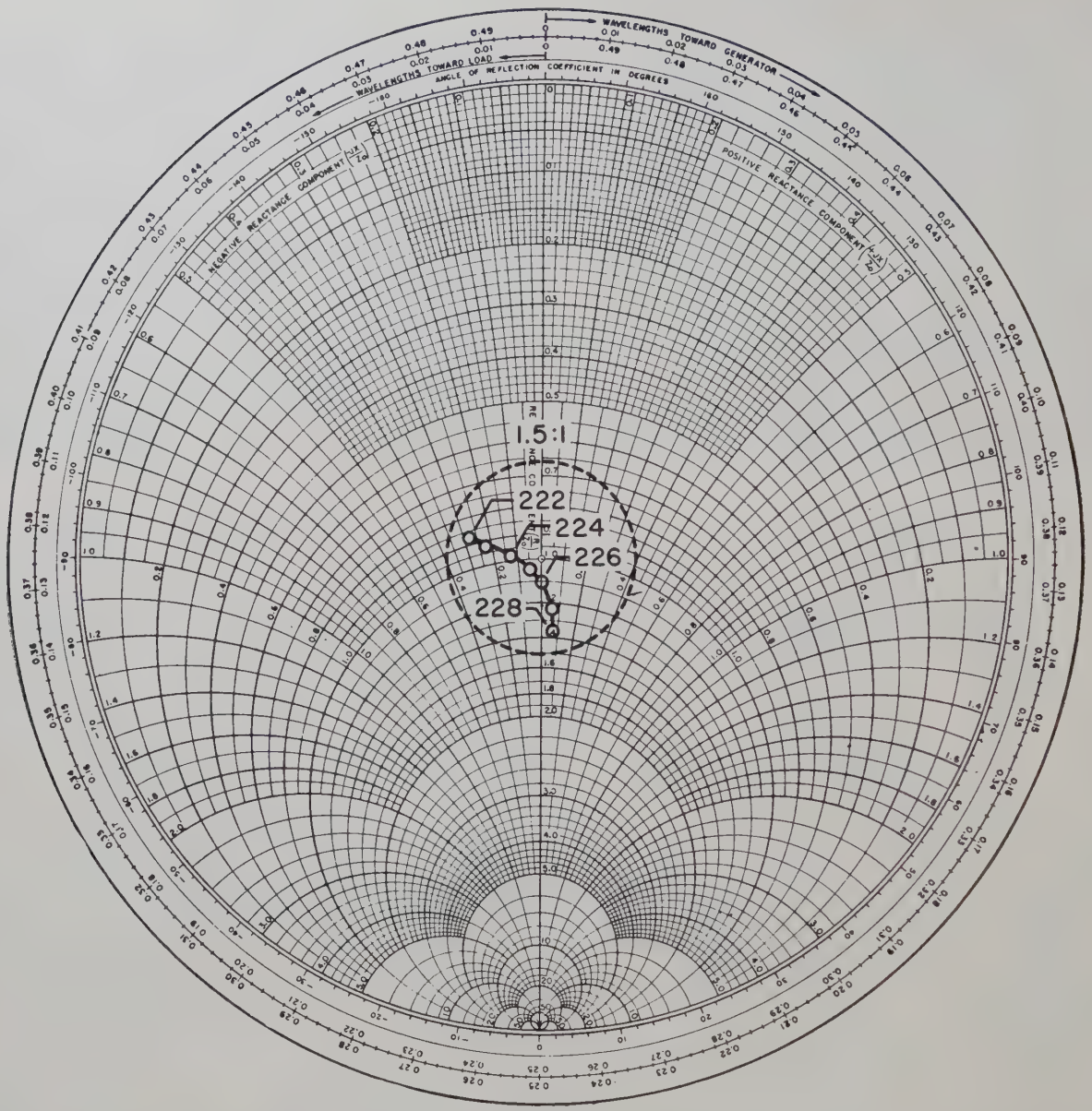

Fig. 6—Impedance plot for ram-pressure-tube antennas.

somewhat dependent on the diameter of the fuselage, is essentially unaffected by its length and shape. Since each transmitter operates with separate antennas there are no losses incurred (such as are commonly encountered in duplexing networks), and damage or malfunction of one transmitter or its antenna does not affect the operation of the remainder of the system.

The mechanical design of the antennas permits their installation on supersonic vehicles without appreciable increase in drag or weight, and since the tuning devices are built into the assembled antenna units, installation problems are minimized.

Measurement of Electric Field Distributions*

R. JUSTICE† AND V. H. RUMSEY‡

Summary—**The usual method of measuring electric field distributions comprises a receiving antenna at the point of observation, connected by means of a transmission line to receiving apparatus at some distant point. The principal advantage of the method described here is that it eliminates the transmission line and thus makes possible many measurements which cannot be done by the usual method. It is based on the fact that the echo from a thin straight conducting wire is proportional to the square of the component of electric field parallel to the wire. The practical application at centimeter wavelengths is described. The method has proven most valuable in a variety of problems involving flush mounted directional antennas, radomes, artificial transmission lines, etc.**

Introduction

HUYGENS' Principle applied to antenna radiation problems states that the radiation pattern of any source is determined by the distribution of the tangential components of electric or magnetic field intensity on any surface which encloses the source.[1,2] This well-known result is particularly useful in problems concerning radiating apertures in perfectly conducting closed surfaces such as a slot antenna mounted in an infinite cylinder or in an infinite ground plane, or more generally, a mathematically closed surface. In such instances the radiation patterns are determined by tangential E in the aperture. The considerable interest in such antennas shows the importance of a system for measuring accurately electric field distributions in the vicinity of such sources of radiation. Conventional probing techniques are frequently impractical since they introduce more disturbing elements into the field than can be tolerated. In particular the transmission line from the probing antenna to the receiving apparatus may so disturb the field as to invalidate the measurement. Furthermore, in making phase measurements, it is necessary to transmit the rf signal picked up by the moving probe back to the fixed receiving apparatus, and thus involve passing the rf through a flexible transmission line (or waveguide). The distortion of the rf signal caused by flexing the transmission line is a further objection to the usual probing method which is serious at short wavelengths (e.g., 3 cm). The purpose of this paper is to describe a reflection method of measuring electric field distributions in the vicinity of the source: its principal advantage is the elimination of the transmission line from the receiving antenna to the receiving apparatus.

Principle of the Method

Consider the measuring system sketched in Fig. 1. An antenna, represented by a horn, is connected to a transmitter through a hybrid junction. The junction is balanced so that when the antenna is radiating in its normal environment no energy is detected in the receiving arm of the junction. If now a conducting scatterer is introduced into the field of the antenna, a signal will be observed at the receiving arm of the hybrid junction.

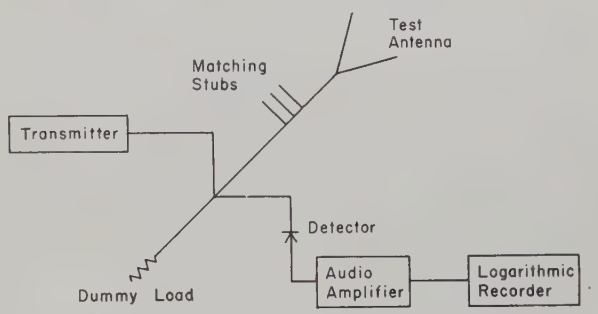

Fig. 1—Schematic of the measuring system.

The principle of the method is to use this signal, denoted by V, as a measure of the electric field, E, at the position of the scatterer. It follows from the reciprocity theorem[3,4] that V and E are related by an equation of the form

$$V = C \iint_{\text{scatterer}} E \cdot J dS, \tag{1}$$

where C is a constant, E = field when the scatterer is absent, J = current distribution on the scatterer. If the scatterer is a very short length of thin straight wire, (1) reduces to

$$V = CE_l Il, \tag{2}$$

where E_l = component of E in the direction of the wire, and Il = current moment of the current on the wire. The value of Il is determined from the condition that the total tangential electric field at the scatterer must vanish, which implies that

$$E_l(J) = -\ (\text{tangential } E_l \text{ at the scatterer}), \tag{3}$$

* Original manuscript received by the PGAP, December 20, 1954; revised manuscript received, April 1, 1955.

† Ohio State Univ., Columbus, Ohio.
‡ University of Illinois, Urbana, Ill.; formerly at Ohio State University.

[1] Larmor, *London Math. Soc. Proceedings*, vol. 1, p. 1; 1904.
[2] S. A. Schelkunoff, *Bell Sys. Tech. Jour.*, vol. 15, p. 92; 1936.
[3] S. A. Schelkunoff, "Electromagnetic Waves," D. Van Nostrand Co., Inc., New York, N. Y., p. 477; 1943.
[4] V. H. Rumsey, "Reaction concept in electromagnetic theory," *Phys. Rev.*, vol. 94, p. 2; September, 1954.

where $E(J)$ = field that would be generated by the current distribution J. If the scatterer is very small compared with the wavelength, $E(J)$ at the scatterer will be very nearly the same as if the scatterer were in "free-space." In this case we can write

$$E_l(J) \simeq K'Il$$

and therefore, from (3),

$$Il \simeq KE_l, \tag{4}$$

where K is a constant. Substitution in (2) for Il from (4) gives

$$V = AE_l^2, \tag{5}$$

where A is a constant, provided the scatterer stays in the same medium (same μ, ϵ and σ). Eq. (5) shows that the echo voltage V is proportional to the square of the component E_l of electric field and the phase angle of V is twice the relative phase angle of E_l. We note that E represents the field when the scatterer is absent; i.e., E is the thing we are trying to measure. This result is the basis of the method of measurement. If the scatterer is moved through the field to be measured and the echo signal is recorded as a function of position of the scatterer, the result is a continuous measurement of the distribution of the component of electric field parallel to the scatterer along the path followed by the scatterer (again note that the electric field referred to is the field that exists when the scatterer is absent).

We note that the validity of the method depends on the scatterer being sufficiently small and thin to make (4) a reliable approximation. The approximation will begin to fail when the scatterer comes close to some reflecting surface, for then we cannot assume that $E(J)$, at points on the scatterer, can be calculated as if the scatterer were in "free space." To estimate the magnitude of this effect, calculations were made for a scatterer in the presence of a plane perfectly conducting reflector. (The calculations are based on an assumed distribution of current on the scatterer, and are therefore approximate, but they should be quite satisfactory for estimating the order of magnitude of the effect). The results are plotted in terms of the error in E due to assuming that (5) is correct (*see* Fig. 2). It will be seen that the error is less than one per cent provided the distance from the reflecting surface is not less than the length of the scatterer. It should be noted that Fig. 2 applies to a plane perfect reflector; presumably the effect will be more or less depending on whether the reflector is concave or convex. In an enclosed region such as a cavity or waveguide, the effect will presumably be significantly greater or, to put it another way, the scatterer will have to be significantly smaller, as one would expect.

We should note that the error due to the size of the scatterer is characteristic of any method of measurement. For example, the magnitude of the error in the standard field probing method is of the same order, if the probe consists of a dipole of total length which is connected to a detector of extremely high impedance (the error being due simply to the finite size of the antenna).

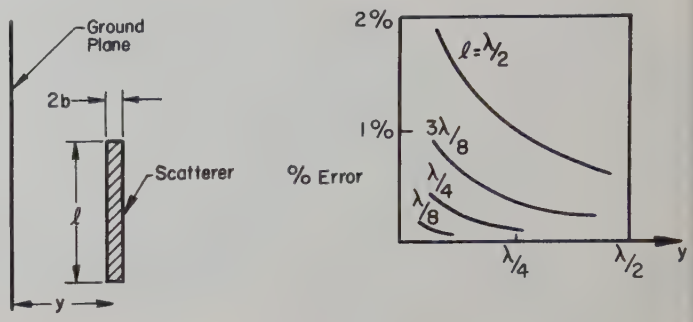

Fig. 2—Scatterer near ground plane, coordinate system and error vs distance from ground plane.

An experimental verification of (5) was obtained by measuring the transverse variation of the electric field in a rectangular waveguide operating in the lowest order TE mode. The excellent agreement between the cosine distribution of the true field and the measured result, as shown in Fig. 3, confirms the prediction that conducting surfaces in the vicinity of the scatterer do not appreciably alter the square law dependence of echo voltage on incident electric field.

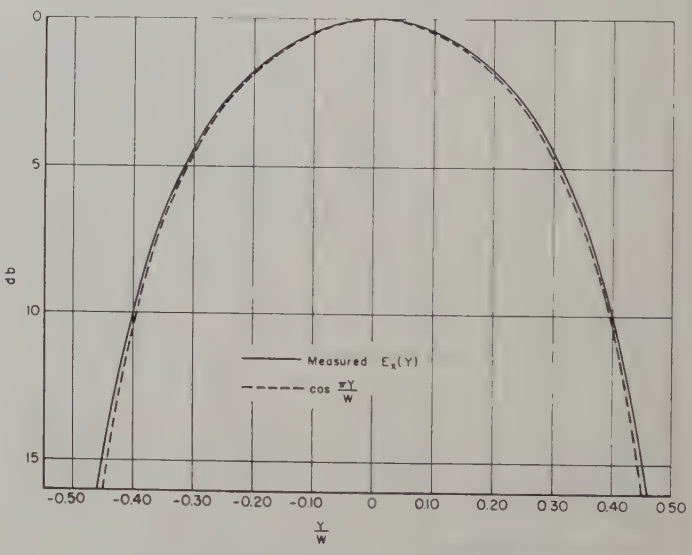

Fig. 3—Measured and calculated fields in a TE_{01} rectangular waveguide.

Instrumentation

A measuring system of the type described above has been in use at the Ohio State University Antenna Laboratory for some time. Some of the problems encountered in developing the system and their solutions are now discussed. An isolation between transmitter and receiver of about 90 db is usually required. The need for such a fine balance of the hybrid junction requires that the transmitter be as nearly monochromatic as possible.

Just how near to monochromatic it has to be depends on the antenna under test. If it is well-matched and broadband, a good balance can be obtained even if the signal has a certain frequency spread; if it is highly selective, an extremely pure signal is required. It has been found that a reflex klystron immersed in a large undisturbed oil bath generates a signal of sufficient purity and stability[5] for the requirements of the measuring system. The success of this device depends on the thermal capacity of the oil being large enough to hold the transmitter temperature constant for the duration of a measurement. The necessary tuning to achieve the required degree of isolation between the transmitting and receiving arms of the junction can be obtained from carefully designed and manufactured triple stub tuners, provided the test antenna is well matched into a waveguide.

In both the original 3,000 mc system, and the 10,000 mc system installed later, it was found that crystal detection was satisfactory. The energy was transmitted unmodulated and then modulated at the receiver by means of a crystal. This scheme was used because it furnished a more nearly monochromatic signal than that obtained by modulating the beam voltage of the klystron. The output of the detector was then fed into a selective audio amplifier whose output in turn was used to drive a logarithmic recorder.

A problem of some importance in the actual experiments is that of supporting the scatterer and moving it through the field. It was found that the scattered field due to a fine nylon thread was completely negligible compared to that due to a conducting scatterer. Hence it was possible to attach the scatterer, usually a fine wire, to the nylon thread which was then pulled through the field. Synchronization of the motion of the scatterer and of the recorder then made it a simple matter to interpret the recorded echo voltage in terms of the electric field distribution.

Another problem of considerable importance involves the ability of the scatterer to discriminate between mutually perpendicular field components; i.e., how thin must the scatterer be to select only the component E_l? Measurements indicate that the length to diameter ratio must be about 30 to reduce the error to less than 10 per cent of the cross polarized component.

Applications

The 3,000 mc system was assembled in order to facilitate the study of traveling-wave slot antennas. In this application many measurements were made of the distribution of tangential electric field in the aperture of such antennas. A typical antenna of the type investigated is illustrated in Fig. 4 together with its coordinate system.

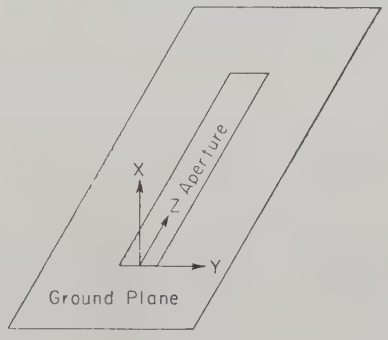

Fig. 4—Slot antenna in ground plane with coordinate system.

Since the phase of the signal V varies as twice the phase of the component E, it is possible to use this system to make phase measurements as well as amplitude measurements. The simplest way to obtain phase information is to unbalance the hybrid junction thus providing a constant reference signal R and then to record the sum of the constant reference signal and the echo signal produced by the scatterer. Thus for each position of the scatterer three voltages are known; namely V, $V+R$ and R where R is the reference signal. Since R is constant for a given measurement the calculation of the relative phase distribution for that measurement follows directly from the application of the law of cosines to a series of distinct positions of the scatterer. Alternatively, it is possible to measure the relative phase distribution along the path of the scatterer by directly measuring the phase variation of the signal V. This latter method has been used successfully at 10,000 mc.[6] The first method is well suited for the measurement of the phase velocity of a guided traveling wave field. A typical result showing the sum of the echo and a fixed signal is shown in Fig. 5.

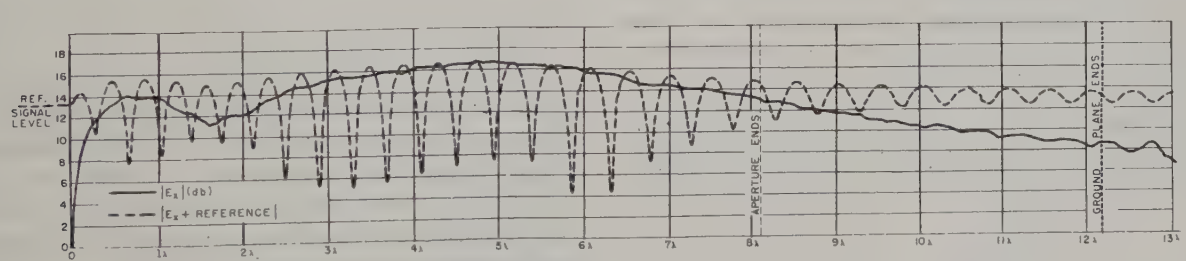

Fig. 5—Amplitude and phase measurement of normal component of electric field in slot antenna.

[5] J. N. Hines, and T. E. Tice, "Frequency stabilisation of klystrons," Ant. Lab. Rep. 478-13, Ohio State Univ.; June, 1953.

[6] J. Bacon, "Automatic phase plotter for microwaves," *Proc. NEC;* 1954.

The minima in the dashed line occur where the echo is 180 degrees out-of-phase with the constant reference signal and therefore the phase difference between echoes at adjacent minima is 360 degrees. Thus the phase difference between the values of E_l at adjacent minima is 180 degrees. The measurements plotted in Fig. 5 (on the previous page) show that the electric field distribution under observation can be approximated by a traveling wave of slightly variable wavelength (or phase velocity), the wavelength being equal to twice the distance between consecutive minima.

Other applications of the method include the study of the effect of radomes on the performance of antennas and antenna systems, and the study of the propagation along artificial transmission lines.

Acknowledgment

This work was carried out under a contract between the Air Force (WPAFB) and the Ohio State University Research Foundation. It is a pleasure to acknowledge the contributions of J. N. Hines, J. H. Richmond and W. E. Nexsen.

Determining the Reflector Surface of a Radar Antenna with Point Source Feed*

PENTTI LAASONEN†

Summary—**In the construction of a radar antenna the basic problem is to give the antenna reflector such a design that the scattering pattern will conform to the required power distribution. An approximative method is given for the determining of the central section of a reflector with point source feed and enveloping the osculating paraboloids, as well as a formula for the computation of the beam reflected by this surface. The central section obtained may be improved successively until adequate accuracy is attained. The method of computation is illustrated by an example.**

THE TWO basic problems encountered in the mathematical treatment of a radar antenna are to determine the beams of an antenna of given shape; i.e., the power distribution in the scattering pattern, and to find such a design of the reflector that it will radiate a pattern of the desired power distribution in the various directions.

Inasmuch as either problem is the inverse of the other as far as its starting point and its aim are concerned, and as problems of the first kind are more easily solved than those of the second kind, the normal procedure will be to find the solution of a problem of the second kind by successive approximations involving the recurrent solving of problems of the first kind. This is why the solution formulas of the first problem will be derived as a first step in the following considerations, the objective of which is to describe the solution of the second problem in the case of a radar antenna with point-feed source.

For the reflected pattern, the following expression will apply for the gain function of the pattern formed upon reflection, in the direction of the vector $\bar{R}^0$:

$$G = \frac{1}{\lambda^2}\left[\,|\,\bar{\imath}_1\cdot\bar{I}\,|^2 + |\,\bar{\imath}_2\cdot\bar{I}\,|^2\right],$$

where λ is the wavelength, $\bar{\imath}_1$ and $\bar{\imath}_2$ are two unit vectors orthogonal to the direction in question and to each other, and $\bar{I}$ is a complex vector defined through the surface integral

$$\bar{I} = \int_a G_f^{1/2} e^{-kj(\bar{r}\cdot\bar{R}^0)}\,\frac{1}{r^2}\left[(\bar{e}^0\times\bar{r})\times d\bar{a}\right]$$

extended over the entire reflector area a.

G_f = gain function of the feed
$k = 2\pi/\lambda$ = propagation constant in the nonlossy media
$\bar{r}$ = vector from feed point to reflector surface
$\bar{e}^0$ = unit vector defining the polarization of the radiation incident upon the reflector
$d\bar{a} = \bar{n}\,da$ = surface element of the reflector surface
$j = \sqrt{-1}$.

We shall limit the following discussion to a reflector of such symmetry that the reflector surface and the primary pattern G_f of the antenna have a common plane of symmetry and that the direction of polarization of the fictive dipole idealizing the radiating waveguide is orthogonal to this plane. We now take the reference system of co-ordinates with the y-axis orthogonal to the said plane and with the unit vectors $\bar{\imath}$, $\bar{\jmath}$ and $\bar{k}$. We shall restrict our problem to determination of gain function G in directions lying in the xz-plane of symmetry only. Consequently, then, $\bar{R}^0$ lies in this plane of symmetry and $\bar{I}$ is orthogonal to it, whence G obtains value

* Original manuscript received, November 12, 1954; revised manuscript received, March 28, 1955.
† Finland Institute of Technology, and State Institute for Technical Research, Helsinki, Finland.

$$G = \frac{1}{\lambda^2} |\, \bar{\jmath} \cdot \bar{I} \,|^2.$$

The polarization vector $\bar{e}^0$ pertaining to the ray $\bar{r}$ incident upon the reflector lies in the plane determined by the direction of polarization $\bar{\jmath}$ of the transmitting dipole and by the ray $\bar{r}$, and it is orthogonal to the latter; i.e., it is obviously the unit vector pertaining to the vector

$$\bar{e} = \bar{\jmath} - (\bar{\jmath} \cdot \bar{r}^0)\bar{r}^0.$$

For the y-component of the vector $(\bar{e} \times \bar{r}) \times d\bar{a}$ in the integrand in the expression of $\bar{I}$ there is now found the expression

$$\begin{aligned} \bar{\jmath} \cdot [(\bar{e} \times \bar{r}) \times d\bar{a}] &= (\bar{\jmath} \cdot \bar{r})(\bar{e} \cdot d\bar{a}) - (\bar{\jmath} \cdot \bar{e})(\bar{r} \cdot d\bar{a}) \\ &= (\bar{\jmath} \cdot \bar{r})(\bar{\jmath} \cdot d\bar{a}) - \bar{r} \cdot d\bar{a} \\ &= -(r_x da_x + r_z da_z). \end{aligned}$$

Since further the square of the length of $\bar{e}$ is $(r_x^2 + r_z^2)/r^2$, we thus have

$$G = \left| \int_a G_f^{1/2} e^{-kj(r - \bar{r} \cdot \bar{R}^0)} \frac{r_x da_x + r_z da_z}{\lambda r \sqrt{r_x^2 + r_z^2}} \right|^2.$$

When it is attempted to concentrate the power in the direction of the xz central plane, it is expedient to shape the reflector to conform with the enveloping surface of such confocal revolution paraboloids pertaining to the directions in this plane that are of interest that the osculating paraboloid corresponding to any direction θ in this plane will be tangent to the envelope along a plane curve; i.e., a parabola, with this particular elevation θ (Fig. 1). If the distance of the intersection of this

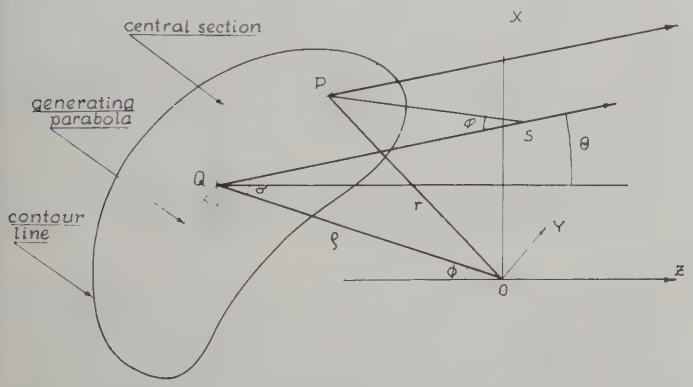

Fig. 1

parabola and the central plane, Q, from the focal point 0 is ρ and the elevation of the radius $0Q$ is ϕ, so that $2\sigma = \phi + \theta$ is twice the angle of reflection, a simple calculation shows the focal distance of the parabola to be $\rho \cos^2\sigma$. Let now $S(\xi, 0, \zeta)$ denote the focus of the parabola, $P(x, y, z)$ an arbitrary point on this parabola, and at the same time also a point on the reflector surface, and let the azimuth angle of this point be $PSQ = \varphi$. The said points have the co-ordinates:

$$\begin{cases} \xi = \rho \sin\phi + \rho \cos^2\sigma \sin\theta \\ \zeta = -\rho \cos\phi + \rho \cos^2\sigma \cos\theta \end{cases}$$

$$\begin{cases} x = \rho \sin\phi + \rho \cos^2\sigma \operatorname{tg}^2 \tfrac{1}{2}\varphi \sin\theta \\ y = 2\rho \cos^2\sigma \operatorname{tg} \tfrac{1}{2}\varphi \\ z = -\rho \cos\phi + \rho \cos^2\sigma \operatorname{tg}^2 \tfrac{1}{2}\varphi \cos\theta. \end{cases}$$

Using the parabolic co-ordinate α defined by the equation

$$\operatorname{tg} \tfrac{1}{2}\alpha = \cos\sigma \operatorname{tg} \tfrac{1}{2}\varphi,$$

instead of the azimuth angle φ, the following expressions are found for the co-ordinates of a point P on the reflector surface:

$$\begin{cases} x = \rho \sin\phi + \rho \operatorname{tg}^2 \tfrac{1}{2}\alpha \sin\theta, \\ y = 2\rho \operatorname{tg} \tfrac{1}{2}\alpha \cos\sigma, \\ z = -\rho \cos\phi + \rho \operatorname{tg}^2 \tfrac{1}{2}\alpha \cos\theta. \end{cases}$$

Differentiation with regard to the variable ϕ shall be indicated by a prime. On the basis of the shape of the central section ($\alpha = 0$) of the reflector the following differential equation between the variables ρ, ϕ and θ is found:

$$\frac{d\rho}{d\phi} = \rho' = \rho \operatorname{tg}\sigma = \rho \operatorname{tg} \tfrac{1}{2}(\phi + \theta), \tag{1}$$

and furthermore the functional determinants

$$\begin{cases} \dfrac{\partial(y, z)}{\partial(\phi, \alpha)} = -\dfrac{\rho^2}{\cos^3 \frac{1}{2}\alpha}(1 + \theta' \operatorname{tg}^2 \tfrac{1}{2}\alpha) \cos\tfrac{1}{2}\alpha \sin\tfrac{1}{2}(\phi - \theta), \\ \dfrac{\partial(z, x)}{\partial(\phi, \alpha)} = -\dfrac{\rho^2}{\cos^3 \frac{1}{2}\alpha}(1 + \theta' \operatorname{tg}^2 \tfrac{1}{2}\alpha) \sin\tfrac{1}{2}\alpha, \\ \dfrac{\partial(x, y)}{\partial(\phi, \alpha)} = +\dfrac{\rho^2}{\cos^3 \frac{1}{2}\alpha}(1 + \theta' \operatorname{tg}^2 \tfrac{1}{2}\alpha) \cos\tfrac{1}{2}\alpha \cos\tfrac{1}{2}(\phi - \theta). \end{cases}$$

In accordance with the theory of surfaces there is

$$d\bar{a} = \left[\frac{\partial(y, z)}{\partial(\phi, \alpha)} \bar{\imath} + \frac{\partial(z, x)}{\partial(\phi, \alpha)} \bar{\jmath} + \frac{\partial(x, y)}{\partial(\phi, \alpha)} \bar{k} \right] d\phi d\alpha.$$

The differential expression appearing in the expression of G is then

$$\begin{aligned} &-\frac{r_x da_x + r_z da_z}{\sqrt{r_x^2 + r_z^2}} \\ &\quad = -\rho(1 + \theta' \operatorname{tg}^2 \tfrac{1}{2}\alpha) \frac{\cos\sigma}{\sqrt{1 + \operatorname{tg}^2\alpha \sin^2\sigma}} d\phi d\alpha. \end{aligned}$$

Let θ_0 be the angle of elevation of the particular direction $\bar{R}^0$ in the xz-plane for which the value of the gain function shall be determined. The exponent in the integrand in the expression of the gain function $G(\theta_0)$ is

$$\begin{aligned} &-kj(r - \bar{r} \cdot \bar{R}^0) \\ &\quad = -\frac{4\pi\rho}{\lambda} j[\cos^2 \tfrac{1}{2}(\phi + \theta_0) + \operatorname{tg}^2 \tfrac{1}{2}\alpha \sin^2 \tfrac{1}{2}(\theta - \theta_0)], \end{aligned}$$

whence the expression of the gain function is ultimately found to be

$$G(\theta_0) = \left| \iint_a (G_f(\phi, \alpha))^{1/2} \frac{\rho}{\lambda} (1+\theta' \operatorname{tg}^2 \tfrac{1}{2}\alpha) \frac{\cos \sigma}{\sqrt{1+\operatorname{tg}^2 \alpha \sin^2 \sigma}} \cdot e^{-(4\pi\rho/\lambda)[\cos^2 (\phi+\theta_0)/2+\operatorname{tg}^2 \alpha/2 \cdot \sin^2 (\theta-\theta_0)/2]i} d\phi d\alpha \right|^2. \quad (2)$$

When the central section of the reflector has a given shape as determined in polar co-ordinates by a function $\rho=\rho(\phi)$, θ (and consequently also σ) will be determined through (1) in terms of ϕ. The gain function G_f expressing the power distribution of the radiation from the waveguide is originally determined through two directional co-ordinates; e.g., the spherical angular co-ordinates

$$\begin{cases} \beta = \operatorname{arctg} (-\sqrt{x^2+y^2}/z), \\ \psi = \operatorname{arctg} (x/y). \end{cases}$$

Since, however, these are related with the variables ϕ and α through the equations

$$\begin{cases} \cos \beta = \cos \phi \cos^2 \tfrac{1}{2}\alpha - \cos \theta \sin^2 \tfrac{1}{2}\alpha, \\ \sin \beta \cos \psi = \sin \alpha \cos \sigma, \end{cases}$$

the function $G_f(\phi, \alpha)$ will thus be determined. All in all, the evaluation of (2) then involves the integration of a definite function of the variables ϕ and α; ϕ designating a certain parabola section of the reflector and α representing the parameter which defines the location of a point upon this parabola. The domain of integration is limited by the contour line of the reflector represented by the boundary function $\alpha=\alpha_c(\phi)$, whence $-\alpha_c(\phi) \leqq \alpha \leqq +\alpha_c(\phi)$.

The double integral in the expression of $G(\theta_0)$ has to be computed for each requisite value of θ_0 by means of some method of numerical integration. The dependence of the integrand of variable α is regular enough, both as regards the exponential function and the factors preceding it; that, e.g., Gauss' method of mean values can be employed with advantage in the integration with regard to α. The integrand being even with regard to α, it is adequate if, for instance, six intermediate points are used, to compute the integrand for the different values of ϕ at three α values chosen in accordance with the mean value method. The dependence of the integrand of variable ϕ is mostly irregular to such a degree that the integration with regard to this variable should be carried out in accordance with some more versatile method; e.g., Simpson's rule, but increasing the number of subdivisions as occasion demands.

The factor in the integrand most strongly dependent on the shape of the central section of the reflector is the exponential function; at various points on the reflector it obtains complex values of absolute value unity, but with phase angles which may vary within a range of several full turns. In order to examine more closely the nature of this exponential function, we shall expand its phase angle to a Taylor series in the vicinity of the value ϕ_0 corresponding, in accordance with (1), to the direction θ_0 under consideration. It will be seen, then, that the first-order term always disappears; the zero- and second-order terms are

$$-\frac{4\pi\rho}{\lambda} j[\ ] = \left\{ -\frac{4\pi\rho_0}{\lambda} \cos^2 \sigma_0 - \frac{\pi\rho_0}{\lambda} \theta_0'(1+\theta_0' \operatorname{tg}^2 \tfrac{1}{2}\alpha)(\phi-\phi_0)^2 + \cdots \right\} j.$$

It is evident from this that the said phase angle has a stationary value along the osculating parabola section ϕ_0 belonging to the direction θ_0, its steepness, however, increasing with the increase of the factor $(\pi\rho_0/\lambda)\theta_0'(1+\theta_0' \operatorname{tg}^2 \tfrac{1}{2}\alpha)$. Due to the integral formula

$$\int_{-\infty}^{+\infty} e^{(a+bt^2)i} dt = e^{(a+\pi/4)i} \sqrt{\frac{\pi}{b}},$$

we thus arrive at the approximative formula

$$G(\theta_0) \approx \frac{\rho_0}{\lambda \left| \theta_0' \right|} \cos^2 \sigma_0 \cdot \left| \int_{(\phi=\phi_0)} (G_f(\phi_0, \alpha))^{1/2} \sqrt{\frac{1+\theta_0' \operatorname{tg}^2 \tfrac{1}{2}\alpha}{1+\operatorname{tg}^2 \alpha \sin^2 \sigma_0}} \, d\alpha \right|^2.$$

This formula also constitutes the starting point for the finding of the first approximate solution to the inverse problem; i.e., that of determining such a central section $\rho=\rho(\phi)$ of the reflector that the gain function of the reflected pattern will be a given function of the directional angle θ_0. If, namely, this formula is approximated further by substituting for its integrand the value it obtains at the center ($\alpha=0$), there results, with an integration interval of the length $2\alpha_c(\phi_0)$, the approximate formula

$$G(\theta) = K \frac{\rho}{\theta'} \cos^2 \tfrac{1}{2}(\phi+\theta) G_f(\phi, 0)(\alpha_c(\phi))^2, \quad (3)$$

where K is a constant.

In addition to this equation relating the variables ρ, ϕ and θ we have the differential equation (1) containing these variables. Eliminating ρ and the indefinite constant K from these equations, we have the differential equation of the second order:

$$\frac{d^2\theta}{d\phi^2} - \left(\frac{G_f'(\phi, 0)}{G_f(\phi, 0)} + 2 \frac{\alpha_c'(\phi)}{\alpha_c(\phi)} \right) \frac{d\theta}{d\phi} + \left(\frac{G'(\theta)}{G(\theta)} + \operatorname{tg} \tfrac{1}{2}(\phi+\theta) \right) \left(\frac{d\theta}{d\phi} \right)^2 = 0,$$

which has a solution satisfying the given boundary conditions $\theta(\phi_1)=\theta_1$, $\theta(\phi_2)=\theta_2$; to this solution corresponds a certain shape of the central section:

$$\rho = \rho_0 e^{\int \operatorname{tg} 1/2(\phi+\theta(\phi))d\phi}.$$

This first approximate solution is, however, most easily obtained directly from (3) by integration of its both members with regard to θ:

$$\int_{\theta_1}^{\theta} G(\theta)d\theta = K\int_{\phi_1}^{\phi} G_f(\phi, 0)(\alpha_c(\phi))^2\theta(\phi)\cos^2\tfrac{1}{2}(\phi+\theta(\phi))d\phi. \qquad (4)$$

It is true that the right member of this equation is not exclusively a function of ϕ, since the integrand contains the unknown function $\theta(\phi)$ immediately as well as through ρ, but a process of iteration starting with an assumed function is generally very rapidly convergent. The constant K is naturally determined in such a way that even the second boundary condition $\theta(\phi_2)=\theta_2$ is satisfied.

When now the power distribution of the pattern actually reflected by this first reflector shape determined in the way described above is calculated from (2) it will not generally coincide with the required $G(\theta)$, but it has a certain imperfect configuration $G(\theta)+\Delta G(\theta)$. A new, improved shape of the reflector is now found by repeating the calculations outlined above, inserting, however, for the required pattern the function $G(\theta)$ modified in the opposite direction; i.e., $G(\theta)-\Delta G(\theta)$. The procedure usually leads quite rapidly to a reflector shape of such perfection that it will reproduce the required pattern with adequate accuracy. This convergence has been verified in practice. Moreover, a reflector based on these calculations has been constructed and measured.

Example

As an illustration of the application of this method we shall consider a problem of schematic simplicity: to design a reflector meeting the following requirements:

1. The power distribution in the primary pattern radiated by the waveguide conforms to the function $G_f=\cos^2\beta$.
2. The reflector area is confined to the region with $G_f \geqq 0.25$.
3. The dimensions of the reflector are determined by the condition that the upper edge of the central section should have the distance 10λ from the feed point.
4. The central section of the beam of this antenna is required to conform to Fig. 2; i.e., there should be

$$\begin{cases} G(\theta)\cdot\sin^2\theta = \text{constant}, & \text{when } \operatorname{arctg} 0{,}1 \leqq \theta \leqq 30°, \\ G(\theta) = \text{constant}, & \text{when } 0 \leqq \theta \leqq \operatorname{arctg} 0{,}1, \\ G(\theta) = 0, & \text{when } \theta < 0 \text{ or } \theta > 30°. \end{cases}$$

It was seen above that the solving of this problem is essentially connected with the determination of the function $\theta(\phi)$ corresponding to the shape of the central section. The boundary values of θ being 0 and 30° and those of ϕ, with $\varphi=0$ and consequently $\alpha=0$, being obviously $-60°$ and $+60°$, the following boundary conditions may be set up for this monotonously changing function:

when $\phi=-60°$, we must have $\theta=30°$,
when $\phi=+60°$, we must have $\theta=0$.

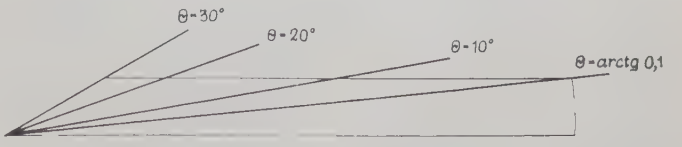

Fig. 2

As a first trial function we shall employ the linear

$$\theta(\phi) = 15° - \tfrac{1}{4}\phi.$$

According to (1), the shape of the central section corresponding to this function is

$$\rho = \rho_0[\cos(\tfrac{3}{8}\phi + 7°{,}5)]^{-8/3}.$$

In Table I, these θ and ρ functions of the first approximation are listed under A. The α_c values pertaining to the reflector edge have been obtained on the basis of the equation

$$\cos\beta = \cos\phi\cos^2\tfrac{1}{2}\alpha - \cos\theta\sin^2\tfrac{1}{2}\alpha \qquad (5)$$

substituting $\beta=60°$, which corresponds to the edge.

TABLE I

	A			B			C
ϕ	θ	ρ/λ	α_c	θ	ρ/λ	α_c	θ
−60°	30°	7.42	0°	30°00	8.455	0°00	30°00
−40°	25°	6.99	47°	20°51	7.833	46°56	20°12
−20°	20°	6.82	58°	9°68	7.469	57°08	8°79
0°	15°	6.99	60°	5°17	7.387	60°00	4°57
+20°	10°	7.42	57°	2°31	7.693	56°88	2°02
+40°	5°	8.44	46°	0°53	8.482	45°67	0°44
+60°	0°	10.00	0°	0°00	10.000	0°00	0°00

The second approximation of the functions θ, ρ and α_c will be found by means of (4). Since the integrand in the left member of this equation is known in terms of θ, and the integrand in the right member can be computed by substituting θ, ρ and α_c in terms of and in accordance with the first approximation, these integrals can be evaluated by means of numerical or graphical integration in terms of θ and ϕ, respectively. Plotting the results in a rectangular (ϕ, θ) system of co-ordinates with the values of the left-hand integral measured along the ϕ axis and those of the right-hand integral along the θ axis, the relation between ϕ and θ can be found by means of a simple nomographic construction shown in Fig. 3. The columns joined under B in the table give the function θ obtained in this way as well as the functions ρ and α_c calculated once more according to equations

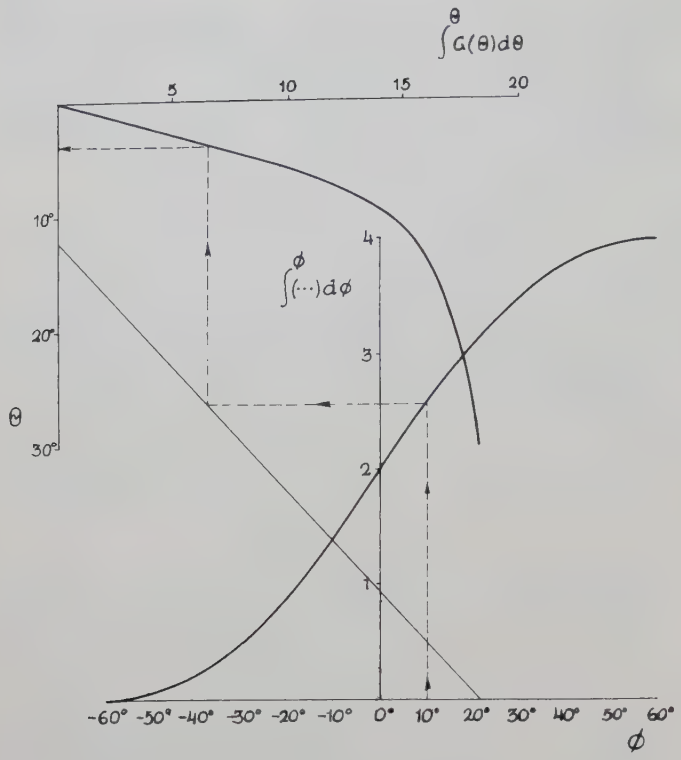

Fig. 3

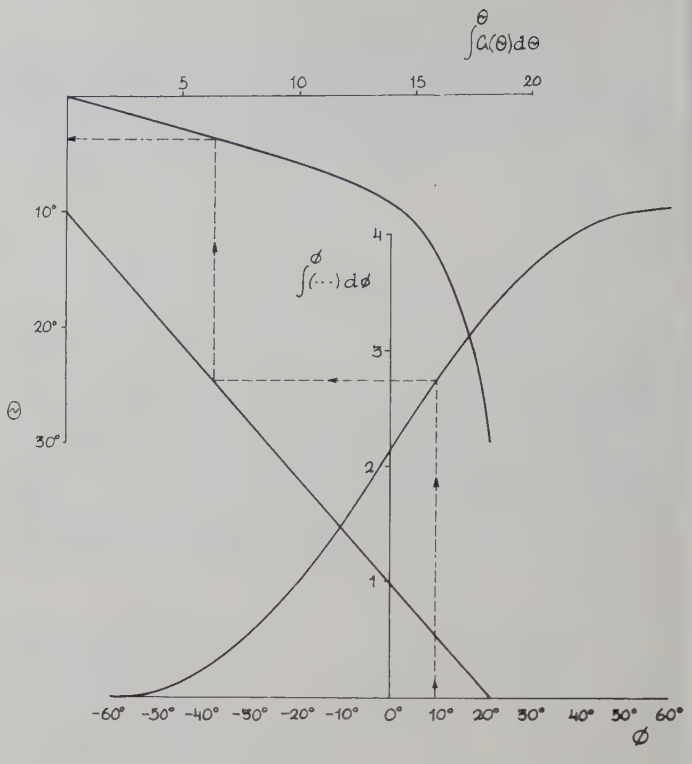

Fig. 4

(1) and (5). For purposes of control, a third approximation of $\theta(\phi)$ has been calculated from these functions, using the nomograph in Fig. 4. The beam corresponding to this reflector shape has then been computed from (2) for a few θ_0 values. The double integral appearing here has been evaluated numerically, integrating first with regard to α, applying the mean value formula of Gauss on the interval $(-\alpha_c, +\alpha_c)$ at two abscissa values $[\pm(1/\sqrt{3})\alpha_c]$, then with regard to ϕ, employing Simpson's rule on the interval $(-60°, +60°)$. The result is shown graphically in Fig. 5 which gives the shape of the central section of the beam; i.e., the gain function $G(\theta)$. The desired shape is also indicated in the figure to make a comparison possible.

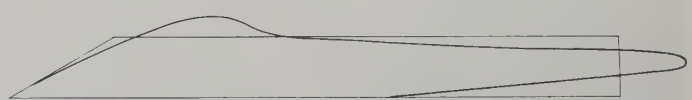

Fig. 5

The next step would be to repeat the calculation, only with the difference of substituting for the desired function $G(\theta)$ such a fictive G which tends to correct for the errors observed; thus, the value corresponding to $\theta = 20°$; e.g., should be smaller in an appropriate degree than the actual value. As this calculation would be quite similar to that carried out in the first step (except for being shorter, since there will not be any great changes in the reflector shape), our example has not been carried further.

Multipath Phase Errors in CW-FM Tracking Systems*

T. E. SOLLENBERGER†

Summary—**High-precision, cw, missile-tracking systems are subject to multipath errors due to ground reflections and reflections from neighboring objects. To reduce the effects of ground reflection, advantage may be taken of the characteristic of frequency modulation to discriminate against a weaker interfering signal. This paper discusses the magnitude of the phase error reduction to be obtained by use of frequency modulation.**

It is demonstrated that the phase error can be reduced to any desired value if sufficient band width is utilized in the frequency modulation signal and significant improvement over an amplitude modulation system can be obtained with a wide-band FM system.

Introduction

IN RECENT years a number of phase-comparison tracking or position location systems have been developed for guided missile testing. In such systems, ranging between the missile and a ground location is accomplished by measuring the phase difference between a reference cw transmission and a replica of the reference transmission which has traveled to the missile and back to the ground location.

Fig. 1 illustrates the principle of operation of a representative system.[1] A cw transmission consisting of a modulated carrier is transmitted to the missile where it is retransmitted, while maintaining coherence of the modulation. This retransmitted signal is received by the three ground receivers. The signal from the ground transmitter is transmitted by ground links to the three ground receivers and serves as a reference from which the phase delay in the modulation is measured. This phase delay is a measure of the sum of the ranges from ground to missile and back to ground. With the measure of three range sums and knowledge of the receiver positions relative to the ground transmitter, the position of the missile in space can be determined.

Because the measurement of phase is ambiguous for every half-wavelength displacement of the remote transponder on the missile, a series of sine wave modulations are placed on the carrier. These modulations usually have a decade relationship and provide coarse and fine range scales. The low-frequency modulation serves to resolve the ambiguity of the next higher frequency modulation.

All such systems employing a phase comparison technique for distance measurement are to some degree susceptible to errors caused by multipath reflections

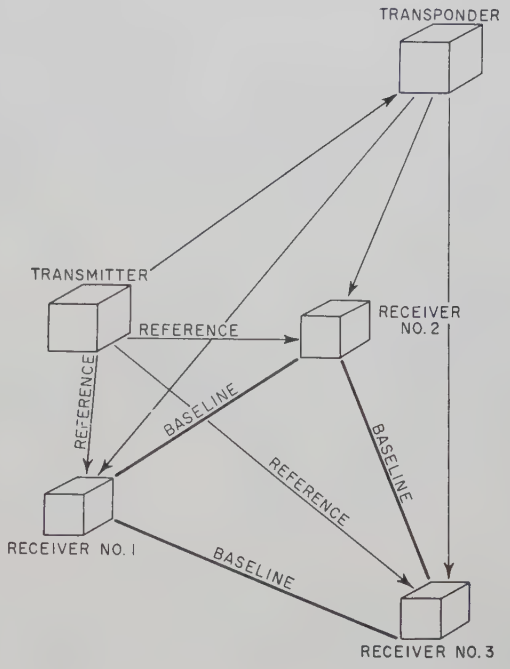

Fig. 1—Typical baseline trajectory-measuring system.

from neighboring objects in the field of the antennas and particularly from the ground plane of the antennas. While these multipath errors may be considered systematic, they are sometimes difficult to recognize and isolate since they are changing with time due to motion of the missile. Methods of reducing errors due to multipath consist of using highly directive antennas and, in the case of ground reflection, lowering the height of the antenna so that the path difference between the direct and reflected rays is reduced. The first method complicates the system since, with directive antennas, it is necessary to rotate the antenna to follow the missile. Reduction of antenna height often means loss of range coverage. Even if ground reflection could be minimized, there would remain problems caused by reflections from neighboring objects such as poles, trees, and buildings.

Fig. 2 illustrates the order of magnitude of phase errors that may be encountered with a double-side-band amplitude-modulation system.[2] These are computed curves for a reflection coefficient of 0.9 and a carrier-to-modulation frequency ratio of 8. The sharp phase-error peaks are due to interference at the carrier frequency. The envelope is a result of interference at the modulation frequency.

* Original manuscript received, October 21, 1954; revised manuscript received, April 14, 1955. This work was supported by Air Force Contract No. AF-08(169)-94.

† The Ralph M. Parsons Co., Electronics Division, Pasadena 2, Calif.

[1] R. W. Johnson, E. I. Bosch, and P. H. Reedy, "Precision Automatic Ranging System—PARAN," Rep. 955-RI, Phase I Tech. Rep., Part I, AF Armament Center, Eglin AFB, Fla. Contract AF 18(600)-202; November, 1953. (Unclassified.)

[2] R. A. Epstein and P. H. Reedy, "Ground-Reflection Phase Errors of CW-AM Tracking Systems," AF Tech. Rep. No. 7, AFMTC, Patrick AFB, Cocoa, Fla., Parsons Aerojet Co.; September, 1951. (Unclassified.)

The thought that frequency modulation may have some immunity to multipath error is supported by the fact that frequency modulation tends to suppress the weaker of two signals in the same channel. It has been previously demonstrated that multipath interference on an FM channel generates a multitude of harmonic distortion components. However, when the modulation consists of one or more discrete frequencies, as is the case in tracking systems, there is a possibility of filtering out most of the distortion components after detection.

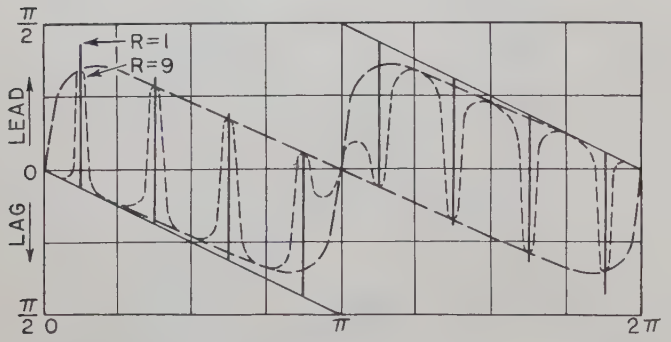

Fig. 2—Phase error in double-side-band AM for carrier-to-modulation frequency ratio of 8. Ordinate is modulation frequency phase error in radians. Abscissa is phase delay modulation of reflected signal in radians.

Calculation of Phase Error

The problem considered here is that of determining the magnitude of phase error on an FM transmission after filtering of distortion. Actual computation of phase error has been carried out for a simple system which has been idealized in several particulars:

1. To start with it is assumed that the transmission consists of a carrier which is frequency-modulated by a single sinusoidal wave form. Later, multitone modulation is also considered.

2. A single interfering multipath reflection, such as from an infinite ground plane of the antenna, is assumed. The case of more than one interfering multipath reflection is not analyzed because of the extremely intractable character of the mathematical manipulations. The case chosen for study is believed to represent a practical situation, since considerable care should normally be exercised to choose an antenna site having no nearby reflecting objects other than the ground plane.

3. Both the amplitude and phase shift of the coefficient of reflection are assumed to be independent of frequency over the bandwidth of the transmission.

4. The receiver contains a perfect limiter preceding the discriminator.

5. Perfect filtering of the modulations takes place after detection so that only the component of distortion at the modulation frequency is retained in the output.

This assumption of a perfect filter is made to facilitate the analysis. In any real system the post-detection bandwidth must be consistent with the information contained in the measurement of phase. This bandwidth is the same as the bandwidth of the doppler frequency shifts on the modulation due to motion of the remote transmitter or transponder and is usually quite small in comparison to the modulation frequency, so that no serious filtering problem arises.

6. Delay associated with the reflection is assumed to be constant and independent of time. This means that the remote transmitter or transponder is not moving. If the distant transmitter were moving, it would be necessary to consider the doppler effect and consequently the frequency difference between the doppler-shifted direct and reflected signals. In the case of reflection from the ground plane, the paths of the direct and reflected signals are nearly parallel when the distance from the transmitter to the receiving antenna is large compared to distance from ground plane to antenna. Both direct and reflected signals are then shifted in frequency almost equally so the frequency difference is quite small.

In the computation of signal distortion, it is entirely feasible to include transmitter motion; however, as discussed later, for the highest velocities encountered, the contributions to phase error by doppler effects are indeed quite small and, therefore, ignored.

The signal at the receiving antenna is the result of direct and reflected signals. Let the field strength of the direct signal at the receiving antenna have an amplitude E_0, and the field strength of the reflected signal at the receiving antenna an amplitude E_r. The amplitudes E_0 and E_r contain the effects of the antenna radiation pattern and the separate space attenuations of direct and reflected signals. The amplitude E_r contains the reflection coefficient of the ground plane as a factor. So far as this discussion is concerned, these effects can be expressed by writing the ratio of reflected-to-direct signals as $E_r/E_0 = R \exp(j\phi)$, where R and ϕ may be thought of respectively as the amplitude and phase shift of an effective reflection coefficient. As stated earlier, both R and ϕ are assumed independent of frequency. It is also assumed that R and ϕ are independent of time. Travel time of the direct signal will be designated by t_1 and time of the reflected signal by t_2. The multipath delay is then, $t_2 - t_1 = t_0$. The frequency-modulated signal for the direct path may be expressed as

$$e_0 = E_0 \exp\left[j \int_0^{t-t_1} \Omega dt\right] = E_0 \exp(jb_1), \qquad (1)$$

where the instantaneous frequency, Ω, is defined by

$$\Omega = \omega_c + \Delta\omega \cos \omega_1 t,$$

with $\Delta\omega = 2\pi x$ frequency deviation and $\omega_1 =$ modulation-angular frequency. For reflected signal, field strength is

$$e_r = E_0 R \exp j\left[\int_0^{t-t_2} \Omega dt + \phi\right] = E_0 R \exp(jb_2). \qquad (2)$$

It is assumed that e_0 and e_r may be combined at the antenna by phasor addition to produce a resultant sig-

nal at the receiver input. Fig. 3 shows the phasor addition to the direct and reflected signals.

The instantaneous phase b of the resultant is

$$b = b_1 + \arctan \frac{R \sin (b_2 - b_1)}{1 + R \cos (b_2 - b_1)}. \tag{3}$$

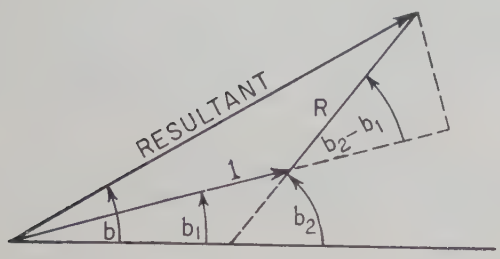

Fig. 3—Phasor addition of direct and reflected signals.

Assuming the use of a perfect limiter, the output of the discriminator is the instantaneous frequency given by

$$\frac{db}{dt} = \frac{db_1}{dt} + \frac{d}{dt} \arctan \frac{R \sin (b_2 - b_1)}{1 + R \cos (b_2 - b_1)} \tag{4}$$

or

$$\frac{db}{dt} = \omega_c + \Delta\omega \cos \omega_1(t - t_1) + \frac{d}{dt} \arctan \frac{R \sin (b_2 - b_1)}{1 + R \cos (b_2 - b_1)}. \tag{5}$$

The dc term ω_c need not be considered. The desired output is the second term, $\Delta\omega \cos \omega_1(t-t_1)$, of which the phase lag $\omega_1 t_1$ is to be measured by comparison with a reference signal. The last term represents nonlinear distortion. We wish, then, to find the magnitude of the component of distortion at frequency ω_1. All other components are assumed to be removed by a perfect filter. It is now convenient to make the following substitutions:

$$\theta_0 = \omega_c t_0 + \phi = \text{phase delay of the carrier}, \tag{6}$$

$$\beta = \Delta\omega/\omega_1 = \text{frequency deviation ratio}, \tag{7}$$

$$B = \omega_1(t - t_1 - t_0/2), \tag{8}$$

$$z = 2\beta \sin \omega_1 t_0/2. \tag{9}$$

With these substitutions, it can be shown that

$$b_2 - b_1 = \theta_0 - z \cos B. \tag{10}$$

Corrington[3] has developed the expansion of the derivative of the arctangent function of (5) which converges for $R<1$. It may seem unrealistic to restrict R to values less than unity since it is quite possible for R to be greater than unity as, for example, in the situation in which the direction of the transmitter coincides with an antenna pattern null. Unfortunately, this appears to be a particularly bad situation for which there is no mitigation other than to avoid it altogether. Because the FM receiver tends to suppress the weaker of two signals, the measured phase closely follows the phase of the reflected signal when $R>1$, obviously an undesirable circumstance. Therefore, in order to prevent the measured phase from oscillating grossly between the phase of the direct signal and the phase of the reflected signal, careful design of the antenna and siting must be used to prevent R from becoming greater than unity. Starting with (3) and using the identity $\tan \gamma/2 = \sin \gamma/(1+\cos \gamma)$, it is not difficult to show that when $R=1$, the phase error is $\omega_1 t_0/2$, or one-half the phase delay on the modulation frequency.

Following Corrington, the expansion of the arctangent in (5) with substitutions of (6), (7), (8), and (9) is

$$\arctan \frac{R \sin (\theta_0 - Z \cos B)}{1 + R \cos (\theta - Z \cos B)} = -\sum_{n=1}^{\infty} \frac{(-R)^n}{n} \sin n\theta_0 \cdot \left[J_0(nz) + 2 \sum_{m=1}^{\infty} (-1)^m J_{2m}(nz) \cos 2mB \right] + \sum_{n=0}^{\infty} \frac{(-R^n)}{n} \cos n\theta_0 \cdot \left[2 \sum_{m=0}^{\infty} (-1)^m J_{2m+1}(nz) \cos (2m+1)B \right], \tag{11}$$

where $J_{2m}(nz)$ and $J_{2m+1}(nz)$ are Bessel coefficients.

In the process of differentiating (11) to find the signal distortion components, the quantities θ_0, z, and B may be considered functions of time by virtue of motion of the transmitter which causes the quantity t_0 to vary with time. The phase B also contains time explicitly. Considering t_0 to be a function of time, the differentiation yields terms proportional to $\omega_c(dt_0/dt)$, $\beta\omega_1(dt_0/dt)$, $\omega_1(dt_0/dt)$, and ω_1. In the case of ground reflection on the assumption of parallel rays, the time delay t_0 is nearly $2h/c \sin \theta$ where h is the antenna height, c the velocity of propagation, and θ the elevation angle. If the elevation angle is changing at the excessive rate of one radian per second, dt_0/dt is less than $2h/c$. Suppose, for a possible tracking system, that

$$h = 1 \text{ meter}$$
$$\omega_c = 10^9$$
$$\omega_1 = 10^6$$
$$\beta = 10.$$

Then,

$$\omega_c dt_0/dt = (2/3)(10)$$
$$\beta\omega_1 dt_0/dt = (2/3)(10)(10^6/10^8) = (2/3)(10^{-1})$$
$$\omega_1 dt_0/dt = (2/3)(10^6/10^8) = (2/3)(10^{-2}),$$

so that all terms proportional to dt_0/dt are negligible in comparison to the term proportional to $\omega_1 (= 10^6)$. It

[3] M. S. Corrington, "Frequency modulation distortion caused by multipath transmission," Proc. IRE, vol. 33, pp. 878–891; December, 1945.

should be noted also that from (4) the dc term ω_c would properly appear as $\omega_c(1-dt_1/dt)$ as a result of the motion of the transponder. This term, having only very low-frequency components corresponding to the motion of the transponder, is filtered from the output. The result, after retaining only the term proportional to ω_1, is

$$\frac{d}{dt}\left[\arctan\frac{R\sin(\theta_0-2\sin B)}{1+R\cos(\theta-2\sin B)}\right] = \omega_1\sum_{m=1}^{\infty}S_m\sin 2mB+\omega_1\sum_{m=1}^{\infty}C_m\sin(2m+1)B, \quad (12)$$

where

$$S_m(\theta_0,R,z) = (-1)^m 4m\cdot\sum_{n=1}^{\infty}\frac{(-R)^n}{n}\sin(n\theta_0)J_{2m}(nz) \quad (13)$$

$$C_m(\theta_0,R,z) = (-1)^m 2(2m+1)\cdot\sum_{n=1}^{\infty}\frac{(-R)^n}{n}\cos(n\theta_0)J_{2m+1})(nz). \quad (14)$$

The term in the expansion at frequency ω_1 is given by $m=0$, so that the output of the discriminator and filter is

$$\begin{aligned}\text{output} &= \Delta\omega\cos\omega_1(t-t_1)+\omega_1C_0\sin B\\ &= \Delta\omega[\cos\omega_1(t-t_1)+C_0/\beta\sin\omega_1(t-t_1-t_0/2)]\\ &= \Delta\omega A\cos[\omega_1(t-t_1)-\alpha], \quad (15)\end{aligned}$$

where

$$\alpha = \arctan\frac{C_0/\beta\cos\omega_1t_0/2}{1-C_0/\beta\sin\omega_1t_0/2} \quad (16)$$

is the desired expression for the phase error due to multipath interference in this FM system.

The coefficient C_0 is given by

$$C_0 = -2\sum_{n=1}^{\infty}\frac{(-R)^n}{n}\cos n(x-\phi)\cdot J_1\left[2n\beta\sin\left(\frac{\omega_1}{\omega_c}\frac{x}{2}\right)\right], \quad (17)$$

where a new parameter has been introduced as $x=\omega_ct_0$, which is the difference in phase of the carrier for the two paths.

Interpretation

The following observations can be made about C_0. First, C_0 is periodic at both the carrier and modulation periods. Second, C_0 has the form of a rapid oscillation modulated by a slowly varying envelope represented by the Bessel function (the ratio ω_1/ω_c is normally quite small in a tracking system). Third, C_0 is bounded independently of β, so that the ratio C_0/β becomes smaller as β becomes larger. This follows from the fact that series for C_0 is absolutely convergent, and its sum less than

$$2\sum_{n=1}^{\infty}\frac{R^n}{n}$$

which is convergent for R less than unity and independent of β.

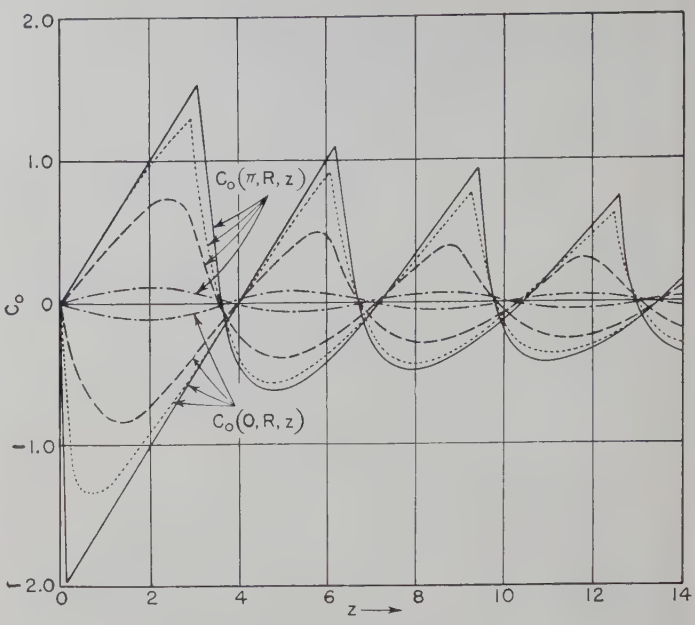

Fig. 4—The functions $C_0(\pi, R, z)$ and $C_0(0, R, z)$. O ——— $R=.1$, – – – – $R=.6$, ····· $R=.9$, –·–·– $R=.1$.

Fourth, when the ratio of modulation frequency to carrier frequency is small, and the argument of the Bessel function may therefore be considered as slowly varying and, for practical purposes, constant, the function C_0 has its maximum and minimum values at the points where $(x-\phi)$ is zero or a multiple of π. This can be seen by differentiating C_0 with respect to x, holding z constant in the Bessel function. It may thus be inferred that the envelope functions of C_0 are given very nearly by

$$C_0 = -2\sum_{n=1}^{\infty}(-1)^n(R^n/n)J_1(nz) \quad (18)$$

and

$$C_0 = -2\sum_{n=1}^{\infty}(R^n/n)J_1(nz). \quad (19)$$

Graphs of these functions are shown in Fig. 4 for several values of R. Using these envelope functions for C_0, the envelope curves of phase error as a function of t_0 can be computed and are shown in Fig. 5 (following page) for $R=0.9$ and several values of β.

A qualitative picture of the reduction of phase error as the deviation ratio is increased can be obtained by plotting the maximum values of the curves in Fig. 5 versus β. This plot is shown in Fig. 6, next page. The

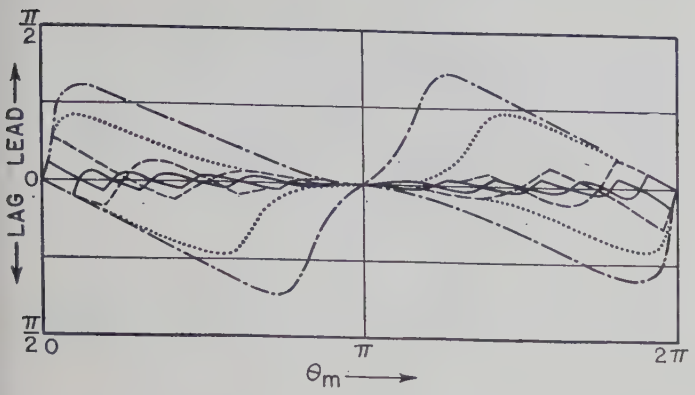

Fig. 5—Envelope of modulation-frequency phase error for FM as a function of phase delay, $\theta_m = \omega_m t_0$ of indirect signal modulation. ——— $\beta = 10$, · · · · · · $\beta = 2$, – – – – $\beta = 5$, –·–·–· $\beta = 1$. $R = 0.9$.

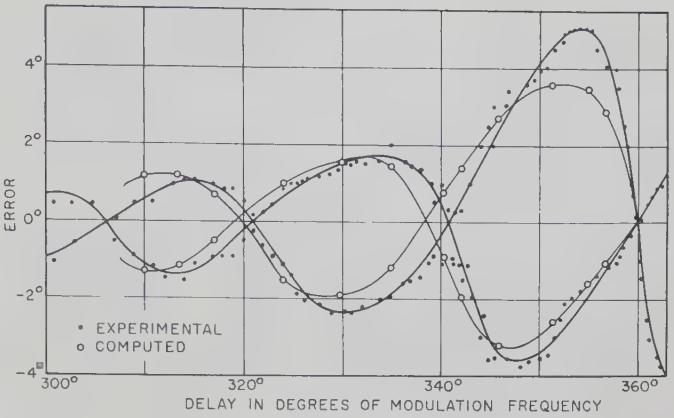

Fig. 7—Phase error vs multipath delay time $\beta = 10$, $R = 0.5$. Delay in degrees of modulation frequency.

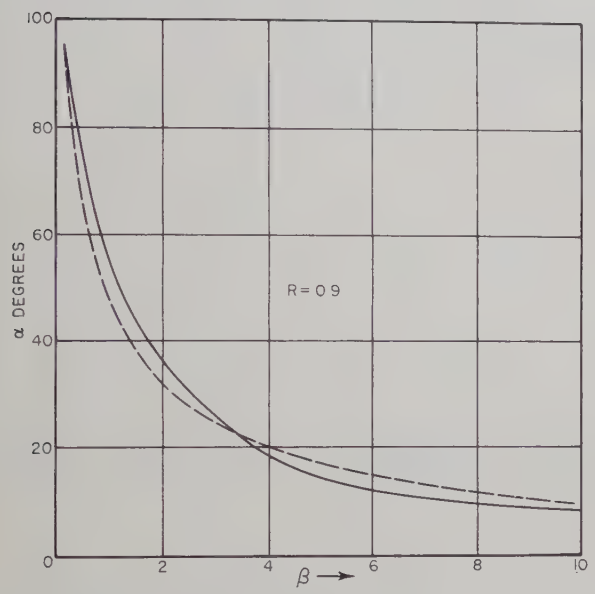

Fig. 6—Phase error at the first maximum of the phase error envelope as a function of β. – – – – lower envelope, ——— upper envelope.

curve is roughly of the form $1/\beta$, and that about 90 per cent of the error reduction takes place for β less than 10.

Multiple Modulation

When more than one modulation frequency is present, the phase-error formula on each frequency still has the same form as (16), but the parameter corresponding to C_0 is then defined by a different series which contains "cross-talk" terms between the modulation frequencies. The distortion term for the case of two modulation frequencies having the relationship $\omega_2 = 10\omega_1$ is derived in the Appendix. The result after the harmonics have been filtered out is

$$\text{distortion} = \omega_1 C_1 \sin B_1 + \omega_2 C_2 \sin B_2, \tag{20}$$

where

$$B_1 = \omega_1(t - t_1 - t_0/2) \tag{21}$$

$$B_2 = \omega_2(t - t_1 - t_0/2), \tag{22}$$

and C_1 and C_2 are defined by the two series (40) and (41) of the Appendix.

The receiver output is proportional to

$$\Delta\omega_1 \cos \omega_1(t - t_1) + \omega_1 C_1 \sin B_1 + \Delta\omega_2 \cos \omega_2(t - t_1) + \omega_2 C_2 \sin B_2. \tag{23}$$

Following the procedure used in the previous section for a single modulation frequency, the phase error for each modulation frequency can be written immediately. For the ω_1 component, the phase error is

$$\alpha_1 = \arctan \frac{C_1/\beta_1 \cos(\omega_1 t_0/2)}{1 - C_1/\beta_1 \sin(\omega_1 t_0/2)}, \tag{24}$$

and for the ω_2 component, the phase error is

$$\alpha_2 = \arctan \frac{C_2/\beta_2 \cos(\omega_2 t_0/2)}{1 - C_2/\beta_2 \sin(\omega_2 t_0/2)}. \tag{25}$$

It is shown in the Appendix that both C_1 and C_2 are bounded independently of β_1 and β_2. That the coefficients C_1 and C_2 are also periodic in the carrier and modulation periods can be seen readily by inserting (28) in (40) and (41). Thus, it is observed from the form of C_1 and C_2 that the behavior of the phase errors is similar to the single modulation-frequency case. Since envelope curves for C_1 and C_2 are not easily derived, computation of phase error envelopes was not undertaken. It is sufficient, however, to note that, since C_1 and C_2 are bounded, the phase errors α_1 and α_2 can be made as small as desired by sufficiently increasing the deviation ratios.

Experimental Data

Fig. 7 shows a plot of experimental data for a single modulation frequency obtained with a mercury delay-line multipath simulator. The experiment was performed by Mr. Leonard Hawn of The Ralph M. Parsons Company Laboratory. Curves in Fig. 7 are the phase

error envelopes; therefore, periodicity at the carrier frequency is not shown. Computed curves of the envelopes obtained from (18) and (19) are also represented in the figure by the large circles. Although the agreement between the experimental data and the computed data points is not precise, it is quite satisfying.

The multipath simulator consisted of a transmitter, receiver, phase meter modulation source, and two paths between the transmitter and receiver. A calibrated mercury delay line provided a means of delaying the signal in one path by a known amount. An attenuator was inserted in the other path to enable the ratio of signal strength of the two paths to be adjusted to a desired value.

The transmitter consisted of a Colpitts oscillator operating at a center frequency of 1.0 mc, a reactance tube, a limiter, and impedance matching amplifiers to the two paths. Double-shielding and low-pass filters in the power-supply leads and modulation-frequency connections were used to prevent leakage to the receiver.

The receiver consisted of a preamplifier, adder, *S*-meter, tandem limiter, wide-band discriminator, rf filter, audio amplifier, cathode follower, and output low-pass filter. The preamplifier compensated for insertion loss of the delay line and partially corrected for frequency and phase response of the delay line. The discriminator design was based on relations given by Granlund,[4] who has demonstrated that, in order for the FM receiver to be effective in suppressing the weaker of two signals, the discriminator bandwidth must exceed the deviation by the factor, $(1+R)/(1-R)$.

The modulation frequency used was 1000 cps. Effective filtering of distortion components was obtained with an *M*-derived 1-kc filter having rejection frequencies of 2.0 and 3.0 kc.

Conclusions

Expressions for the phase error introduced by a single multipath reflection have been derived for the cases of one and two modulation frequencies. Experimental data obtained with a multipath simulator show good agreement with computed values of phase errors. Study of the behavior of the phase errors for these rather idealized cases substantiates the prediction that the use of wide-band frequency modulation can result in a significant reduction of phase error due to multipath signals. The improvement over the use of amplitude modulation is illustrated by comparison of Figs. 2 and 5. For $\beta=1$, the phase error in the FM case has about the same order of magnitude as in the AM case. As β is increased to a value of 10, the phase error is decreased about one-fifth. For a cw tracking system having a highest modulation frequency of 1 megacycle, the frequency deviation corresponding to $\beta=10$ is 10 megacycles and requires a bandwidth at least this amount. Although a further increase in frequency-deviation ratio can result in further reduction of phase error, the necessary bandwidth may become excessive when considered from the point of view of broadband design and spectrum availability.

Appendix

Multiple Modulation Derivations

If there are N modulation components, the instantaneous angular frequency of the frequency-modulation signal is

$$\Omega = \omega_c + \sum_N \Delta_N\omega \cos \omega_N t, \tag{26}$$

where $\Delta_N\omega$ is the angular deviation associated with the Nth-frequency component. Following the same procedure used in developing the resultant phase for one modulation frequency,

$$b_2 - b_1 = \omega_c t_0 + \phi - \sum_N z_N \cos B_N, \tag{27}$$

where

$$Z_N = 2\beta_N \sin \frac{\omega_N t_0}{2} \tag{28}$$

and

$$B_N = \omega_N\left(t - t_1 - \frac{t_0}{2}\right). \tag{29}$$

Using the series expansion of the arctangent[5] and inserting (27) and (28),

$$\arctan \frac{R \sin (b_2 - b_1)}{1 + R \cos (b_2 - b_1)} = -\sum_{n=1}^{\infty} (-1)^n \frac{R^n}{n} \sin n\left(\theta_0 - \sum_N z_N \cos B_N\right). \tag{30}$$

The right side of (30) can be expanded further, using the appropriate trigonometric identities until the individual harmonics of B_N appear; however, the result is very complicated, and the task of sorting out the terms of a single frequency is extremely tedious if the number of modulation frequencies exceeds two. To illustrate the result, only two modulation frequencies are considered. Eq. (30) is first differentiated to find the instantaneous frequency. The result of the differentiation is

$$\frac{d}{dt}\left[\arctan \frac{R \sin (b_2 - b_1)}{1 + R \cos (b_2 - b_1)}\right] = \sum (-1)^n R^n \cos n(\theta_0 - z_1 \cos B_1 - z_2 \cos B_2) \cdot [z_1\omega_1 \sin B_1 + z_2\omega_2 \sin B_2]. \tag{31}$$

Using the identity for the cosine of the difference of two angles, (31) becomes

[4] J. Granlund, "Interference in Frequency Modulation Reception," MIT Res. Lab. of Electronics, Tech. Rep. No. 42, p. 8; January, 1949.

[5] E. T. Whittacker and G. N. Watson, "A Course of Modern Analysis," 4th ed., Cambridge University Press, Cambridge, England, p. 190; 1952.

$$\frac{d}{dt}\left[\arctan\frac{R\sin(b_2-b_1)}{1+R\cos(b_2-1)}\right]$$

$$= -\sum_{n=1}^{\infty}(-1)^n R^n[\cos n(\theta_0 - z_1\cos B_1)\cos(nz_2\cos B_2) + \sin n(\theta_0 - z_1\cos B_1)\sin(nz_2\cos B_2)]$$

$$\cdot[z_1\omega_1\sin B_1 + z_2\omega_2\sin B_2] = -\sum_{n=1}^{\infty}(-1)^n R^n$$

$$\cdot[z_1\omega_1\sin B_1\cos n(\theta_0 - z_1\cos B_1)\cos(nz_2\cos B_2 + z_1\omega_1\sin B_1\sin n(\theta_0 - z_1\cos B_1)\sin(nz_2\cos B_2) + z_2\omega_2\sin B_2\cos n(\theta_0 - z_2\cos B_2)\cos(nz_1\cos B_1) + z_2\omega_2\sin B_2\sin n(\theta_0 - z_2\cos B_2)\sin(nz_1\cos B_1)]. \quad (32)$$

Four identities are useful at this point:

$$\cos(nz\cos B) = J_0(nz) + 2\sum_{v=1}^{\infty}(-1)^v J_{2v}(nz)\cos 2vB \quad (33)$$

$$\sin(nz\cos B) = -2\sum_{v=0}^{\infty}(-1)^v J_{2v+1}(nz)\cos(2v+1)B \quad (34)$$

$$\sin B\cos n(\theta_0 - z\cos B) = 2\sum_{m=1}^{\infty}(-1)^m\frac{2m+1}{nz}J_{2m+1}(nz)\sin[(2m+1)B]\cos(n\theta_0) + 2\sum_{m=1}^{\infty}(-1)^m\frac{2m}{nz}J_{2m}(nz)\sin 2mB\sin(n\theta_0) \quad (35)$$

$$\sin B\sin n(\theta_0 - z\cos B) \equiv 2\sum_{m=0}^{\infty}(-1)^m\frac{2m+1}{nz}J_{2m+1}(nz)\sin[(2m+1)B]\sin(n\theta_0) - 2\sum_{m=1}^{\infty}(-1)^m\frac{2m}{nz}J_{2m}(nz)\sin 2mB\cos(n\theta_0). \quad (36)$$

The third identity, (35) is proved by Corrington,[3] and proof of (36) can be established by following his method as presented. Introduction of these four identities in (32) leads directly to

$$\frac{d}{dt}\left[\arctan\frac{R\sin(b_2-b_1)}{1+R\cos(b_2-b_1)}\right]$$

$$= -\sum_{n=1}^{\infty}(-R)^n z_1\omega_1\left\{2\sum_{m=0}^{\infty}(-1)^m\frac{2m+1}{nz_1}J_0(nz_2)J_{2m+1}(nz_1)\times\sin[(2m+1)B_1]\cos(n\theta_0) + 4\sum_{m=0}^{\infty}\sum_{v=1}^{\infty}(-1)^{(m+v)}\frac{2m+1}{nz_1}J_{2v}(nz_2)J_{2m+1}(nz_1)\times\cos 2vB_2\sin[(2m+1)B_1]\cos(n\theta_0) + 2\sum_{m=1}^{\infty}(-1)^m\frac{2m}{nz_1}J_0(nz_2)J_{2m}(nz_1)\sin 2mB_1\sin(n\theta_0) + 4\sum_{m=0}^{\infty}\sum_{v=1}^{\infty}(-1)^{(m+v)}\frac{2m}{nz_1}J_{2v}(nz_2)J_{2m}(nz_1)\times\cos 2vB_2\sin 2mB_1\sin(n\theta_0) - 4\sum_{m=0}^{\infty}\sum_{v=0}^{\infty}(-1)^{(m+v)}\frac{2m+1}{nz_1}J_{2v+1}(nz_2)J_{2m+1}(nz_1)\times\cos[(2v+1)B_2]\sin[(2m+1)B_1]\sin(n\theta_0) + 4\sum_{m=1}^{\infty}\sum_{v=0}^{\infty}(-1)^{(m+v)}\frac{2m+1}{nz_1}J_{2v+1}(nz_2)J_{2m}(nz_1)\times\cos[(2v+1)B_2]\sin 2mB_1\cos(n\theta_0)\right\} - \sum_{n=1}^{\infty}(-R)^n z_2\omega_2\left\{\begin{array}{l}\text{Same as above except with } z_1\\ \text{and } z_2 \text{ interchanged and } B_1\\ \text{and } B_2 \text{ interchanged}\end{array}\right\}. \quad (37)$$

Inspection of (37) reveals that there is an infinite number of terms at the fundamental frequencies, ω_1 and ω_c. These terms are produced when the beat frequencies, which may be designated by $k\omega_1 \pm q\omega_2$, equal either ω_1 or ω_2. The numbers k and q stand for the integers $2v+1$, $2v$, and $2m$, whenever applicable. No attempt will be made here to follow through the long process of sorting out the fundamental components, and only the first few terms for the condition that $\omega_2 = 10\omega_1$, will be written down to illustrate the result. Thus, the following is obtained from the distortion term, (37).

Fundamental Component of Distortion =

$$-2\omega_1\sum_{n=1}^{\infty}\frac{(-R)^n}{n}J_0(nz_2)J_1(nz_1)\cos(n\theta_0) - 2J_1(nz_2)J_{10}'(nz_1)\sin(n\theta_0) + 2J_2(nz_2)J_{20}'(nz_1)\cos(n\theta_0) + 2J_3(nz_2)J_{30}'(nz_1)\sin(n\theta_0) - 2J_4(nz_2)J_{40}'(nz_1)\cos(n\theta_0) - 2J_{50}(nz_1)J_5'(nz_2)\sin(n\theta_0) + \text{an infinite series of higher order terms}$$

$$-2\omega_2\sum_{n=1}^{\infty}\frac{(-R)^n}{n}J_0(nz_1)J_1(nz_2)\cos(n\theta_0) - 2J_{10}(nz_1)J_1'(nz_2)\sin(n\theta_0) + 2J_{20}(nz_1)J_2'(nz_2)\cos(n\theta_0) + 2J_{30}(nz_1)J_3'(nz_2)\sin(n\theta_0) - 2J_{40}(nz_1)J_4'(nz_2)\cos(n\theta_0) - 2J_{50}(nz_1)J_{50}'(nz_2)\sin(n\theta_0) + \text{an infinite series of higher order terms,} \quad (38)$$

where J' denotes the first derivative of the Bessel function with respect to nz_1 or nz_2 as required.

The fundamental component of distortion, therefore, has the form

$$\omega_1 C_1\sin B_1 + \omega_2 C_2\sin B_2. \quad (39)$$

With the introduction of $J_0'(z) = -J_1(z)$, the coefficients C_1 and C_2 can be written compactly as double summations thus:

$$C_1 = -2\sum_{n=1}^{\infty}\frac{(-R)^n}{n}\cdot\Big[-\sum_{k=0}^{\infty}(-1)^k e_k J_{2k}(nz_2)J'_{20k}(nz_1)\cos(n\theta_0) - 2\sum_{k=0}^{\infty}(-1)^k J_{2k+1}(nz_2)J'_{10(2k+1)}(nz_1)\sin(n\theta_0)\Big] \quad (40)$$

and

$$C_2 = -2\sum_{n=1}^{\infty}\frac{(-R)^n}{n}\cdot\Big[-\sum_{k=0}^{\infty}(-1)^k e_k J_{20k}(nz_1)J'_{2k}(nz_2)\cos(n\theta_0) - 2\sum_{k=0}^{\infty}(-1)^k J_{10(2k+1)}(nz_1)J'_{2k+1}(nz_2)\sin(n\theta_0)\Big], \quad (41)$$

where e_k is equal to two when k is not zero and e_k is equal to one when k is zero. It is desirable to show that both C_1 and C_2 are bounded independently of z_1 and z_2. Consider first the series for C_1. Each term of the absolute series for C_1 is less than the corresponding term of

$$\sum_{n=1}^{\infty}\frac{R^n}{n}\Big[\sum_{k=0}^{\infty}e_k\,|J_{2k}(nz_2)|\,|J'_{20k}(nz_1)| + 2\sum_{k=0}^{\infty}|J_{2k+1}(nz_2)|\,|J'_{10(2k+1)}(nz_1)|\Big]. \quad (42)$$

Since $J_{-n}=(-1)^n J_n$, this series can be written conveniently as

$$\sum_{n=1}^{\infty}\frac{R^n}{n}\sum_{k=-\infty}^{\infty}|J_k(nz_2)|\,|J'_{10k}(nz_1)|. \quad (43)$$

Using Cauchy's inequality[6]

$$\Big[\sum_{k=-\infty}^{\infty}|J_k(nz_2)|\,|J_{10k}'(nz_1)|\Big]^2 \leqq \sum_{k=-\infty}^{\infty}|J_k(nz_2)|^2\cdot\sum_{k=-\infty}^{\infty}|(J'_{10k}(nz_1)|^2 = \sum_{k=-\infty}^{\infty}[J_k(nz_2)]^2\cdot\sum_{k=-\infty}^{\infty}[J'_{10k}(nz_1)]^2. \quad (44)$$

Now[7]

$$\sum_{k=-\infty}^{\infty}J_k^2(z) = 1^* \quad (45)$$

and

$$\sum_{k=-\infty}^{\infty}[J'_{10k}(z)]^2 < \sum_{k=-\infty}^{\infty}[J_k'(z)]^2 = 1. \quad (46)$$

This last inequality is obvious since the sum of the series formed by using only every 10th term is less than the sum of the series over all values of k. It is not difficult to show that

$$\sum_{k=-\infty}^{\infty}J_k'(z)^2 = 1$$

by use of the recurrence formula

$$2J_k'(z) = J_{k-1}(z) - J_{k+1}(z),$$

and the relations

$$\sum_{k=-\infty}^{\infty}J_k(z)J_{k+2}(z) = 0 \text{ (Ref. 7), and } \sum_{k=-\infty}^{\infty}J_k^2(z) = 1.$$

Thus, it is clear that

$$\sum_{k=-\infty}^{\infty}|J_k(nz)_2|\,|J'_{10k}(nz_1)| < 1 \quad (47)$$

and, therefore,

$$|C_1| < 2\sum_{n=1}^{\infty}\frac{R^n}{n} \quad (48)$$

which is convergent for $R<1$.

An identical result applies also to C_2.

[6] G. H. Hardy, "A Course of Pure Mathematics," 9th Ed., The Macmillan Co., New York, N. Y., p. 490; 1946.

[7] G. N. Watson, "Theory of Bessel Functions," The University Press, Cambridge, Mass., p. 31; 1952.

Application of the Reaction Concept to Scattering Problems*

M. H. COHEN†

Summary—**Rumsey's "reaction concept" is applied to scattering problems by considering volume polarization currents which generate the scattered field. The scattering cross section is discussed. Approximation formulas are developed and illustrated by calculations for the echo width of a circular cylinder as a function of dielectric constant. Calculations are made for four plane-wave type trial fields in the cylinder; these are compared with the exact solution and with integral equation solutions through the second order. In this case the reaction method gives better results than the integral equation method, for the same amount of labor.**

Introduction

IN A RECENT paper Rumsey[1] defined an electromagnetic reaction and showed why it is to be regarded as a basic physical observable. His argument, briefly, is as follows. Any microwave measurement consists of measuring, not the electric field (force on a unit charge) at a point; but rather, the signal at the terminals of an antenna. Thus two antennas, for transmission and reception, are inherent in a measurement. (In the radar case these may degenerate into the same antenna.) The antennas may be considered as sources of two distinct fields, and the reaction between these sources is the observable quantity.

Let a and b represent the two sources,[2] consisting of distributions of electric currents $\boldsymbol{J}(a)$ and $\boldsymbol{J}(b)$, and magnetic currents $\boldsymbol{K}(a)$ and $\boldsymbol{K}(b)$. The fields radiated by these sources are $\boldsymbol{E}(a)$, $\boldsymbol{H}(a)$, and $\boldsymbol{E}(b)$, $\boldsymbol{H}(b)$. Then the reaction between the sources is denoted by the symbol $\langle a, b\rangle$ and it is defined by

$$\langle a, b\rangle = \iiint_{V_b} [\boldsymbol{E}(a)\cdot\boldsymbol{J}(b) - \boldsymbol{H}(a)\cdot\boldsymbol{K}(b)]\,dv. \qquad (1)$$

The integration volume contains $\boldsymbol{J}(b)$ and $\boldsymbol{K}(b)$. Under suitable conditions the reciprocity theorem holds:

$$\langle a, b\rangle = \langle b, a\rangle. \qquad (2)$$

It can be shown that, as a phasor, the reaction $\langle a, b\rangle$ represents half the time-dependent portion of the instantaneous power expended by source a on source b. If source b is a unit current source, then $\langle a, b\rangle$ represents the open circuit voltage received at b when a alone is radiating. Further significance of the reaction is discussed by Rumsey.[1]

An important application of the reaction concept consists in finding suitable approximation formulas in problems where the exact solution is not known (or is useless because of computational difficulties). If one has an assumed current which generates an approximation to the desired field then parameters in the assumption can be "fixed" by requiring, as far as possible, that it have the same reactions with other sources that the correct current does. This generally gives the customary stationary, or variational, formulas.

In this paper the application of the reaction concept to scattering problems will be discussed by using volume currents which generate the scattered field. This follows directly from Rumsey's work,[1] although he confined himself to surface currents. Approximation formulas will be developed and illustrated by calculations for an infinite circular cylinder. The value in these calculations is that the exact solution for this problem is known, and thus some measure of the worth of the different approximations and current assumptions is obtained. It is hoped that this will furnish insight into suitable approximation procedures to be used for other problems.

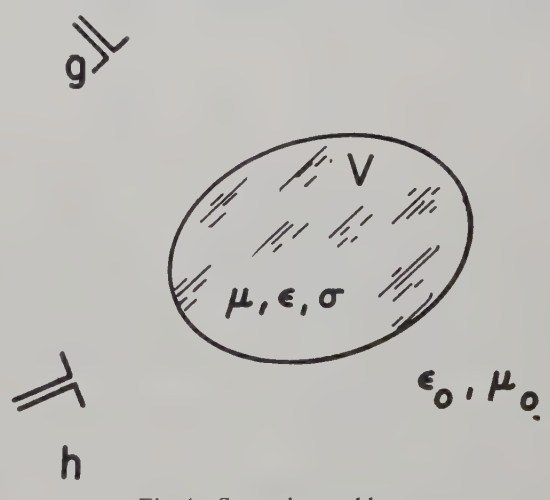

Fig. 1—Scattering problem.

Scattering by a Finite Isotropic Body

Let a source of monochromatic electromagnetic energy at g (Fig. 1) illuminate a finite isotropic scattering body with the bulk constants μ, ϵ, and σ. Let $\boldsymbol{E}$, $\boldsymbol{E}^i$, and $\boldsymbol{E}^s$ represent the total, incident, and scattered electric fields, respectively. The incident field is that obtained in the absence of the scatterer, and the scattered field is defined by

$$\boldsymbol{E}^s = \boldsymbol{E} - \boldsymbol{E}^i. \qquad (3)$$

* Original manuscript received, October 12, 1954. Portions of this paper were presented at the Washington Meeting of the American Physical Society, April 29, 30, and May 1, 1954; and at the joint URSI-IRE-AGU Meeting in Washington on May 3–6, 1954. It is partially contained in Report 475-14, Antenna Laboratory, Ohio State University, June 30, 1954.

† School of Electrical Engineering, Cornell University, Ithaca, N. Y.; formerly Antenna Laboratory, Ohio State University, Columbus, Ohio.

[1] V. H. Rumsey, "Reaction concept in electromagnetic theory," *Phys. Rev.*, vol. 94, pp. 1483–1491; June, 1954. The notation used in this paper follows that used by Rumsey.

[2] It is implied that both sources oscillate at the same frequency. The time convention $\exp(-i\omega t)$ is used.

It can be shown by a direct manipulation of Maxwell's equations that the source of the scattered field may be taken to be the volume polarization and conduction currents radiating in free space. In general there are both electric and magnetic currents, given by

$$J = -i\omega(\epsilon - \epsilon_0)E + \sigma E, \tag{4}$$

and

$$K = -i\omega(\mu - \mu_0)H. \tag{5}$$

For convenience, let

$$\kappa = -i\omega(\epsilon - \epsilon_0) + \sigma \tag{6}$$

and

$$\gamma = -i\omega(\mu - \mu_0), \tag{7}$$

so that

$$J = \kappa E \tag{8}$$

and

$$K = \sigma H. \tag{9}$$

This representation for the source of the scattered field is different from the surface currents used by Rumsey.[1] Some consequences of the difference are discussed.

We wish to investigate the field at h (Fig. 1) and so we put an antenna there, according to the above discussion. Let $J(h)$, $K(h)$ represent a distribution of sources which generates the field obtained when the antenna at h is radiating. Also, let c and d represent the sources of the scattered fields obtained when the sources g and h, respectively, are radiating. That is,

$$\begin{aligned} J(c) &= \kappa E(g) \qquad J(d) = \kappa E(h) \\ K(c) &= \gamma H(g) \qquad K(d) = \gamma H(h). \end{aligned} \tag{10}$$

Then the measure of the total field at h, due to the source g, is the reaction $\langle g, 1, h\rangle$, where the internal numeral 1 means that the sources radiate in the presence of the scatterer. Similarly, the measure of the scattered field at h is the reaction $\langle c, 2, h\rangle$, where the internal numeral 2 means that the sources radiate in the absence of the scatterer. The formula for $\langle c, 2, h\rangle$ is

$$\langle c, 2, h\rangle = \iiint_V [E(c)\cdot J(h) - H(c)\cdot K(h)]dv, \tag{11}$$

where the integration volume contains $J(h)$ and $K(h)$. By the reciprocity theorem,

$$\begin{aligned} \langle c, 2, h\rangle &= \langle h, 2, c\rangle \\ &= \iiint_V [E^i(h)\cdot J(c) - H^i(h)\cdot K(c)]dv \\ &= \iiint_V [\kappa E^i(h)\cdot E(g) - \gamma H^i(h)\cdot H(g)]dv, \end{aligned} \tag{12}$$

where the integration is over the volume of the scatterer.

The reaction $\langle c, 2, h\rangle$ is proportional to the scattered signal received at h. When $E(g)$ and $H(g)$ are known (or can be approximated), the reaction can be computed by (12), since $E^i(h)$ and $H^i(h)$ are characteristic of the receiving antenna.

Consider $\langle h, 2, c\rangle$. It may be regarded as the signal induced at the "terminals" of the source c, by the incident field due to h. From (3) then, we have

$$\langle h, 2, c\rangle + \langle d, 2, c\rangle = \langle h, 1, c\rangle, \tag{13}$$

and similarly,

$$\langle g, 2, d\rangle + \langle c, 2, d\rangle = \langle g, 1, d\rangle \tag{14}$$

$$\langle h, 2, g\rangle + \langle d, 2, g\rangle = \langle h, 1, g\rangle \tag{15}$$

$$\langle g, 2, h\rangle + \langle c, 2, h\rangle = \langle g, 1, h\rangle. \tag{16}$$

From elementary combinations of these formulas (and the reciprocity theorem), the following reciprocal relations are derived:

$$\langle c, 2, h\rangle = \langle d, 2, g\rangle \tag{17}$$

$$\langle c, 1, h\rangle = \langle d, 1, g\rangle. \tag{18}$$

Scattering Cross Section

The scattering cross section is ordinarily defined as the cross section of an isotropic scatterer which gives the same scattered intensity as the target does, for an incident plane wave. For a complete description, it is considered to be a two-by-two matrix with components $A_{\rho k}$, where

$$A_{\rho k} = \lim_{R_h\to\infty} 4\pi R_h^2 \frac{|E_\rho^s|^2}{|E_k^i|^2}. \tag{19}$$

The subscript k refers to orthogonal linear components in the plane normal to the incident propagation vector; the subscript ρ refers to orthogonal linear components in the plane normal to the scattered propagation vector (along the line from the target to point h, Fig. 1). R_h is the distance from the target to the point h.

Let the source of the incident wave be the source g, a distant dipole with components I_k. The polarization currents c_k are those induced by E_k. Let the source h be a distant dipole with components I_ρ. Then the reaction $\langle c_\rho, 2, h_k\rangle$, proportional to the ρ-component of scattered field for a k-polarized incident wave, is given by

$$\langle c_k, 2, h_\rho\rangle = \iiint_V E^s(I_k)\cdot J(h_\rho)dv = E_\rho^s(I_k)I_\rho. \tag{20}$$

As $R_h\to\infty$, $|E_\rho^i|\to\omega\mu_0 I_\rho/(4\pi R_h)$, at the target. Hence

$$A_{\rho k} = \frac{(\omega\mu_0)^2|\langle c_k, 2, h_\rho\rangle|^2}{4\pi|E_k^i|^2|E_\rho^i|^2}. \tag{21}$$

By (17), the scattering cross section satisfies the reciprocal relation:

$$A_{\rho k} = A_{k\rho}. \tag{22}$$

Approximations

The "reaction method" of approximation consists of assuming functions which approximate the polarization

currents c and d and forcing them, as far as possible, to have the same reaction relations that the correct sources do. The adjustable parameters contained in the assumption are thereupon fixed.

The reaction relations satisfied by c and d are contained in (13) through (16). They may be generalized to

$$\langle g, 2, x\rangle + \langle c, 2, x\rangle = \langle g, 1, x\rangle \tag{23}$$

and

$$\langle h, 2, y\rangle + \langle d, 2, y\rangle = \langle h, 1, y\rangle, \tag{24}$$

where x and y are any sources. The approximations to the sources c and d, denoted by sources a and b, are to be substituted into these equations. Adjustable constants in the approximations are fixed when sources are substituted for x and y.

Now consider what the possible substitutions for x and y are. There are six sources in the problem: a, b, c, d, g, and h. Two of these, c and d, are unknown; and g and h cannot be used because $\langle g, 1, g\rangle$, $\langle g, 1, h\rangle$, and $\langle h, 1, h\rangle$ cannot be calculated. Therefore we must use a or b. But they can be subdivided into component electric and magnetic currents; reactions can be computed separately for them, so there are four possibilities for x and for y. We now fix the choices for x and y by noting that there are two approximations to the reaction $\langle c, 2, h\rangle$, obtained by substituting a and b for c and d in the two sides of (17). These are the same when we substitute $\boldsymbol{J}(b)$ and $\boldsymbol{K}(b)$ for x in (23), and $\boldsymbol{J}(a)$ and $\boldsymbol{K}(a)$ for y in (24), so this is the choice.

When these substitutions are made into (23) and (24), we have

$$\begin{aligned}
&\langle g, 2, \boldsymbol{J}(b)\rangle + \langle a, 2, \boldsymbol{J}(b)\rangle = \langle g, 1, \boldsymbol{J}(b)\rangle\\
&\langle g, 2, \boldsymbol{K}(b)\rangle + \langle a, 2, \boldsymbol{K}(b)\rangle = \langle g, 1, \boldsymbol{K}(b)\rangle\\
&\langle h, 2, \boldsymbol{J}(a)\rangle + \langle b, 2, \boldsymbol{J}(a)\rangle = \langle h, 1, \boldsymbol{J}(a)\rangle\\
&\langle h, 2, \boldsymbol{K}(a)\rangle + \langle b, 2, \boldsymbol{K}(a)\rangle = \langle h, 1, \boldsymbol{K}(a)\rangle
\end{aligned} \tag{25}$$

The total fields of sources g and h are needed in the right-hand sides of these equations. They are unknown, but by the requirements implicit in (8) and (9), they must be proportional to the assumed currents. That is,

$$\boldsymbol{E}(g) = \kappa^{-1}\boldsymbol{J}(c) \approx \kappa^{-1}\boldsymbol{J}(a), \tag{26}$$

and so on. In integral form, then, (25) become

$$\langle g, 2, \boldsymbol{J}(b)\rangle + \langle a, 2, \boldsymbol{J}(b)\rangle = \iiint_V \kappa^{-1}\boldsymbol{J}(a)\cdot\boldsymbol{J}(b)\,dv \tag{27}$$

$$\langle g, 2, \boldsymbol{K}(b)\rangle + \langle a, 2, \boldsymbol{K}(b)\rangle = \iiint_V \gamma^{-1}\boldsymbol{K}(a)\cdot\boldsymbol{K}(b)\,dv \tag{28}$$

$$\langle h, 2, \boldsymbol{J}(a)\rangle + \langle b, 2, \boldsymbol{J}(a)\rangle = \iiint_V \kappa^{-1}\boldsymbol{J}(b)\cdot\boldsymbol{J}(a)\,dv \tag{29}$$

$$\langle h, 2, \boldsymbol{K}(a)\rangle + \langle b, 2, \boldsymbol{K}(a)\rangle = \iiint_V \gamma^{-1}\boldsymbol{K}(b)\cdot\boldsymbol{K}(a)\,dv. \tag{30}$$

Eqs. (27) through (30) are four simultaneous equations, from which four parameters, one each in $\boldsymbol{J}(a)$, $\boldsymbol{K}(a)$, $\boldsymbol{J}(b)$, and $\boldsymbol{K}(b)$, can be determined. By adding (27) to (28), and (29) to (30), it is shown that

$$\langle a, 2, h\rangle = \langle b, 2, g\rangle. \tag{31}$$

Thus the two approximations to $\langle c, 2, h\rangle$ are equal.

In many cases the *distributions* of currents may be reasonably guessed at, whereas their *levels* (phases and amplitudes) with respect to the incident fields cannot. To consider this case,[3] let

$$\begin{aligned}
\boldsymbol{J}(a) &= \alpha\kappa\boldsymbol{\Phi} \qquad \boldsymbol{J}(b) = \delta\kappa\boldsymbol{\Psi}\\
\boldsymbol{K}(a) &= \beta\sigma\boldsymbol{\Theta} \qquad \boldsymbol{K}(b) = \eta\gamma\boldsymbol{\Upsilon},
\end{aligned} \tag{32}$$

where $\boldsymbol{\Phi}$, $\boldsymbol{\Theta}$, $\boldsymbol{\Psi}$, and $\boldsymbol{\Upsilon}$ are functional approximations to the total fields, and α, β, δ, and η are adjustable constants. Then, from (27) and (28),

$$\iiint_V \boldsymbol{E}^i(g)\cdot\kappa\boldsymbol{\Psi}\,dv + \iiint_V \boldsymbol{E}^i(a)\cdot\kappa\boldsymbol{\Psi}\,dv = \iiint_V \alpha\boldsymbol{\Phi}\cdot\kappa\boldsymbol{\Psi}\,dv \tag{33}$$

$$\iiint_V \boldsymbol{H}^i(g)\cdot\gamma\boldsymbol{\Upsilon}\,dv + \iiint_V \boldsymbol{H}^i(a)\cdot\gamma\boldsymbol{\Upsilon}\,dv = \iiint_V \beta\boldsymbol{\Theta}\cdot\gamma\boldsymbol{\Upsilon}\,dv. \tag{34}$$

Here $\boldsymbol{E}^i(a)$ and $\boldsymbol{H}^i(a)$ must be computed from the assumed currents $\boldsymbol{J}(a)$ and $\boldsymbol{K}(a)$ which radiate in free space.

Eqs. (33) and (34) are a simultaneous pair for the determination of α and β. A similar pair for the determination of δ and η are obtained from (29) and (30). The desired reaction is now given by

$$\begin{aligned}
&\langle c, 2, h\rangle \approx \langle a, 2, h\rangle = \langle h, 2, a\rangle,\\
&\langle h, 2, a\rangle = \iiint_V [\alpha\boldsymbol{E}^i(h)\cdot\kappa\boldsymbol{\Phi} - \beta\boldsymbol{H}^i(h)\cdot\gamma\boldsymbol{\Theta}]\,dv.
\end{aligned} \tag{35}$$

The above approximation procedure differs from Rumsey's "testing" technique[1] by the necessity for making the integral approximations to the right-hand sides of (25). This comes about because we have used polarization currents rather than the equivalent surface currents used by Rumsey. In general there is no clear choice for the more useful representation, in terms of surface or volume currents. However, in the important special case when $\mu=\mu_0$ the magnetic polarization currents are zero, and we would have to make only one guess, for the distribution of electric field, to use the volume currents. On the other hand, to use free-space calculations, both electric and magnetic surface currents are needed (except for perfect conductors), and to use them we would have to guess at the distributions of tangential electric *and* magnetic fields.

Higher Order Approximations

Higher order approximations may be made by assuming that the currents a and b are combinations of ele-

[3] This is the only case considered by Rumsey.

mentary distributions. The phase and amplitude of each elementary source are to be found from (25). Let

$$J(a) = \sum_{i=1}^{n} \alpha_i \kappa \Phi_i \qquad J(b) = \sum_{k=1}^{n} \delta_k \kappa \Psi_k$$

$$K(a) = \sum_{j=1}^{n} \beta_j \gamma \Theta_j \qquad K(b) = \sum_{l=1}^{n} \eta_l \gamma \Upsilon_l. \tag{36}$$

Then, from (25),

$$\langle g, 2, \Psi_k \rangle + \langle a, 2, \Psi_k \rangle = \langle g, 1, \Psi_k \rangle, \quad k = 1, \cdots n, \tag{37}$$

and

$$\langle g, 2, \Upsilon_l \rangle + \langle a, 2, \Upsilon_l \rangle = \langle g, 1, \Upsilon_l \rangle, \quad l = 1, \cdots n. \tag{38}$$

Eqs. (37) and (38) are a set of $2n$ equations for the $2n$ unknown coefficients α_i and β_j, and the coefficients δ_k and η_l are similarly found.

Stationary Properties

It can be shown that the reaction when computed by (35) is stationary with respect to first-order variations of the total fields about their true values. Eqs. (37) and (38) result when the fields are expanded as in (36) and the Ritz procedure is used to find the coefficients.

Since the work of Levine and Schwinger,[4] the variational method has been widely used in problems of scattering by conductors,[5,6] and in a few problems concerning dielectrics.[1,7] In standard derivation, motivation of the manipulation of the equations to arrive at stationary form is obscure, whereas the reaction concept leads one naturally and pictorially to it. It enables one to proceed when there is a variety of stationary forms.[1] It also is more general, since discussion is not limited to far fields; characteristics of transmitting and receiving antennas are explicitly introduced.

Application to a Circular Cylinder

As an example of the use of the above theory, we shall compute the back-scattering cross section of a lossless circular cylinder. The cylinder has a diameter equal to one free-space wavelength ($a/\lambda_0 = \frac{1}{2}$); it has unit relative permeability and its relative dielectric constant is ϵ_r. Its axis is the z-axis, as in Fig. 2. A plane wave, $e^{ik_0 x}$, is incident from the left and has its electric vector parallel to the z-axis. By symmetry the total field also has only a z-component. There is therefore only one component in

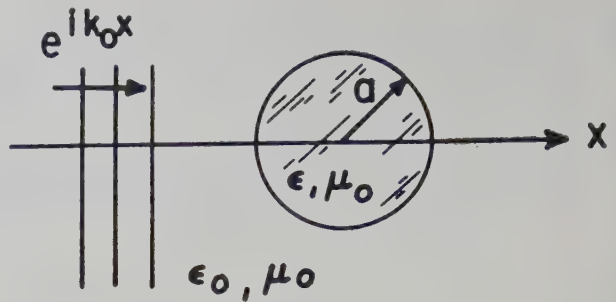

Fig. 2—Plane wave incident on a circular dielectric cylinder.

the scattering cross-section matrix. Since this is a two dimensional problem, we redefine the cross section as

$$\sigma_2 = \lim_{r \to \infty} 2\pi r \frac{|E^s|^2}{|E^i|^2}. \tag{39}$$

The source notation of the field vectors is omitted because we are interested in the back-scattered cross section (echo width) and the same antenna is used for transmission and reception. In a manner analogous to that used for the three dimensional cross section it is shown that the echo width is related to the reaction by

$$\sigma_2 = (4k_0)^{-1}(\omega\mu_0)^2 |E^i|^{-4} |\langle c, 2, g \rangle|^2. \tag{40}$$

In this formula source g is a distant line source, the source of the plane wave, and k_0 is the propagation constant of free space. The reactions are surface integrals containing only one term (since the magnetic currents are zero); e.g.,

$$\langle c, 2, g \rangle = \langle g, 2, c \rangle = \iint_A E^i(g) J(c) ds$$

$$= \iint_A E^i(g) \kappa E(g) ds, \tag{41}$$

where the integration is over the cross section of the cylinder. When the total field in the scattering body is unknown the reaction in (41) may be approximated by using the methods outlined above in connection with (26) through (29), and with (35).

The circular cylinder was chosen for illustrative calculations because the exact solution is known,[8] and approximations are not trivial. Calculations were made for four different assumptions for the field in the cylinder. These are compared with the exact solution, and also with integral equation solutions through the second order.[9,10] It is hoped these comparisons will yield information of use in other problems which are not soluble.

[4] H. Levine and J. Schwinger, "On the theory of diffraction by an aperture in an infinite plane screen," *Phys. Rev.*, vol. 74, pp. 958–974; October, 1948; vol. 75, pp. 1423–1432, May, 1949.

[5] C. H. Papas, "Diffraction by a Cylindrical Obstacle," *Jour. Appl. Phys.*, vol. 21, pp. 318–325; April, 1950.

[6] R. G. Kouyoumjian, "The Calculation of the Echo Areas of Perfectly Conducting Objects by the Variational Method," Ohio State University Res. Found. Antenna Lab. Rep. 444–13; November, 1953.

[7] J. R. Lurye, "Electromagnetic Scattering Matrices of Stratified Anisotropic Media," Rep. EM-11, N. Y. Univ. Math. Res. Group; May, 1951.

[8] P. Frank and R. Von Mises, "Die Differentialgleichungen und Integralgleichungen der Mechanik und Physik, Mary S. Rosenberg, N. Y., p. 869; 1943.

[9] W. Sternberg, "Anwendung der integralgleichungen auf beugung und eigensschwingungen in der electromagnetischen lichtheorie," *Z. Phys.*, vol. 64, pp. 638–649; September, 1930.

[10] D. R. Rhodes, "An Investigation of Pulsed Radar Systems for Model Measurements," Rep. 475-6, Antenna Lab., The Ohio State University Res. Found., chap. 5; December, 1953.

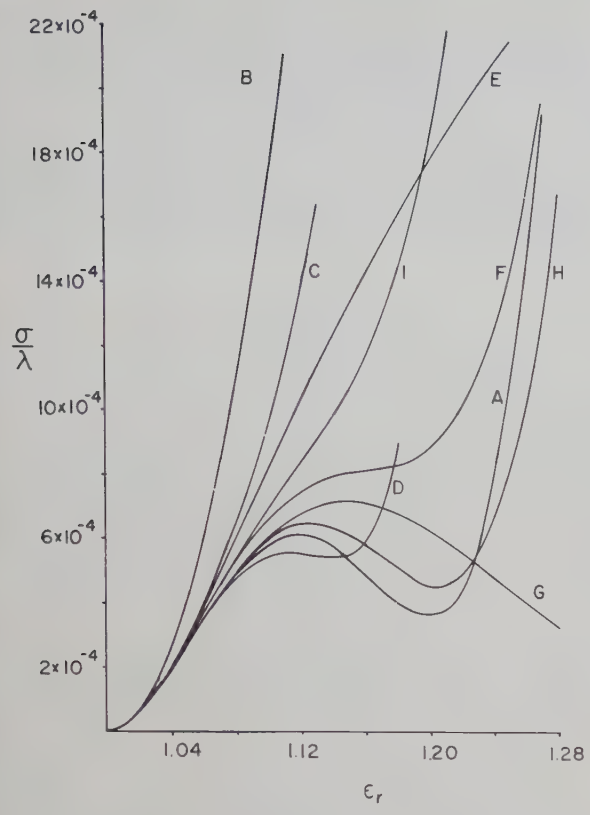

Fig. 3—Echo width of circular cylinder vs relative dielectric constant for various approximations. The approximations are defined in Table I.

The calculation procedure is discussed in the Appendix, and the results are represented in Fig. 3. The various curves are identified in Table I.

TABLE I

IDENTIFICATION OF CURVES IN FIGURE 3

Curve	Method	Assumption for the total field in cylinder[a]	Labor of calculations
A[b]	Boundary value (exact solution)	—	First-order
B[b]	Zero-order integral equation	e^{ik_0x}	zero
C[b]	First-order integral equation	e^{ik_0x}	first
D[b]	Second-order integral equation	e^{ik_0x}	second
E	Reaction	$\alpha_1 e^{ik_0x}$	first
F	Reaction	$\alpha_2 e^{ik_0x}+\alpha_3 e^{-ik_0x}$	first
G	Reaction	$\alpha_4 e^{ik_1x}$	second
H	Reaction	$\alpha_5 e^{ik_1x}+\alpha_6 e^{-ik_1x}$	second
I	Second-order integral equation	$\alpha_1 e^{ik_0x}$	second

[a] k_0, k_1 are the propagation constants of free space and of the medium in the cylinder, respectively.
[b] Curves A, B, C, and D are reproduced from Rhodes work.[10]

The labor of calculation increases with the order. For example, curves C and E are merely different combinations of the same integrals. Curve F requires the evaluation of a second double surface integral, so it requires about twice the labor of E. Curves G and H have k_1 in the exponential rather than k_0, and the integrals have to be separately evaluated for every value of dielectric constant; this is not the case for the other curves. The calculation for curve D includes the evaluation of a triple surface integral. In many cases, particularly where some of the integration has to be done numerically, this would be much more laborious than the evaluation of the double surface integrals for curves G and H.

Curve I was obtained by using $\alpha_1 e^{ik_0x}$ (the reaction determined field for curve E) instead of e^{ik_0x} as a starting function in the integral equation iteration (See Appendix). The zero-order solution so obtained is just the reaction solution (curve E), and it turns out that the first-order solution is identical to the zero-order solution. The second order solution is represented by curve I in Fig. 3. This calculation consists of a recombination of the integrals used for curve D. It is seen that it gives a result which is farther from the exact curve (A) than curve D is (over the range of dielectric constants considered). This is somewhat surprising, since I springs from an apparently better initial field assumption. Moreover, the zero- and first-order approximations (E) are closer to the exact curve than the corresponding approximations with the simpler field assumption (B and C). However, neither B, C, nor E is at all representative of the exact curve, except in the region of very low dielectric constant. Conclusions based on these curves in other regions may be very misleading.

Curve H is the only one which has the correct shape over the resonance region. The field assumption for this curve is presumably better than any of the others and it was expected that it would give a better approximation than the other reaction calculations. It is also superior to curves D and I, although this could not have been guessed beforehand.

The field assumption for curve H is

$$E \approx \alpha_5 e^{ik_1x} + \alpha_6 e^{-ik_1x}. \tag{42}$$

The first term corresponds to a forward-traveling plane wave; and the second, to a reflection from the "back face." It is similar to the field inside an infinite slab; the difference of course is in the coefficients, which are determined by the reaction equations. They were separately evaluated and their amplitudes are represented in Figs. 4(a) and (b), where they are compared with the amplitudes of the internal waves in a slab one free-space wavelength thick, excited by a plane wave as shown. It is seen that the respective amplitudes in Fig. 4 are nearly equal. Hence the amplitudes of the reaction-determined fields are very close to what might be guessed at from elementary considerations. The phases, however, are important, and cannot be arrived at by such means.

Observe that there is a substantial difference between curves G and H, even though $|\alpha_5| \gg |\alpha_6|$. The explanation of this is that we have computed a *back-scattering* parameter, and the reaction between the forward wave (e^{ik_1x}) and the source is much less than the reaction between the backward wave (e^{-ik_1x}) and the source.

Note that the coefficients in the field assumptions are functions of the aspect; for a given field assumption they have to be separately evaluated for every aspect of interest. Hence a complete calculation of scattered field would be very laborious. However, it would undoubtedly yield interesting and valuable information.

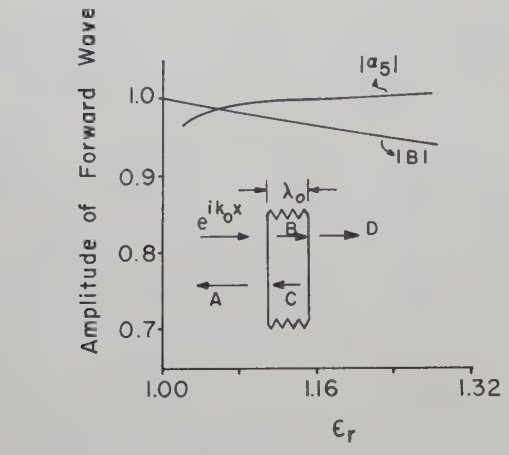

(a)

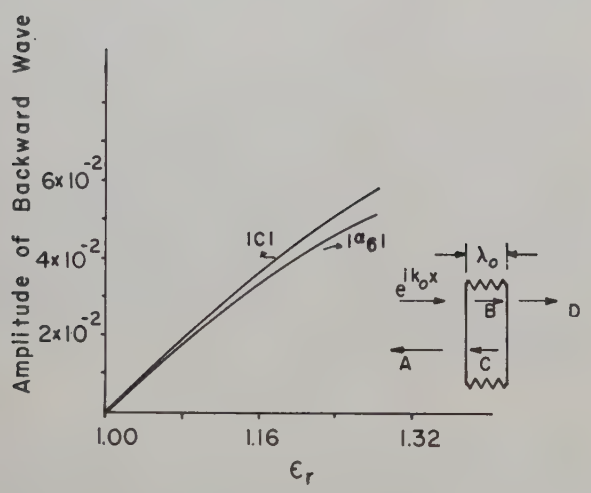

(b)

Fig. 4—(a) Comparison of forward waves in cylinder and slab. (b) Comparison of backward waves in cylinder and slab.

It is sometimes stated that variational calculations are insensitive to the choice of trial function and therefore they give good results. Such remarks are misleading and must be interpreted with great caution. The curves in Fig. 3, for example, show a very marked dependence on the trial function; only one of four functions gives a good result over the resonance region. If the current assumption is the exact current, all calculation methods give the correct answer, and the simplest method is chosen. If the approximation to the current is poor then no method can be relied upon to give a reasonable result, for a reasonable amount of labor. In principle, of course, one can get a formal convergent sequence for the echo width, either by successive iterations of the integral equation, or by using the Ritz method with a complete set of trial functions. As a practical matter, though, calculations beyond the first few orders are generally prohibitive of labor. Higher order variational calculations are more feasible than successive iterations because the latter require increasing orders of integration; the former require only double volume or surface integrals, which have a chance of being done numerically.

Conclusions

The following conclusions have been established only for the particular field assumptions used here and for bodies whose dimensions are on the order of a wavelength, with relative dielectric constant less than 1.3. However, it is felt that they are valid over greater ranges and possibly for other field assumptions. They at least can serve as a guide in other problems, particularly those where the exact solution is not known. Much more experience would be required to firmly establish them over wide conditions.

1. The reaction (variational) solution is superior to the iterated integral equation solution, for the same amount of labor.
2. The approximation $E \approx \alpha_5 e^{ik_1 x} + \alpha_6 e^{-ik_1 x}$ is "close" to the correct field in the cylinder, in the sense that it gives an echo width which is close to the correct value over the first resonance region. This does not necessarily imply that it would give good angle-scattering results.
3. It is very important to have a good current assumption.

Appendix

The formula for echo width (40) may be written as

$$\sigma_2 = u^2 \tag{43}$$

where

$$u = c \iint_A E^i E ds \tag{44}$$

and

$$c = \tfrac{1}{2} k_0^{3/2} \left| E^i \right|^{-2} (\epsilon_r - 1). \tag{45}$$

The different methods essentially consist in finding functions for E to be used in the integral in (44).

Integral Equation Method

From (3) one may write

$$E = E^i + \iint_A \Gamma_{2\kappa} E ds, \tag{46}$$

which is an integral equation of the second kind for E, the unknown z-component of total electric field. Γ_2 is a two-dimensional free-space Green's Function;[11] it is

[11] P. M. Morse and H. Feshbach, "Methods of Theoretical Physics," McGraw-Hill Book Company, Inc., New York, p. 811; 1953.

the electric field produced by a unit line source, all of whose elements are in phase and in the z-direction:

$$\Gamma_2 = -\tfrac{1}{4}\omega\mu_0 H_0^{(1)}(k_0 r), \tag{47}$$

where H_0 (1) is the zero-order Hankel function representing an outgoing wave.

The iterated solution to (46) is found by making a zero-order guess for E, called E_0. Then

$$E_1 = E^i + \int\int_A \Gamma_{2\kappa} E_0 ds$$

$$E_2 = E^i + \int\int_A \Gamma_{2\kappa} E_1 ds, \tag{48}$$

and so on. Different order approximations to σ_2 are found when approximations to E are substituted into (44). Born approximations[12] result from initial choice

$$E_0 = e^{ik_0 x}. \tag{49}$$

This is the choice discussed by Sternberg,[9] and by Rhodes;[10] the first three approximations to the echo width of the circular cylinder using this initial choice were computed by Rhodes. His results are reproduced in Fig. 3 as curves B, C, and D.

A second series of calculations was made using

$$E_0 = \alpha_1 e^{ik_0 x}, \tag{50}$$

where α_1 was determined by the reaction calculation. With this assumption, it can be shown that $u_0 = u_1$, so that the zero- and first-order approximations are the same, and are equal to the reaction, or variational, solution. Second order solution is in Fig. 3 as curve I.

Reaction (Variational) Method

The four assumptions for the total field used in the reaction calculations are given in Table I. The most involved calculation, for curve H, will now be discussed. Let

$$\phi_1 = e^{ik_1 x} \tag{51}$$

and

$$\phi_2 = e^{-ik_1 x}$$

so that the field assumption is

$$E \approx \alpha_5\phi_1 + \alpha_6\phi_2. \tag{52}$$

[12] L. I. Schiff, "Quantum Mechanics," McGraw-Hill Book Company, Inc., New York, N. Y., p. 159; 1949.

We now use (37) to find coefficients. Simultaneous solution of (37) and (38) is not necessary because magnetic currents are zero. From (37), then, we have

$$\int\int_A \phi_\mu e^{ik_0 x} ds + \int\int_A \int\int_{A'} \phi_\mu \Gamma_{2\kappa}(\alpha_5\phi_1' + \alpha_6\phi_2') ds' ds$$

$$= \int\int_A \phi_\mu(\alpha_5\phi_1 + \alpha_6\phi_2) ds, \quad \mu = 1, 2. \tag{53}$$

Let

$$N_\mu = \int\int_A \phi_\mu e^{ik_0 x} ds, \qquad \mu = 1, 2, \tag{54}$$

and

$$D_{\mu\nu} = D_{\nu\mu} = \int\int_A \phi_\mu\phi_\nu ds$$

$$- \int\int^A \int\int_{A'} \phi_\mu \Gamma_{2\kappa} \phi_\nu' ds' ds, \quad \begin{matrix}\mu = 1, 2 \\ \nu = 1, 2.\end{matrix} \tag{55}$$

Then the coefficients are given by

$$\alpha_5 = (N_1 D_{22} - N_2 D_{12})/(D_{11}D_{22} - D_{12}^2), \tag{56}$$

and

$$\alpha_6 = (N_2 D_{11} - N_1 D_{21})/(D_{11}D_{22} - D_{12}^2).$$

Thus

$$u = c(\alpha_5 N_1 + \alpha_6 N_2), \tag{57}$$

where α_5 and α_6 are given in (56).

The evaluation of the double surface integrals is rather tedious. The procedure used was to express the Hankel function and the exponentials as sums of Bessel functions. Their products are integrable and the resulting series converge fairly rapidly.[10]

ACKNOWLEDGMENT

It is a pleasure to acknowledge the helpful suggestions and criticisms given by Professor V. H. Rumsey. Acknowledgements are also due Dr. D. R. Rhodes for the use of his results on the integral equation solution, and Dr. T. H. Crowley for many helpful discussions.

This work was done at the Antenna Laboratory of the Ohio State University, under a contract between the Wright Air Development Center and The Ohio State University Research Foundation.

Radiation Patterns of Slotted-Elliptic Cylinder Antennas*

J. Y. WONG†

Summary—An expression is developed for the radiation pattern of an array of thin axial slots arbitrarily disposed around the circumference of an elliptic cylinder. Calculated azimuthal patterns are presented for single slots on elliptic cylinders of vanishing thickness. The results can be applied to approximate the pattern of practical cylinders having very thin cross sections.

Introduction

THE PATTERN of slots located on cylinders of elliptic cross section has become an increasingly important problem in the design of slotted-cylinder antennas. A paper directly applicable to this problem was given by Sinclair[1] who calculated the far fields of small dipole and loop antennas in the vicinity of elliptic cylinders. In a previous paper[2] an expression for the radiation field of axial and transverse slots in cylinders of elliptic cross section was derived by a method based on the application of diffraction theory and the principle of reciprocity. Attention was devoted primarily to the radiative properties of transverse slot radiators. A different approach to the elliptic cylinder problem was extended by Wait.[3] The tangential component of the electric field in the slot was assumed to be a prescribed function and the integrals in the formal solution were evaluated by the saddle point method for the far-zone fields.

The material contained in this paper is an extension of the work previously carried out for the axial slot problem. A general expression is developed for the pattern of an array of axial slots located arbitrarily around an elliptic cylinder. Calculated azimuthal patterns are presented for single slots and for special cases of dual slots located on elliptic cylinders of vanishing thickness. The results can be applied to approximate the pattern of slots in very thin cylinders such as wing and tail surfaces of aircraft.

Pattern of an Array of Axial Slots

The expression[4] for the radiation field in the horizontal plane, $\theta = 90°$, produced by an axial slot located at $(u_0, v, 0)$ on the surface of an elliptic cylinder defined by u_0 is given by:

$$E_\phi = A \sum_{m=0}^{\infty} B_m{}^e Se_m(c, \cos v) Se_m(c, \cos \phi) + B_m{}^0 So_m(c, \cos v) So_m(c, \cos \phi), \quad (1)$$

where

$$B_m{}^e = \frac{i^m}{N_m{}^e He_m{}^{(2)\prime}(c, \cosh u_0)}, \quad \text{and}$$

$$B_m{}^0 = \frac{i^m}{N_m{}^0 Ho_m{}^{(2)\prime}(c, \cosh u_0)}.$$

The primes on the functions $He_m{}^{(2)\prime}(c, \cosh u_0)$ and $Ho_m{}^{(2)\prime}(c, \cosh u_0)$ denote derivatives with respect to the variable u. In (1), the parameter A depends upon the type of excitation, but is independent of the azimuthal angle ϕ. Consequently, it is not necessary to know A in order to compute relative radiation pattern.

Consider the case of an array of "p" axial slots located arbitrarily on the periphery of the cylinder. The geometry of such an array is illustrated in Fig. 1. The

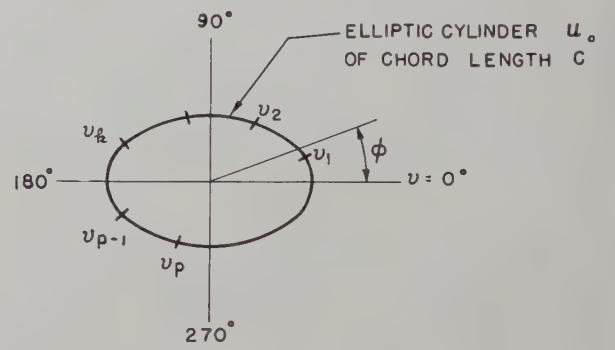

Fig. 1—Array of p axial slots.

total field of the array can be computed by adding the fields contributed by each slot, taking into account the magnitude and phase of the exciting voltages of the various slots. Examination of the derivation reveals that the reference for the phase of each slot is at the axis of the elliptic cylinder, consequently it is not necessary to introduce any phase factor involving the distance of each slot from the axis. The expression for the total field of an array of p slots becomes

$$E_\phi = \sum_{k=1}^{p} \sum_{m=0}^{\infty} A_k e^{i\psi_k} \{ B_m{}^e Se_m(c, \cos v_k) Se_m(c, \cos \phi) + B_m{}^0 So_m(c, \cos v_k) So_m(c, \cos \phi) \}, \quad (2)$$

where A_k is the ratio of the voltage fed to the kth slot and the voltage fed to slot number 1; *i.e.*, $A_k = V_k / V_1$. ψ_k is the phase angle by which voltage V_k leads the reference voltage V_1.

* Original manuscript received by the PGAP, February 9, 1955; revised manuscript received, June 22, 1955.

† Radio and Electrical Engineering Division, National Research Council, Ottawa, Canada.

[1] G. Sinclair, "The pattern of antennas located near cylinders of elliptical cross section," PROC. IRE, vol. 39, pp. 660–668; June, 1951.

[2] J. Y. Wong, "Radiation conductance of axial and transverse slots in cylinders of elliptical cross section," PROC. IRE, vol. 41, pp. 1172–1177; September, 1953.

[3] J. R. Wait, "Fields Produced by an Arbitrary Slot on an Elliptic Cylinder," Defence Res. Telecommun. Establishment, Ottawa, Canada; Rep. 19-0-8; June, 1954.

[4] Wong, *op. cit.*, p. 1173, Eq. (7).

For the particular case of two slots located on the major or minor axis of the cylinder, (2) can be simplified considerably because advantage can be taken of the special properties of the angular Mathieu functions, $Se_m(c, \cos v)$ and $So_m(c, \cos v)$. From the equivalent series expansions of the angular functions, it is readily apparent that the following relationships exist:

$$Se_m(c, \cos v) = Se_m(c, \cos(-v)),$$
$$So_m(c, \cos v) = -So_m(c, \cos(-v)).$$

Values of the functions for particular angles of v are listed in Table I.

TABLE I

SPECIAL VALUES FOR THE EVEN AND ODD ANGULAR FUNCTIONS

v	m	$Se_m(c, \cos v)$	$So_m(c, \cos v)$
0	even	1	0
	odd	1	0
90°	even	$Se_m(c, \cos 90°)$	0
	odd	0	$So_m(c, \cos 90°)$
180°	even	1	0
	odd	−1	0

Expressions for the azimuthal pattern for some special cases of single slots and dual slots are shown below:

1. Single slot at $v = 0°$ (major axis),

$$E_\phi = \sum_{m=0}^{\infty} B_m{}^e Se_m(c, \cos\phi). \quad (3)$$

2. Single slot at $v = 90°$ (minor axis),

$$E_\phi = \sum_{m=0}^{\infty} B_{2m}{}^e Se_{2m}(c, \cos 90°) Se_{2m}(c, \cos\phi) + B_{2m+1}^{0} So_{2m+1}(c, \cos 90°) So_{2m+1}(c, \cos\phi). \quad (4)$$

3. Two slots at $v_1 = 0°$ and $v_2 = 180°$,

   a. Equal in-phase voltages ($V_1 = V_2$, $x = 0°$),

$$E_\phi = \sum_{m=0}^{\infty} B_{2m}{}^e Se_{2m}(c, \cos\phi). \quad (5)$$

   b. Equal out-of-phase voltages ($V_1 = V_2$, $\psi = 180°$),

$$E_\phi = \sum_{m=0}^{\infty} B_{2m+1}{}^e Se_{2m+1}(c, \cos\phi). \quad (6)$$

4. Two slots at $v_1 = 90°$ and $v_2 = 270°$,

   a. Equal in-phase voltages,

$$E_\phi = \sum_{m=0}^{\infty} B_{2m}{}^e Se_{2m}(c, \cos 90°) Se_{2m}(c, \cos\phi). \quad (7)$$

   b. Equal out-of-phase voltages,

$$E_\phi = \sum_{m=0}^{\infty} B_{2m+1}{}^0 So_{2m+1}(c, \cos 90°) So_{2m+1}(c, \cos\phi). \quad (8)$$

Discussion of Results

In order to facilitate the computations of the radiation patterns, only the case of a degenerate elliptic cylinder ($u_0 \to 0$) is considered. Simplification of the expressions result, because advantage can be taken of the joining factors associated with the various radial and angular Mathieu functions.[5] Patterns are computed for three different sizes of cylinder. The values chosen for the major axis or chord dimension C, are 0.55λ, 1.0λ, and 1.42λ. The results of these calculations are shown in Figs. 2, 3, 4, 5, and 6. The elliptic cylinder is oriented so that the major axis coincides with the ordinate axis of the coordinate system (0°–180° line).

Eq. (3) represents the pattern of a single axial slot located on the major axis of the cylinder. It is not difficult to demonstrate that (3) yields a circular pattern for this particular case. Simplification of (3) results by making use of the following identities:[6]

$$He_m{}^{(2)\prime}(c, 1) = -\frac{i}{Je_m(c, 1)}, \quad (9)$$

and

$$e^{ic(\cosh u \cos v \cos\phi)} = (8\pi)^{1/2} \sum_{m=0}^{\infty} \frac{i^m}{N_m{}^e} Je_m(c, \cosh u) \cdot Se_m(c, \cos v) Se_m(c, \cos\phi). \quad (10)$$

Substituting (9) and (10) in (3) and simplifying, yields the following expression:

$$E_\phi = \frac{1}{(8\pi)^{1/2}} e^{i(ka \cos\phi - (\pi/2))}. \quad (11)$$

Eq. (11) can be recognized as the equation of a circle, hence the pattern of a slot located on the edge of a degenerate elliptic cylinder is circular. Furthermore the pattern is independent of the size of cylinder. This result could have been inferred from physical reasoning. A magnetic dipole located parallel to the edge of a degenerate elliptic cylinder does not excite any current on the cylinder, consequently the presence of the cylinder can in no way affect the radiation.

Patterns of a single axial slot located on the minor axis are illustrated in Fig. 2. Most of the energy is concentrated in a single lobe in the forward region, although some diffraction of the energy occurs around the edges of the cylinder.

The effect of offsetting the slot from the center line for the case $C/\lambda = 0.55$ is shown clearly in Fig. 3. The parameter x refers to the amount of offset and a refers to one-half the chord dimension. As the slot approaches the edge of the cylinder, two effects occur. The pattern

[5] "Tables Relating to Mathieu Functions," prepared by the Computation Lab. of the Nat. Appl. Math. Lab. Nat. Bur. Standards, Columbia University Press, New York, N. Y.; 1951.

[6] P. M. Morse and H. Feshbach, "Methods of Theoretical Physics," Part II, McGraw-Hill Book Co., Inc., New York, N. Y., pp. 1572–1573; 1953.

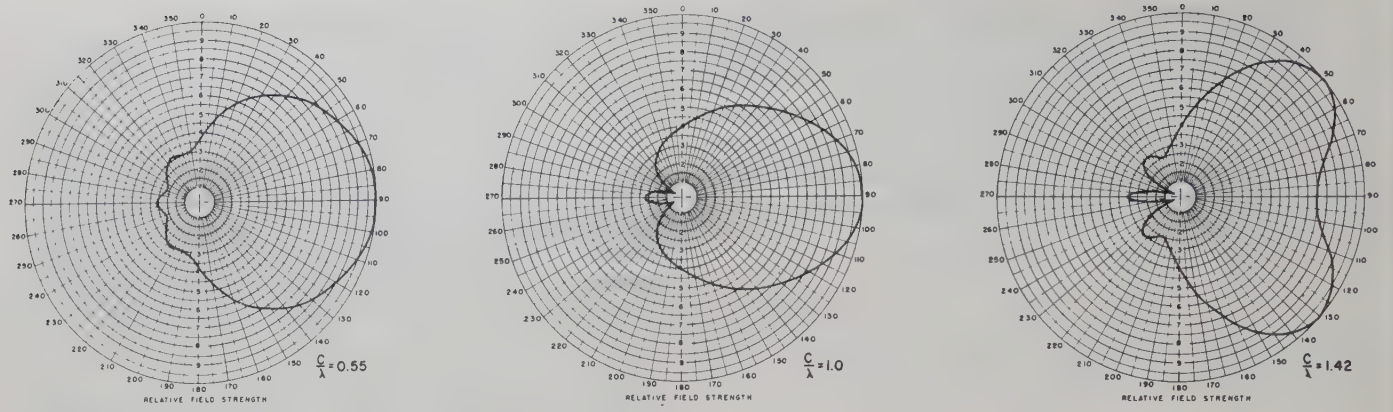

Fig. 2—Pattern of single slot located at $v=90°$.

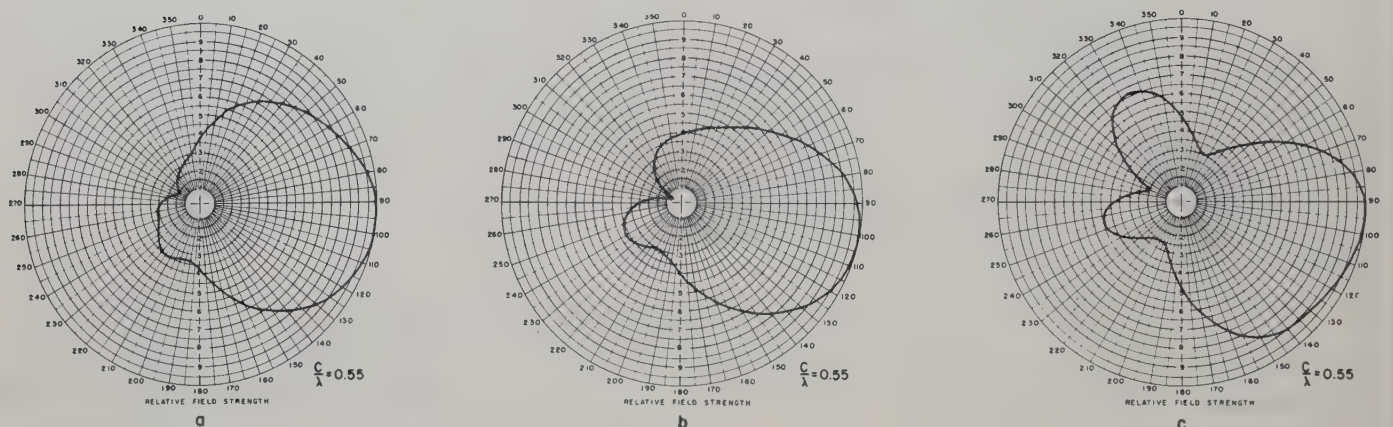

Fig. 3—Effect of offsetting slot from the minor axis. (a) Pattern of slot located at $v=80°$ ($x=0.17a$). (b) Pattern of slot located at $v=60°$ ($x=0.50a$). (c) Pattern of slot located at $v=40°$ ($x=0.76a$).

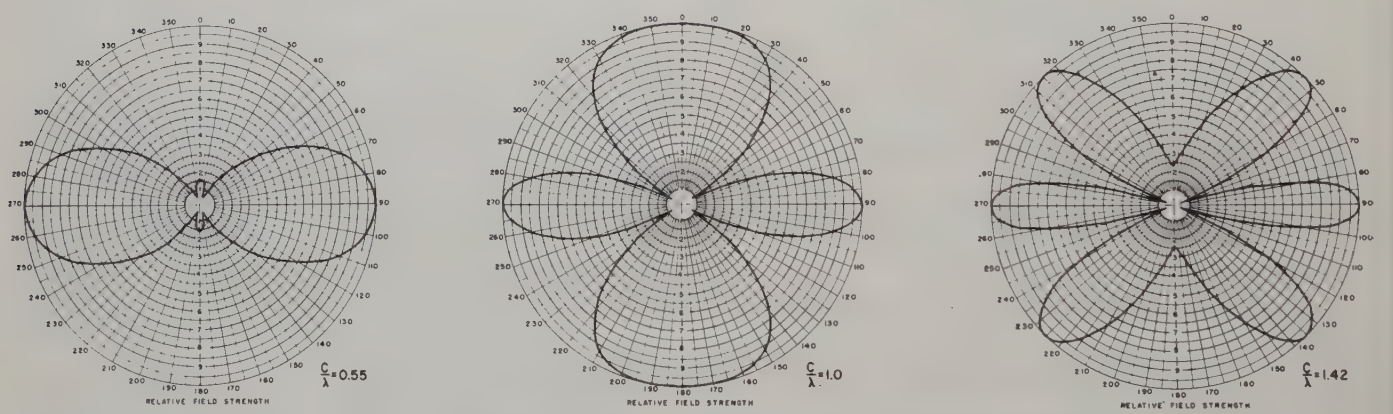

Fig. 4—Pattern of two slots located at $v_1=0°$ and $v_2=180°$ fed with equal in-phase voltages.

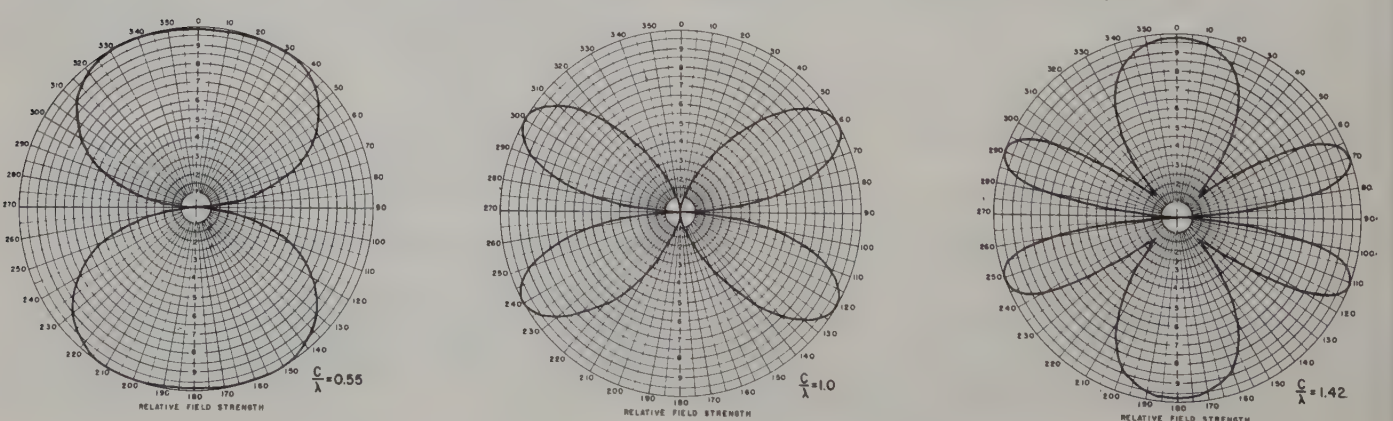

Fig. 5—Pattern of two slots located at $v_1=0°$ and $v^2=180°$ fed with equal out-of-phase voltages.

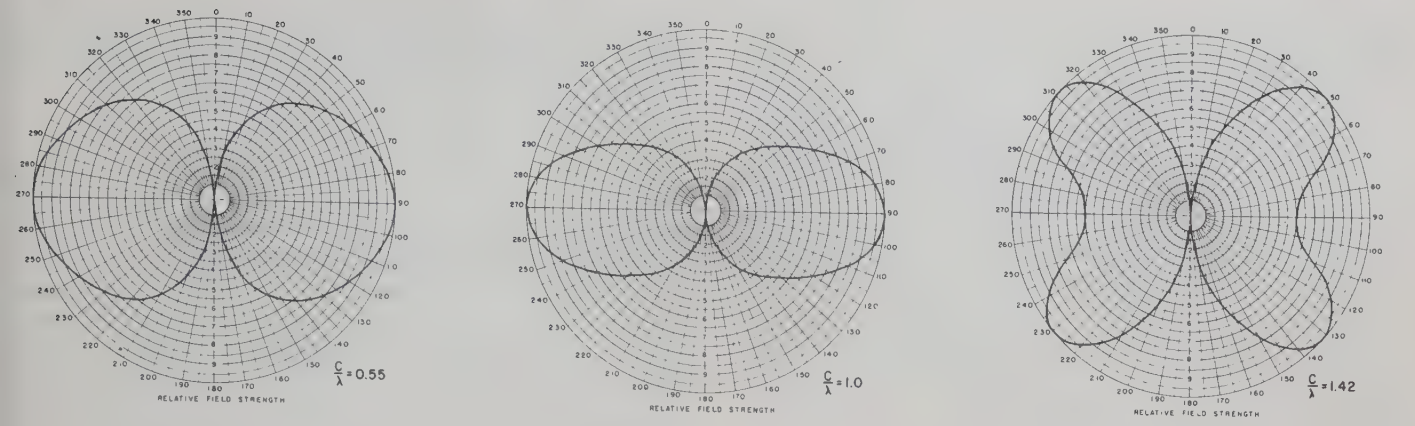

Fig. 6—Pattern of two slots located at $v_1 = 90°$ and $v_2 = 270°$ fed with equal out-of-phase voltages.

of the main lobe becomes more asymmetrical with the maximum directed away from the side containing the slot, and secondly more radiation is encountered in the shadow region.

The patterns of some special cases of dual slots are shown in Figs. 4, 5, and 6. Applying the results obtained for a single slot an an edge, it is apparent that for the case of a pair of axial slots located on the major axis of the cylinder, the patterns are the same as two free-space dipoles placed at a distance C apart, either in phase or 180° out-of-phase.

It was found that the case of two slots located on the minor axis excited with equal in-phase voltages yielded an omnidirectional pattern. If one examines the electric field lines produced by a symmetrical balanced antenna located on either side of a thin conducting plane, it can be seen that the fields at the edges combine in such a manner as to eliminate any diffraction effects.

Acknowledgment

The aid of Miss N. M. McDougall, who performed the computations, is gratefully acknowledged.

The Transmission-Line Properties of a Round Wire between Parallel Planes*

H. A. WHEELER†

Summary—**A transmission line is useful as a primary standard of impedance if there is a formula relating its wave resistance to its cross sectional shape. For this purpose, the round wire between parallel planes is computed to a very close approximation. The method is based on dividing the usual single pole into a pair of spaced half-poles, between parallel lines on the plane of cross section. The resulting formula covers all shape ratios to a high degree of approximation. Simple explicit formulas are given for the shape ratio and the wave resistance, each in terms of the other, sufficiently close for practical purposes. For example, a line made of perfect conductors (assumed) and air dielectric (laboratory conditions), has a wave resistance of 50.000±.003 ohms if the ratio of radii is 0.54850 =1/1.82315.**

* Original manuscript received, February 18, 1955, revised manuscript received, May 20, 1955. This paper presents a small part of the treatment of the same subject in Wheeler Monographs, No. 19, June, 1954. Reprints of this complete paper are available from the author on request.

† Wheeler Laboratories, Great Neck, N. Y.

I. Introduction

UNIFORM transmission lines of certain shapes of cross section are useful as primary standards of impedance because it is possible to compute the relation between their wave resistance and their cross-sectional dimensions. The simplest case is the coaxial line whose inner and outer conducting surfaces have circular cross section.

Another shape of coaxial line has come into use because it offers some advantages of mechanical construction and of accessibility for standing-wave detection. This shape is the round wire between parallel planes [4, 5, 13, 15, 20, 21]. It offers a problem in approximation because the relation between its wave resistance and its cross-sectional shape ratio is not expressed exactly by any of the usual tabulated functions.

The formulation and computation of this relation is the subject of this paper.

The method of computation on the plane of cross section is a change from the usual single pole between parallel lines, to a pair of spaced half-poles giving an equipotential line closely approximating circle representing the inner conducting surface. This method places the wave resistance between upper and lower limits which are close together for the usual cases. The closest approximation is a mean value between these limits, which is found to be closer than required for practical applications. This complete formulation requires elaborate computation, though relying only on hyperbolic and more elementary functions.

For practical purposes, a simple series is derived for explicit computation of either the shape ratio or the wave resistance in terms of the other. Each series converges so rapidly that the first two terms are sufficient for the usual requirements.

For use as a primary standard of impedance, the 50-ohm line is computed to 5 places. The correction is applied for air dielectric in laboratory conditions. The remaining corrections are those for the skin effect in the conductors and for the curtailment of the parallel planes down to finite width; both are given and are shown to be small.

The present formulas are shown to be a great advance over the formula of Wholey and Eldred [13] which is the most advanced solution previously published.

Only the simplest and most useful formulas are presented herein. The complete treatment has been given by the writer [21].

II. Symbols

r = radius of round wire.
c = distance from center of wire to each plane.
$c' = (4/\pi)c$ = radius of round shield equivalent (for small wire) to parallel planes.
R = wave resistance of line (ohms).
$R_c = 120\ \pi$ (approximate) = wave resistance of free space (ohms).
$R_c/2\pi = 60$ ohms (approximate).
a = offset of half-pole.
$\rho = (\pi/4)\ r/c = r/c'$; $\alpha = (\pi/4)\ a/c = a/c'$; parameters (radians).

III. The Basis for the Formulas

Fig. 1 shows the cross section of a round wire between two planes. The outer contour of the wire is the circle of radius r and the inner contour of the planes is the pair of parallel straight lines at a distance c from the center of the circle. Perfect conducting material (free of resistance) is assumed for all contours. The wave resistance of the space between the conductors is taken to be $120\ \pi$ ohms, which is approximately that of free space or air dielectric.

The outer circle, of radius $c' = (4/\pi)c$, is the circular outer contour which is equivalent to the parallel planes if the wire is small ($r/c \ll 1$) [15]. To simplify some of the formulas, they are expressed in terms of the ratio,

$$\rho = \frac{r}{c'} = \frac{\pi}{4}\,\frac{r}{c},$$

which approaches the limiting value $\pi/4$ as the wire approaches contact with the planes.

The formulas to be presented are based on a refinement beyond the usual formula for a small wire between parallel planes. This refinement preserves the parallel planes and enables closer computation of the potential on the wire. The usual single pole in the center of the wire is divided into a pair of half-poles located at a distance of a on opposite sides of the center as shown in Fig. 1.

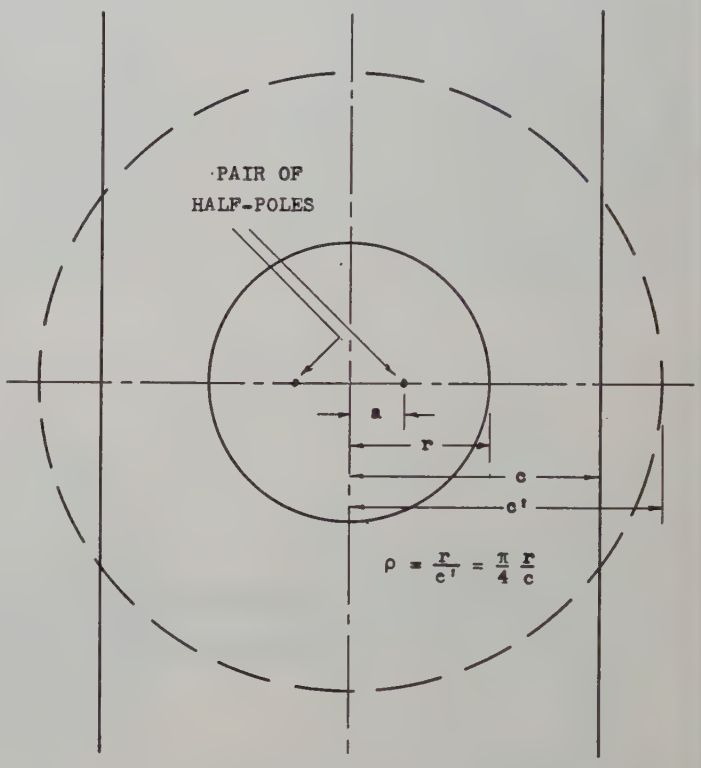

Fig. 1—Cross section of round wire between parallel planes, approximately to scale for $R = 50$ ohms.

If the circular contour were replaced by the pair of half-poles, the potential on the locus of the circle would have a cyclic variation around the circumference. The distance of the half-poles from the center is chosen so that the potential on the circle has equal maximum values on four points (the two points nearest to the planes and the two points farthest from the planes). This gives nearly uniform potential around the circle.

By the usual methods, it is then possible to compute the maximum potential at these four points and the minimum potential at intermediate points on the four quadrants of the circle. A circular conductor at this locus would assume a constant potential having a value which is a mean between the computed maximum and

minimum values. Since these values are close together, the mean value gives an extremely close approximation. This rather elaborate computation is formulated and exemplified in Reference 21; it will not be given here but some of its results will be utilized.

The evaluation of the proper distance to each half-pole has been reduced to a simple formula by considerable effort. It is given here, after which the remaining derivations become routine. It is expressed in terms of the angular parameter,

$$\alpha = \frac{a}{c'} = \frac{\pi}{4}\frac{a}{c} = \frac{1}{2}\,\text{anticos}\,\sqrt{\cosh 2\rho \cos 2\rho}$$
$$= \tfrac{1}{2}\,\text{antisin}\,2\sqrt{\sinh^2\rho \sin^2\rho - \tfrac{1}{2}(\sinh^2\rho - \sin^2\rho)}$$
$$= \sqrt{2/3}\,\rho^2 + \cdots. \qquad (1)$$

IV. Formulas

Simple Logarithmic Formula

The simple logarithmic formula for a small wire between two planes has been known for many years [4, 5, 6, 9, 10, 11]. It is the first term in a series expansion for a small wire. By the present procedure (mean value), the second term has been added. The resulting formula is

$$R = 60\left(\ln\frac{1}{\rho} - \frac{2}{9}\rho^4 - \cdots\right)\ \text{ohms}. \qquad (2)$$

The coefficient of the second term is the mean of 23/90 and 17/90 for the maximum and minimum values of potential; these values are only $\pm 1/30$ from the mean value 2/9.

New Logarithmic Formula

The best simple formula that has been derived is the following, an outcome of the present study.

$$R = 60\left[\ln\frac{\sqrt{1+2\sinh^2\rho} + \sqrt{1-2\sin^2\rho}}{\sqrt{2(\sinh^2\rho + \sin^2\rho)}} - \frac{1}{30}\rho^4 + .014\rho^8 \pm \cdots\right]\ \text{ohms}. \qquad (3)$$

The main term in this formula is based on the maximum potential on the locus of the circle. It alone is closer than any previously published formula, for all shapes from a small wire to a large wire near contact, Even in latter extreme case, its relative error is less than 0.12 (as compared with nearly unity for Reference 13).

The second term in (3) is the correction to obtain the mean value for small wires (as mentioned above). The third term is a further correction to obtain the mean value for a rather large wire (20-ohm line). Any smaller wire has a remaining correction much less than the third term. For a 50-ohm line, (2) is within 1/4000 and (3) is within 1/100,000 (the third term being about 1/50,000), whereas the closest previous formula is off by 1/300 [13].

Explicit Formula for Shape

The most remarkable outcome of this derivation is a simple explicit formula for the ratio of radii in terms of the wave resistance. This formula is in the form of a series which, for a small wire, converges so rapidly that the first two terms meet all the usual needs. It gives a close approximation for all shape ratios, even near contact.

$$\frac{r}{c} = \frac{4}{\pi}\exp\frac{-R}{60}\left(1 - \frac{2}{9}\exp\frac{-4R}{60} - .00736\exp\frac{-8R}{60} + .01932\exp\frac{-12R}{60} - .00434\exp\frac{-16R}{60} \pm \cdots\right). \qquad (4)$$

In the parentheses, the coefficients of the third, fourth and fifth terms are approximated on a logical basis in Reference 21; the remaining error is less than these terms. For example, if $R = 50$ ohms, the first two terms leave a relative error of about 1/300,000. The first two terms are more than adequate for slide-rule computations and all practical purposes if $R > 20$ ohms, leaving a relative error less than 1/5000.

Precise Properties of Free Space

Very close computation requires that the wave resistance (R_c) be evaluated closer than the assumed value ($120\pi = 60 \times 2\pi$). This requires small corrections for free space and air. According to the latest authority [18], the wave velocity in free space is

$$299.793 = 300 - 0.207 = 300/1.00069\ \text{meters}/\mu\text{sec}. \qquad (5)$$

Since the magnetic constant in free space is exactly $0.4\,\pi$ microhenries per meter, this correction of velocity is caused by electric constant being slightly greater than that corresponding to 300 meters per μsec.

Precise Properties of Air Dielectric

The dielectric constant in air is slightly greater than that in free space, in proportion to the density of dry air and, in greater degree, to the density of water vapor. These factors have been formulated and a standard atmosphere has been specified as typical of laboratory conditions [7]. This atmosphere is defined:

Condition	*Standard*
Temperature	= 25°C
Relative humidity	= 0.60
Altitude	= 0 (sea level)
Total pressure	= 1 atmosphere

For present purposes, some limits of variation are stated:

Condition	*Limits*
Temperature	±5°C
Relative humidity	±0.20
Pressure variation with time	±1/60 atmosphere
Pressure variation with altitude	−1/25 atmos (+1000 feet)

The standard conditions, modified to the extent of these variations, give a dielectric constant of

$$1.00070 \pm .00010. \quad (6)$$

Dividing the free-space velocity (5) by the square root of this dielectric constant,

$$300/(1.00104 \pm .00005) = 300 - 0.31 \pm .02$$
$$= 299.69 \pm .02 \text{ meters}/\mu\text{sec}. \quad (7)$$

This value is taken to be typical of laboratory space in regions of low altitude.

The wave resistance in this air dielectric is 0.4 π times the velocity:

$$R_c = 120\pi/(1.00104 \pm .00005)$$
$$= 376.60 \pm .02 \text{ ohms}, \quad (8)$$
$$R_c/2\pi = 60/(1.00104 \pm .00005)$$
$$= 59.938 \pm .003 \text{ ohms}. \quad (9)$$

For very close computation, the latter value is used instead of 60 ohms in various formulas such as (2) to (4). The tolerances of variations in the atmosphere leave an uncertainty of $\pm 1/20{,}000$ of the wave resistance of the transmission line. For a 50-ohm line, this is only $\pm .0025$ ohms, which is negligible in practice.

Skin Effect

A transmission line to be used as a standard of impedance is usually in the form of a slotted line for standing-wave observations. In this application, its length should be at least one-half wavelength and preferably one wavelength. Since a slotted length longer than one meter is inconvenient for laboratory use, the slotted line is most useful at wavelengths less than 2 meters, or frequencies above 150 mc. In this case, the skin depth in copper or silverplate is less than 5.4 microns or 0.21 mil-inch [17]. After computing the dimensions for a perfect conductor, each surface exposed to the field in the line should be raised by $\frac{1}{4}$ the skin depth. Such a correction can be computed for any one frequency, or a mean value taken for a frequency band. However, it is so small that it is usually negligible in any of the nonmagnetic metals used for structure or plating, such as silver, copper, gold, aluminum, or brass.

Finite Parallel Planes

The computations are based on parallel planes extending indefinitely far from the wire between them. In practical construction, the use of a finite width of both planes introduces some uncertainty in the wave resistance. For any width, the edges may be closed (except for a slot) to form a shield of rectangular cross section, in which case the change of wave resistance can be computed for a small wire (by the method of images, from the formulas in References 4, 5, 11). This change is tabulated for various ratios of the width of each plane, over the separation ($2c$) between planes.

Width Fraction Separation	*Reduction of Wave Resistance*
2	0.45 ohm
2.5	.094
3	.020
3.5	.0041
4	.00084

From this table, the width of the planes can be made sufficient to subordinate this correction. Leaving the edges open has the opposite effect, increasing the resistance, but less than $\frac{1}{4}$ as much. However, the open edges leave some uncertainty depending on the external contours and environment.

End Connections and Supports

One end of the slotted line should be precisely matched to an extension line of equal wave resistance, usually of coaxial circular cross section, which connects with the impedance under test. The matching of this connection is not adapted for computation, but can be accomplished by experimental adjustment of the contours. If the line is long enough to need supports at both ends, and perhaps also distributed along its length, there remains a difficult problem of providing a dielectric support in a form that is reliable and computable.

Computation of 50-ohm Line

A 50-ohm line is of particular interest for use as a slotted line for standing-wave tests of reflection, so it has been computed closer than the variation of air dielectric in laboratory conditions. From (4), the approximate value of the shape ratio is $r/c = 0.54896$; this has been verified by mean-value computation and (3). Applying the corrections for free space and air dielectric, the final computation gives

$$r/c = 0.54850 = 1/1.82315 \quad (10)$$

for

$$R = 50.000 \pm .003 \text{ ohms}.$$

Comparison with Published Curves

Referring to the writer's previously published curves [15], the present derivation indicates that, for the round wire between parallel planes, the previous curve is about 1 ohm too low in the transition region of 20 to 50 ohms.

V. Conclusions

The round wire between parallel planes has yielded to a simple and direct computation of its properties, to a degree of approximation more than adequate for the usual applications. Simple explicit formulas are given for the shape ratio and the wave resistance, each in terms of the other. The complete interpolation formula covers the entire range of shape ratio and wave resistance.

VI. Bibliography

[1] Richmond, H. W., "On the Electrostatic Field of a Plane or Circular Grating Formed of Thick Rounded Bars." *Proceedings of the London Mathematical Society*, Ser. 2, Vol. 22 (1923), pp. 389–403. (Reported by Smythe, 16 below.)

[2] Becker, G. F., and Van Orstrand, C. E., "Hyperbolic Functions." Smithsonian, 1924. (Hyperbolic functions; sine and cosine of radians; exponentials; numerical constants; 5 places, long tables.)

[3] Peirce, B. O., "A Short Table of Integrals." 3 ed., Boston, Ginn and Company, 1929. (Natural logarithms, 5 places, long table.)

[4] Frankel, S., "Characteristic Impedance of Parallel Wires in Rectangular Troughs." Proceedings of the IRE, Vol. 30 (April, 1942), pp. 182–190. (Including small wire between parallel planes.)

[5] Wheeler, H. A., "Inductance of Straight Wires in Rectangular Shields." Hazeltine Report 1318W, June 9, 1942. (Including small wire between parallel planes.)

[6] Schelkunoff, S. A., "Electromagnetic Waves." D. Van Nostrand Company, 1943. (Small wire near 1, 2, 3, 4 plane boundaries, pp. 169–87.)

[7] Montgomery, C. G., "Technique of Microwave Measurements." Radiation Laboratory Series, Vol. 11, McGraw-Hill Book Company, 1947. (L. B. Young, pp. 390–393, dielectric properties of air with humidity, standard conditions, nomogram.)

[8] Wheeler, H. A., "Slide Rule Operations for Radio Problems." Wheeler Monographs, no. 2, May 1948. (Quadratic sum, p. 15. Small wire between parallel planes, p. 24. Conversion between radians and degrees, p. 28–29.)

[9] Schelkunoff, S. A., "Applied Mathematics." New York, D. Van Nostrand Company, 1948. (Small wire near 2 or 3 plane boundaries, pp. 289–93; small wire in approximately square shield, pp. 298–300.)

[10] Bewley, L. V., "Two-Dimensional Fields in Electrical Engineering." New York, The Macmillan Company, 1948. (Small wire between parallel planes, pp. 55, 153.)

[11] Wheeler, H. A., "The Piston Attenuator in a Waveguide below Cut-off." Wheeler Monographs, no. 8, January, 1949. (Small wire between parallel planes; coupling between two wires; p. 24.)

[12] Harnwell, G. P., "Principles of Electricity and Electromagnetism." 2 ed., New York, McGraw-Hill Book Co., 1949. (Dielectric constant of air, p. 84.)

[13] Wholey, W. B., and Eldred, W. N., "A New Type of Slotted Line Section." Proceedings of the IRE, Vol. 38 (March, 1950), pp. 244–248. (Approximate formula for moderately large wire between parallel planes.)

[14] Smythe, W. R., "Static and Dynamic Electricity." 2 ed., New York, McGraw-Hill Book Company, 1950. (Mapping grid of wires, any size, approximately round, pp. 98–100; implicit solution, transmission line properties would be in terms of elliptic integrals.)

[15] Wheeler, H. A., "Transmission-Line Impedance Curves." Proceedings of the IRE, Vol. 38 (December, 1950), pp. 1400–1403. (Including wire of any size between parallel planes. References to earlier work.)

[16] Hodgman, C. D., "Mathematical Tables." 9 ed., Chemical Rubber Publishing Co., 1952. (Numerical constants; common logarithms; sine, cosine, tangent, of radians; natural logarithms; exponentials; hyperbolic functions; 5 places, short tables.) See also "Handbook of Chemistry and Physics," same tables.

[17] Wheeler, H. A., "Universal Skin-Effect Chart for Conducting Materials." *Electronics*, Vol. 25 (November, 1952), pp. 152–154. (Formulas and references.)

[18] DuMond, J. W. M., and Cohen, E. R., "Least-Squares Adjustment of the Atomic Constants, 1952." *Review of Modern Physics*, Vol. 25 (July, 1953), pp. 691–708. (Wave velocity in free space.)

[19] Comrie, L. J., "Chamber's Shorter Six-Figure Mathematical Tables." Chemical Rubber Publishing Co., 1954. (Excellent tables of natural functions and antifunctions: circular, hyperbolic, exponential, logarithms.)

[20] Chisholm, R. M., "The Characteristic Impedance of 'Trough' and 'Slab' Transmission Lines." Presented to the IRE at Washington, D. C., May 6, 1954. (Variational double integral used to derive very complicated series for small wire between parallel planes; computation for $50 \pm .001$ ohms in free space.) Not yet published.

[21] Wheeler, H. A., "The Transmission-Line Properties of a Round Wire between Parallel Planes," Wheeler Monographs, no. 19, June 1954. (The complete treatment, from which the present paper is a small part.)

[22] Love, A. E. H., "Electrostatic Problems Related to a Perforated Strip." *Quarterly Journal of Mathematics* (Oxford Series), Vol. 9 (1938), pp. 246–258. (Another solution for a round wire between parallel planes.)

Current Distribution on Wing-Cap and Tail-Cap Antennas*

IRENE CARSWELL†

Summary—**Surface current distributions on aircraft are examined for wing-cap and tail-cap antennas in the hf band using scale models. Current paths involved in structural resonances are investigated, and the effect of such resonances on antenna impedance is discussed. Measured results are also applied to the interpretation of radiation patterns.**

A technique is described for measuring the relative amplitude and phase of the surface current, and for determining the direction of current flow. In this method the detector is placed in the model and the probe is driven by an external source of rf power. This technique permits the frequency to be changed easily. The system is more sensitive than others described in the literature, since a higher power source can be used when it is not required to be enclosed in the aircraft model.

Introduction

IN THE hf frequency range, where the principal dimensions of an aircraft are comparable to the wavelength, current paths composed of portions of the fuselage, wings, and tail surfaces are known to be responsible for resonance effects in the input impedance curves of wing-cap and tail-cap antennas.[1] Frequencies at which the principal current paths on an aircraft may become resonant have been predicted by a backscattering method.[2] Determination of the nature of these resonances, and verification of the frequencies at which they occur, is of interest in connection with the excitation of an aircraft as an antenna, since both the input impedance and radiation patterns are affected.[3] Current distribution is a fundamental electrical property for investigation, since the other quantities are dependent on it in the usual antenna analysis procedures.

* Original manuscript received by the PGAP January 10, 1955; revised manuscript received June 22, 1955.

† Stanford Research Inst., Menlo Park, Calif.

[1] J. V. N. Granger, "Wing-Cap and Tail-Cap Aircraft Antennas," Tech. Rep. 6, Contract AF 19(122)-78; SRI Proj. 188, Stanford Res. Inst., Menlo Park, Calif.; March, 1950.

[2] A. S. Dunbar, "Electromagnetic Resonance Phenomena in Aircraft Structures," Tech. Rep. 8, Contract AF 19(122)-78; SRI Project 188, Stanford Res. Inst., Menlo Park, Calif.; May, 1950.

[3] J. V. N. Granger and T. Morita, "Radio frequency current distributions on aircraft structures," Proc. IRE, vol. 39, pp. 932–938; August, 1951.

When an antenna is mounted on the surface of an aircraft structure, rf currents are not confined to the antenna alone, but flow on the conducting surface of the aircraft as well. If the relative amplitude and phase of the surface current could be determined experimentally, it would be possible to locate resonant path-lengths, and to discuss, at least qualitatively, their effect on input impedance and radiation patterns.

This paper describes a measuring technique for obtaining the distribution of surface current density. The method was applied to determine the current distributions on a 749 Constellation aircraft. All measurements contained in this report were made on a 1/43-scale model aircraft, constructed of cast aluminum. The measured distributions are given and the relation of these distributions to the measured input impedance and radiation patterns is discussed.

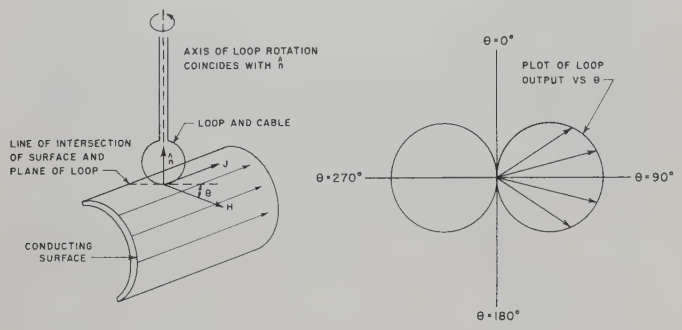

Fig. 1—Orientation and response of loop probe.

Method of Measurement

Loop Probe

If the conductivity of the model is high, and skin depth is small, it is known from Maxwell's equations that the current vector and magnetic field vector are perpendicular to each other at the conducting surface, and mutually perpendicular to a vector directed outwardly normal to the current-carrying surface. This relationship is expressed by the boundary condition,

$$\hat{n} \times \vec{H} = -\vec{J},$$

where $\hat{n}$ is the unit vector normal to the current carrying surface, $\vec{H}$ is the magnetic vector, and $\vec{J}$ is the surface current density. Therefore a loop probe held perpendicular to the surface of the model will indicate the magnitude and direction of surface current density by virtue of the proportionality of its output to the number of linkages with the magnetic flux.[4] The ideal response of the loop, as illustrated in Fig. 1, is a figure eight having maxima when the loop plane coincides with the direction of the surface current at a given point; nulls when the loop plane parallels the magnetic vector.

Ideally, the shielded-loop probe should not respond to the codirectional electric field, or "dipole mode." Practically, however, some response to this mode will exist, due to slight mechanical dissymmetries in the structure. Response of the loop probe to electric field pickup is indicated by the variation of the output of the measuring system from the desired cosine form, which is illustrated in Fig. 1.

When the electric field has components that are not parallel to the line of probe symmetry, such as occur near cusps in the conducting surface, and near regions of impressed field, errors in the measurement will be unavoidable. This fact must be considered in interpreting the data.

Amplitude Measurement

The measuring technique utilized in this investigation differs somewhat from others described in the literature.[4] Instead of driving the antenna terminals and measuring the current picked up in the loop probe, the loop is driven and the current in the antenna terminals is measured. By locating the detecting equipment inside the aircraft model, as illustrated in Fig. 2, and

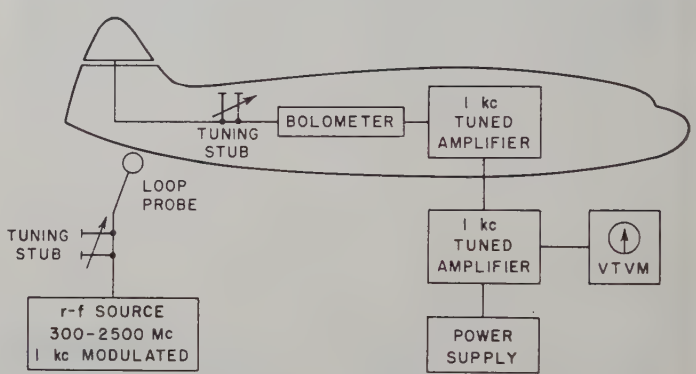

Fig. 2—Block diagram of apparatus for determining amplitude of current.

bringing out the detected audio component on high-resistance leads, the rf field around the model is not disturbed.[5] This audio signal is amplified and presented to the observer on a vacuum-tube voltmeter. The source of power is an rf oscillator modulated at 1,000 cps, whose output is carried to the loop probe by double-shielded coaxial cable. The direction of the loop plane at maximum output coincides with the direction of current flow, and the amplitude of maximum at that point is relative amplitude of surface current density with respect to an arbitrarily chosen reference.

Elliptically-polarized currents can occur on portions of the surface where the lines of current flow change direction during the rf cycle. Their presence is indicated by a "filling in" of the nulls in the output as the loop

[4] J. V. N. Granger and T. Morita, "Current Distribution on Aircraft," Tech. Rep. 78, Cruft Lab., Harvard Univ., Cambridge, Mass.; November, 1949.

[5] R. M. Hatch, Jr., "Improvements in Instrumentation for the Investigation of Aircraft Antenna Radiation Patterns by Means of Scale Models," Tech. Rep. 26, Contract AF 19(604)-266, SRI Project 591, Stanford Res. Inst., Menlo Park, Calif.; August, 1952.

probe is rotated. Regions of elliptical polarization are shown in the current plots as areas where no current distribution data was obtained.

Phase Measurement

The phase of the surface current density is measured by comparing the signal from the probe with the signal received from a dipole illuminating the model and connected to the same source. Reference to Fig. 3 shows that the dipole is mounted in such a way that its distance from the model is variable. Since the phase of the signal in the far field is a known linear function of the distance from the antenna under test, the dipole is an rf phase shifter. When this signal is combined with the signal from the loop probe and impressed on a bolometer detector, the output is presented to the observer as a succession of maxima and minima as the dipole is moved. It is important that the amplitudes of the two signals be of the same order of magnitude, in order for the minima to be well defined. It is convenient to define a position of the dipole at which a sharp null is observed when the loop is in a reference position on the aircraft model, as zero relative phase. The relative phase of the current at any other point on the model is then computed from the distance in wavelengths that the dipole must be moved to produce a new minimum voltage.

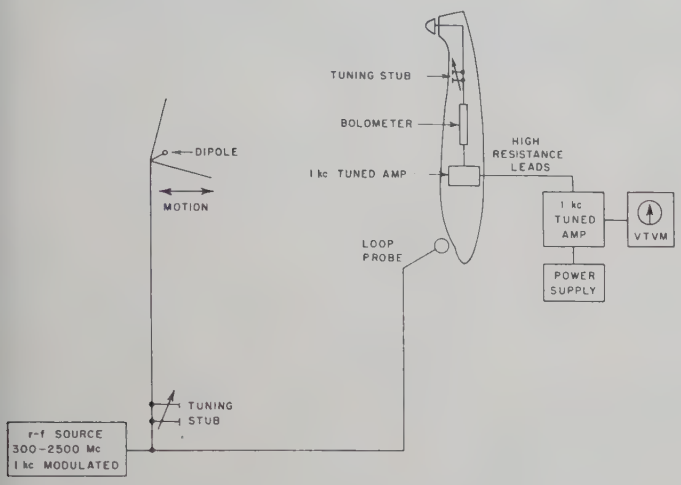

Fig. 3—Block diagram of apparatus for determining relative phase of surface current density.

Measured Results

Fig. 4 shows a contour plot of the amplitude of the current distribution on a 749 Constellation aircraft excited by a wing-cap antenna at a full-scale frequency of 11.2 mc. At this frequency a pathlength L composed of the leading edge of the driven wing and the side of the fuselage forward of the wing, is one wavelength long. Examination of Fig. 4 shows that the level of cur-

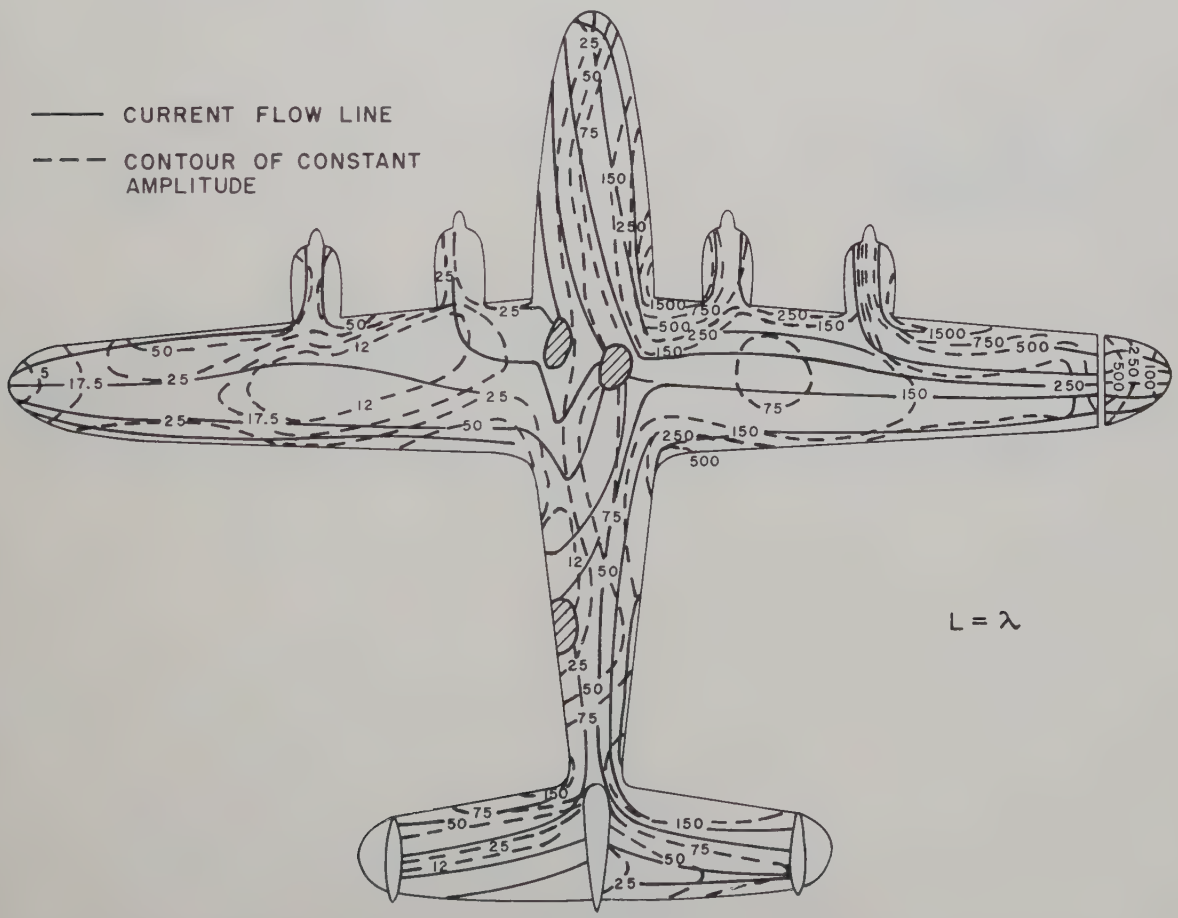

Fig. 4—Contour plot of amplitude of surface current on constellation aircraft excited by a wing-cap antenna at a full-scale frequency of 11.2 mc.

rent amplitude along this path is high when compared to relative amplitude elsewhere on the model surface. Reference to the input impedance curve of Fig. 5[6] reveals a sharp peak in the curve of input resistance at 11.2 mc.[7] Resonance of the wing and fuselage current path appears to be responsible for this effect.

A contour plot of relative amplitude at 7.1 mc is shown in Fig. 6 for the same antenna. Although the wingspan is approximately a wavelength long at this frequency, no strong resonance is apparent, either in the plot of current distribution or in the input impedance curve of Fig. 5. Inspection of Fig. 6 reveals that undriven wing is only weakly coupled to radiating structure. Currents flowing on driven wing tend to divide principally between fore and aft portions of fuselage where no resonant pathlength exists at this frequency.

In the vicinity of 24 mc, another resonant peak occurs in the resistance of the wing-cap antenna. Fig. 7 shows the distribution of the current amplitude at this frequency. It should be noted that at 24 mc, the wing chord is no longer small compared with the span and the wavelength, and the diameter of the fuselage is an appreciable fraction of the wavelength. The quasi-static

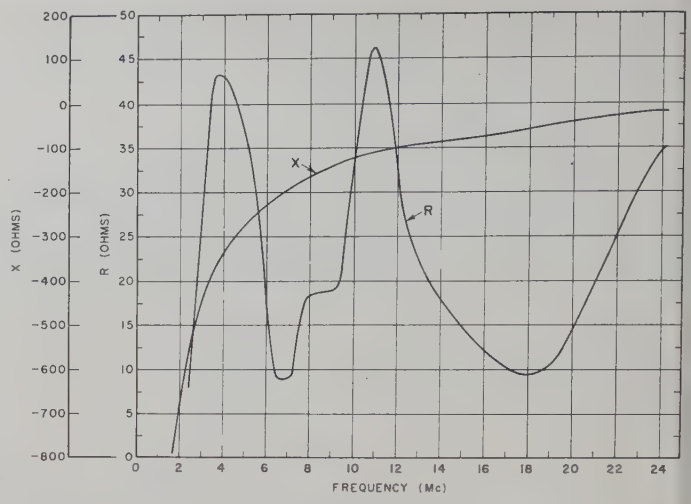

Fig. 5—Impedance of cap-type antenna on wing tip of constellation aircraft.

assumptions of longitudinal current flow and static amplitude distribution at any cross section, which are valid at lower frequencies, are not applicable here.[8] At 24 mc, the wingspan is nearly three wavelengths long, as is a path involving the driven wing, the leading edge of the horizontal stabilizer, and the slide of the fuselage aft of the wing root. At the junction of the wing and fuselage, the wing chord is nearly a half-wavelength

[6] Presented here through the courtesy of the Lockheed Aircraft Corp., Burbank, Calif.

[7] J. Taylor, "Flush-Mounted H-F Antennas for the 1049 Constellation Aircraft," Final Report, SRI Project 409, Stanford Res. Inst., Menlo Park, Calif.; February, 1952.

[8] J. V. N. Granger and T. Morita, *op. cit.*

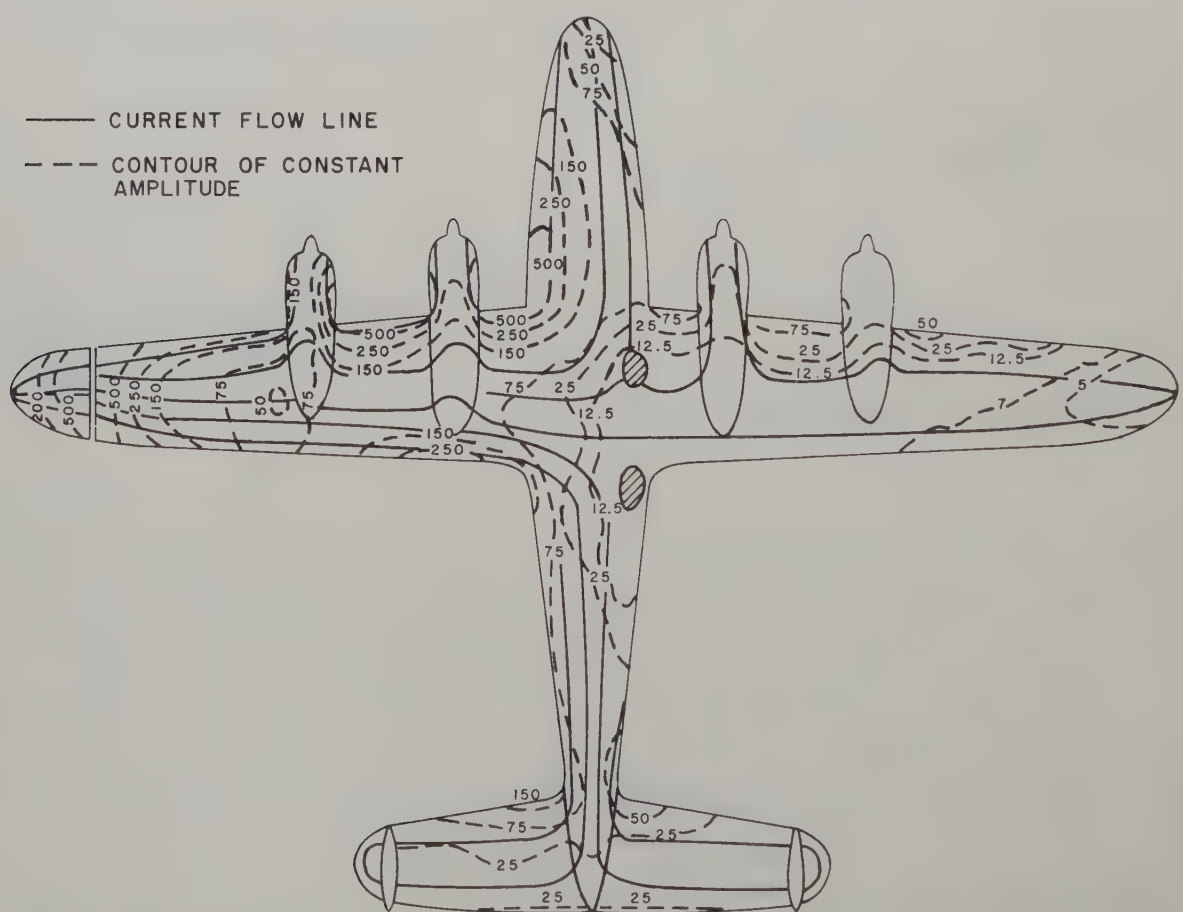

Fig. 6—Contour plot of amplitude of surface current on a constellation aircraft exited by a wing-cap antenna at a full-scale frequency of 7.1 mc.

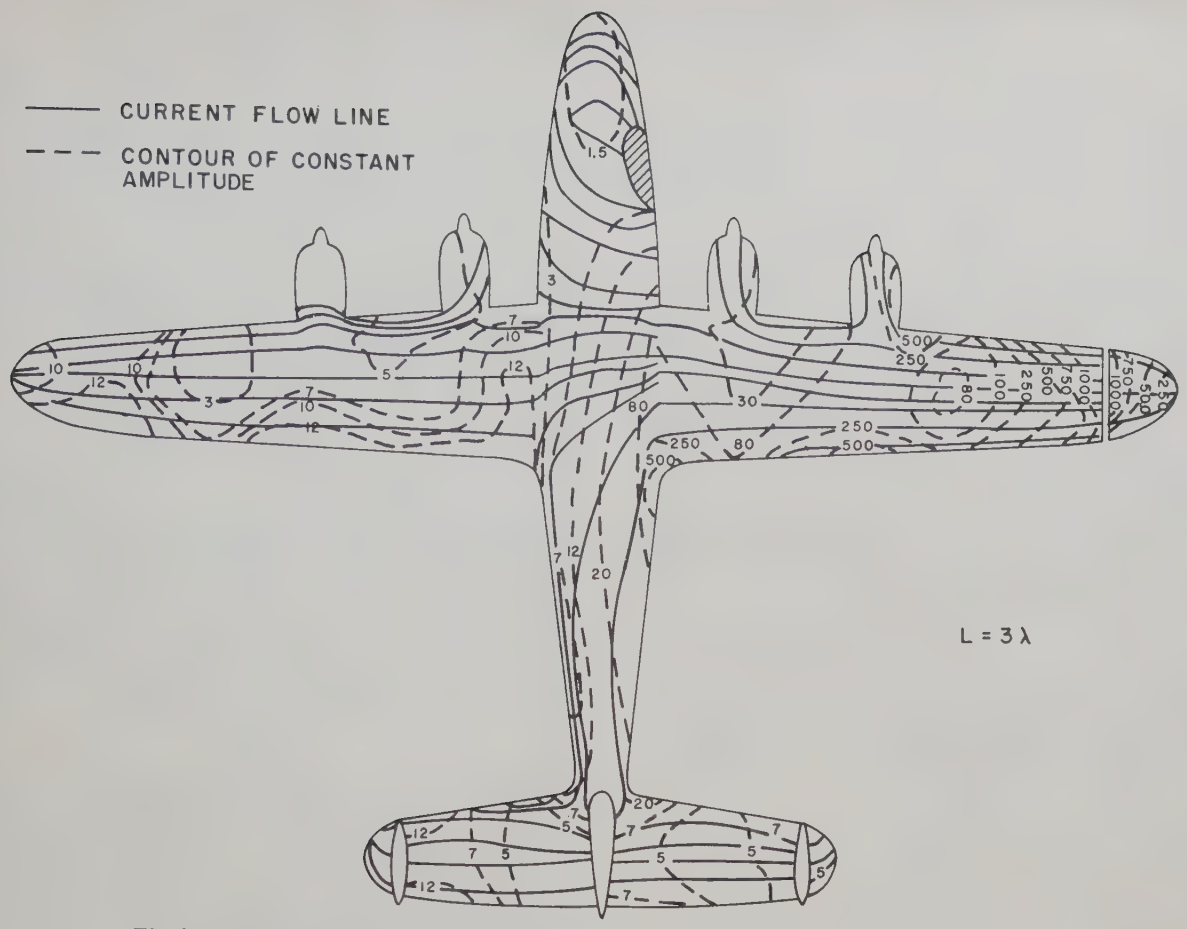

Fig. 7—Contour plot of amplitude of surface current on a constellation aircraft excited by a wing-cap antenna at a full-scale frequency of 24 mc.

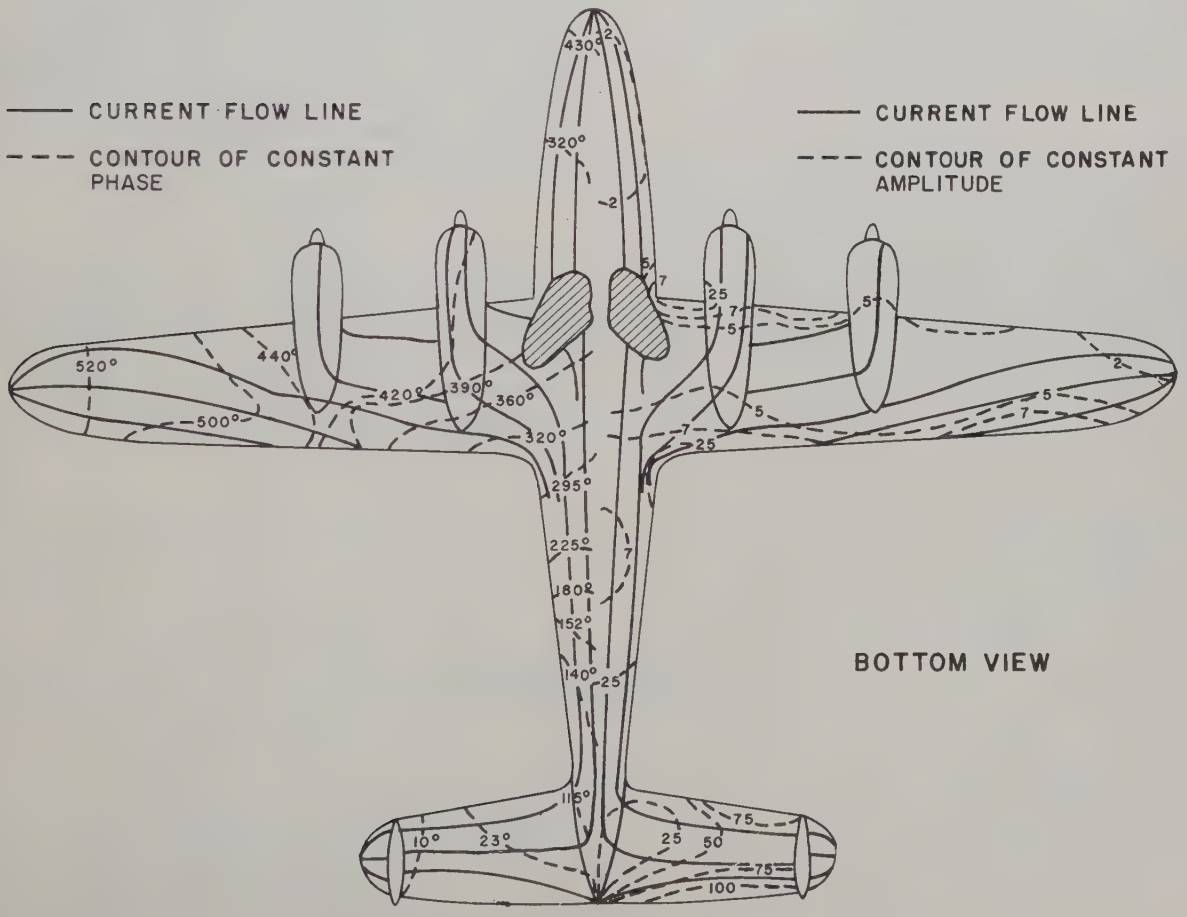

Fig. 8—Contour plot of surface current amplitude and phase on a constellation aircraft excited by a tail-cap antenna on the center fin at a full-scale frequency of 15 mc.

long, and the chord of the isolated wing-tip is a quarter-wavelength long at its base, where the driving voltage is impressed.

Amplitude and phase of surface current on Constellation with center fin isolated are in Fig. 8 on the previous page. Since system possesses symmetry about center line of fuselage, only half of each contour is plotted. The measurements were made at 15 mc, where the span of the horizontal stabilizer is a half-wavelength, and where a peak in the input resistance is known to exist. Inspection of the amplitude distribution reveals that the currents on the horizontal stabilizer are high, whereas the coupling to the rest of the structure is low. The phase angle increases with distance from the source, as would be the case for a lossy transmission line. It lags with respect to the antenna terminals, and is not constant at the cross sections.

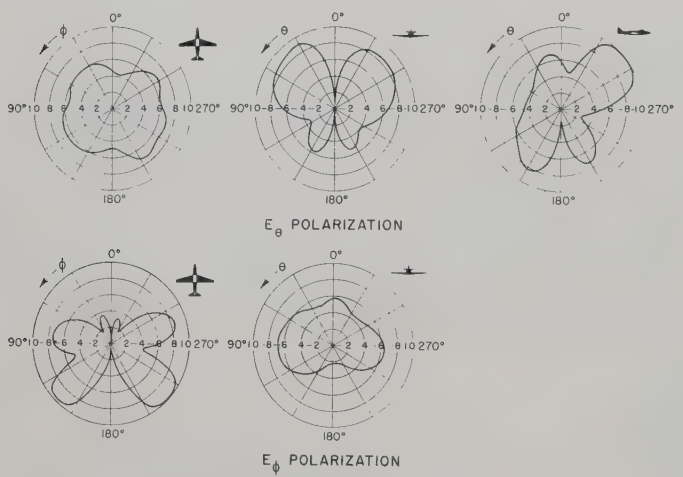

Fig. 9—Field pattern of a tail-cap antenna on center fin of a lockheed constellation at 15 mc.

The field pattern of a tail-cap antenna on the center fin of the Constellation is illustrated in Fig. 9, where the standard spherical coordinate system has been used to define the principal planes. The azimuth angle ϕ is measured in the counterclockwise direction from the nose of the model. The angle of elevation θ is measured from a point directly above the model and is 90 degrees at the horizontal plane. Some of the ways in which the measured current distribution at 15 mc affects the radiation pattern at this frequency may be pointed out. It must be emphasized, however, that exact interpretations must await the completion of further work. The transverse-plane E_θ pattern appears to be the result of the current on the center fin, modified by the effect of current excited on the horizontal stabilizer. The longitudinal pattern is approximately that of a bent dipole consisting of the center fin plus the top of the fuselage aft of the wing, modified by the contribution of currents on the sides and bottom of the fuselage, which are lagging in phase, and are of lower amplitude. It should be noted that the currents on the fuselage forward of the wing are too low to affect the major lobes of the pattern. The E_ϕ azimuth pattern exhibits nulls fore and aft, and off the wing tips, as would be expected. It approximates the radiation from a horizontal dipole about one wavelength long, with modifications due to the currents on the statilizer and wings.

Summary

This paper has described a technique for measuring the relative amplitude and phase of the surface current excited on the skin of an aircraft by antennas in the hf range. Measured results have been obtained at several frequencies for wing-cap and tail-cap antennas, using scale models of the aircraft, and proportionately increased operating frequencies. An attempt has been made to establish relationships between the current distribution data and the appropriate radiation pattern and input impedance information, at least to a first approximation. Further work will be necessary before more exact interpretations are possible.

Acknowledgment

The author wishes to acknowledge the constributions made to this work by Dr. J. V. N. Granger, who suggested the basic problem, and by Dr. J. T. Bolljahn during many helpful discussions. Many of the experimental results reported herein were measured by Mrs. J. K. Snipes and Jean Hughes Waters.

communications

Note on a Method for Calculating Coupling Coefficients of Elements in Antenna Arrays*

V. T. NORWOOD†

AN EXPLICIT expression for calculating coupling coefficients for each element of a traveling-wave array is derived below. The coupling coefficients are shown to be completely determined by the desired current distribution across the aperture, the waveguide attenuation, and the percentage of the total power which is jettisoned into the load. The advantages of the explicit expression over the difference equation method previously used are (1) facility in determining the proper balance between the amount of power assigned to the terminal load and the maximum permissible coupling between an element and the array, and (2) computing simplification; i.e., a computing error affects only one coefficient without causing errors in every successive coefficient. The importance of these points is dramatized by considering the work involved in the design of a 1,000-element Dolph-Tchebyscheff array.

The value of the power at various points in the array is indicated in Fig. 1. The subscript in the first position refers to the power into a kth element (P_{ik}), radiated by a kth element (P_{rk}), or just beyond a kth element (P_{0k}).

Assume that

$$P_{i1} = 1 \text{ (total power in).} \tag{1}$$

The following relationships can be readily deduced:

$$P_{0k} = e^{\alpha l} P_{i(k+1)} \text{ (α attenuation in guide)} \tag{2}$$

$$P_{ik} = P_{0k} + P_{rk}. \tag{3}$$

The power radiated from each slot is proportional to the desired aperture distribution (in terms of power), normalized to 1 for the last element. We shall call these coefficients C_k.

$$P_{rk} = C_k P_{rn}. \tag{4}$$

Combining (2) and (3) yields

$$P_{i(k+1)} = (P_{ik} - P_{rk})e^{-\alpha l} \tag{5}$$

or

$$= (P_{ik} - C_k P_{rn})e^{-\alpha l}.$$

Starting with $P_{il}=1$ we may deduce the kth term after writing a few terms.

$$P_{i1} = 1$$

$$P_{i2} = (1 - C_1 P_{rn})e^{-\alpha l}$$

$$P_{i3} = [(1 - C_1 P_{rn})e^{-\alpha l} - C_2 P_{rn}]e^{-\alpha l}$$

$$P_{i4} = \{[e^{-2\alpha l} - C_1 P_{rn} e^{-2\alpha l} - C_2 P_{rn} e^{-\alpha l}]C_3 P_{rn}\}e^{-\alpha l}$$

$$P_{i(k+1)} = e^{-\alpha l k} - P_{rn} \sum_{d=1}^{k} e^{-\alpha l d} C_{k-d+1}. \tag{6}$$

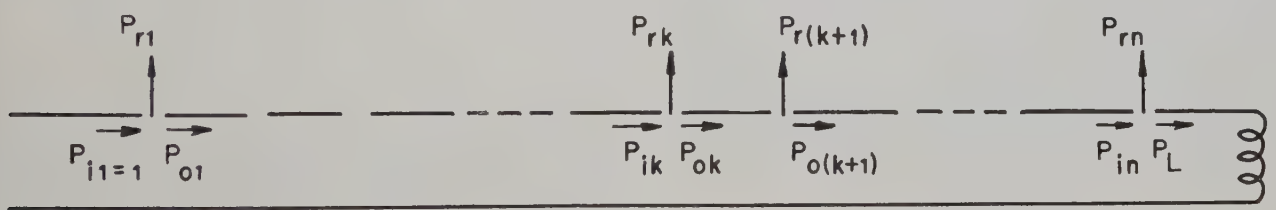

Fig. 1—Schematic representation of power in a slot array.

Eq. (6) is then written for $k=n$, and the expression $P_{in}-P_L$ is substituted for P_{rn}. The resulting expression can be solved to show the relationship between P_{rn} and P_L (the power into the load). (Alternatively everything could have been written in terms of P_{in}.)

$$P_{i(n+1)} = e^{-n\alpha l} - P_{rn} \sum_{d=1}^{n} e^{-\alpha l d} C_{n-d+1}, \tag{7}$$

but $P_{i(n+1)}$ is $P_{0n}e^{-\alpha l}$ or $P_L e^{-\alpha l}$; therefore

$$P_{rn} = \frac{e^{-n\alpha l} - P_L e^{-\alpha l}}{\sum_{1}^{n} e^{-\alpha l d} C_{n-d+1}}. \tag{8}$$

* Original manuscript received May 3, 1955.
† Research and Development Labs., Hughes Aircraft Co., Culver City, Calif.

We may now write the coupling coefficient

$$\frac{P_{rk}}{P_{0k}} = \gamma = \frac{C_k P_{rn}}{e^{\alpha l}\left[e^{-k\alpha l} - P_{rn}\sum_{d=1}^{k} e^{-\alpha l d} C_{k-d+1}\right]}, \qquad (9)$$

which can be expressed in terms of l, P_L, and α. It should be noted that the summation terms are independent of load considerations and these should be computed first in the design of an actual array. With these values at hand a trial value for P_L may be substituted into the expression of γ and a little practice quickly enables one to determine the maximum conductance value by computing conductances for about three consecutive elements. Two or three values for P_L usually result in appropriate maximum conductance, set as a design criterion. An analytic method for solving this extremal problem is easily derived, but expressions are unwieldy except for a few trivial aperture distributions. After l, P_L, and α are determined, P_{rn} becomes a constant and computing is straightforward.

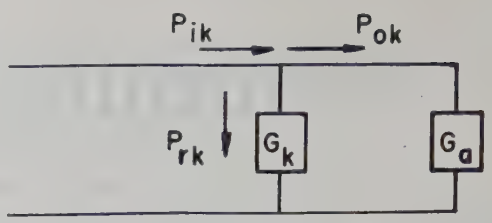

Fig. 2—Equivalent circuit of a slot in an array.

Fig. 2 shows an equivalent circuit of an element and the lumped conductance of the remainder of the array (for example, a waveguide slot array). By conventional circuit relationships,

$$\frac{P_{rk}}{P_{0k}} = \frac{G_k}{G_a}. \qquad (10)$$

For G_a equal to unity (a common assumption in the design of linear arrays) the ratio P_{rk}/P_{0k} reduces to the conductance of the element as it is measured in a transmission line.

On-Axis Defocus Characteristics of the Paraboloidal Reflector*

D. K. CHENG† AND S. T. MOSELEY‡

Summary—**Lack of an adequate test site often requires the use of on-axis defocusing to obtain simulated Fraunhofer radiation patterns in the optical-Fresnel region from microwave reflector-type antennas. This note presents a way of determining the required amount of defocus from the viewpoint of aperture phase correction. It is shown that the important part of the main lobe of the radiation pattern can be approximately reproduced in the optical-Fresnel region with proper amount of defocus. For a given amplitude illumination function, the change in beamwidth with the position of the primary source can also be predicted.**

Introduction

THE TREND toward higher operating frequencies and larger aperture dimensions for microwave reflector-type antennas has brought about the need for taking far-zone (Fraunhofer region) radiation patterns at distances far too great for the average available test site. This has led to a defocusing practice whereby the antenna feed is displaced along the principal axis away from the reflector in the attempt to simulate far-zone patterns in the quasi-near zone (optical-Fresnel region). The amount of defocus required for a given test site is usually determined somewhat empirically by an approximate geometrical optics method.

This note presents an analytical method of determining the required amount of defocus from the viewpoint of aperture phase correction for the circular aperture diffraction problem. Proper defocusing calls for the cancellation of the effect of the Fresnel phase term in the diffraction integral by a phase term as a result of defocusing. The required amount of defocus is also determined from the criterion that the beamwidth of the main lobe in the simulated pattern be a minimum. It will be shown that the minimum beamwidth criterion coincides with the condition for maximum radiation amplitude along the reflector axis.

The Defocus Integral

If it is assumed that the aperture field is linearly polarized, that the aperture dimensions and the radii of curvature of the reflector are large compared with a wavelength, and that the reflector is in the far-zone of the primary source, the diffraction problem reduces to a scalar one and the normalized diffraction integral, which gives the Fresnel pattern in a horizontal plane,

* Original manuscript received by the PGAP, March 16, 1955. The work described in this note was done under Contracts AF 30(602)-925 and AF 30(602)-1360 sponsored by the Rome Air Dev. Center, USAF. Presented at the IRE Western Convention, Los Angeles, Calif., August 25, 1954.

† Elec. Engrg. Dept., Syracuse University, Syracuse, N. Y.
‡ Signal Corps, U. S. Army Pacific Headquarters, Honolulu, Hawaii.

can be approximated as[1]

$$I(u) = \int_0^1 F(r)e^{-jkD^2r^2/8R} rJ_0(ur)dr. \tag{1}$$

In (1), D is the aperture diameter; R, the distance of measurement; r, the radial dimension in the aperture plane normalized with respect to $D/2$; $u=(\pi D/\lambda)\sin\theta$, θ being the azimuth angle; $k=2\pi/\lambda$; and $F(r)$, the circularly symmetrical amplitude illumination function over the aperture. The exponential term is the Fresnel-zone contribution; terms above the second order are neglected.

When the primary source is displaced from the focus of a paraboloidal reflector by a distance ϵ along the reflector axis in the direction away from the reflector with a view to simulating far-zone patterns in the quasi-near zone, there will be a relative phase variation over the aperture. The phase variation referred to the center point is found with good approximation to be[2]

$$\delta = -\frac{2\epsilon}{1+\left[\frac{D}{4f}\right]^2 r^2} = -2\epsilon\left[1-\frac{r^2}{\left[\frac{4f}{D}\right]^2+r^2}\right]. \tag{2}$$

The normalized diffraction integral now becomes

$$I(u) = \int_0^1 F(r)e^{jk(\delta-D^2r^2/8R)} rJ_0(ur)dr. \tag{3}$$

This integral is difficult to evaluate. However, examination of (3) reveals that a far-zone pattern will be obtained if ϵ is chosen to make the exponent vanish or equal to a constant. Unfortunately this cannot be done exactly for all values of r. It has been found[2] that an acceptable and convenient approximation for δ is

$$\delta = -2\epsilon\left[1-\frac{r^2}{\left[\frac{4f}{D}\right]^2+1}\right]. \tag{4}$$

Eq. (4) is exact for $r=0$ (center) and $r=1$ (edge of aperture). For other values of r, the $|\delta|$ given by (4) is slightly larger than that given by (2); the error decreases when the (f/D) ratio of the reflector increases. Using (4), the required amount of defocus can be readily determined:

$$\frac{\epsilon}{f} = \frac{f}{R}\left[1+\left(\frac{D}{4f}\right)^2\right]. \tag{5}$$

If it is desirable to express R in multiples of D^2/λ, $R=nD^2/\lambda$, (5) reduces to

$$\frac{\epsilon}{\lambda} = \frac{f}{n}\left[\left(\frac{f}{D}\right)^2+\left(\frac{1}{4}\right)^2\right]. \tag{6}$$

[1] S. Silver, "Microwave Antenna Theory and Design," M.I.T. Rad. Lab. Ser., vol. 12, McGraw-Hill Book Co., Inc., New York, N. Y., ch. 6; 1949.

[2] S. T. Moseley, "On-Axis Defocus Characteristics of the Paraboloidal Reflector," Final Report for Contract No. AF 30(602)-925, Syracuse Univ. Res. Inst.; August, 1954.

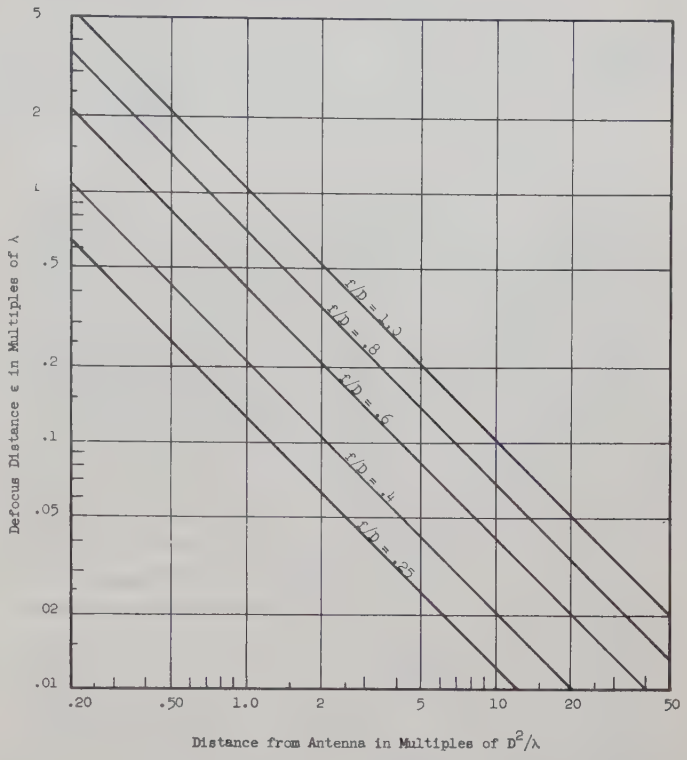

Fig. 1—Defocus chart for paraboloidal reflectors.

Fig. 1 shows a plot of (ϵ/λ) vs n for five values of f/D in log-log scale; they are parallel straight lines. It is noted that for $n=2$ $(R=2D^2/\lambda$, which is normally considered as an adequate far-zone distance), appreciable defocus is still necessary, the required amount being larger for larger f/D ratio.

The Minimum Beamwidth Criterion

The previous derivation for the required amount of defocus is independent of the amplitude illumination function $F(r)$. In this section, the criterion that proper defocusing give a minimum 3-db beamwidth will be used; the problem of simulating far-zone patterns in the quasi-near zone then reduces to that of finding a relation between ϵ and n such that u_1 is a minimum for

$$20\log_{10}\left|\frac{I(0)}{I(u_1)}\right| = 3. \tag{7}$$

In order to evaluate the diffraction integral, an amplitude function of the type

$$F(r) = \left[1-\left(\frac{2r}{D}\right)^2\right]^2 \tag{8}$$

will be assumed. Substitution of (4) and (8) in (3) results, with $y=2r/D$,

$$|I(u)| = \left|\int_0^1 (1-y^2)^2 e^{-jB\pi y^2} yJ_0(uy)dy\right|, \tag{9}$$

where

$$B = \frac{1}{4n} - \frac{4\epsilon}{\lambda\left[1+\left(\frac{4f}{D}\right)^2\right]}. \tag{10}$$

Eq. (9) can be integrated through repeated integration by parts to give

$$|I(u)| = 8\left|\sum_{m=0}^{\infty}\binom{m+2}{2}(2jB\pi)^m \frac{J_{m+3}(u)}{u^{m+3}}\right|. \quad (11)$$

In order to determine the values of u_1, the infinite summation in (11) is separated into real and imaginary parts and a table is constructed of 20 $\log_{10}|I(0)/I(u)|$ vs u for various values of B. The u_1 values that satisfy (7) are then determined by interpolation. Fig. 2 is a plot of half-power beamwidth, $2u_1 = kD \sin\theta_1$, vs ϵ/λ with n as a parameter for a paraboloidal reflector with $f/D = 0.35$. It is distinctly seen from the curves that for every value of n, as far as the Fresnel approximations in (9) hold, there exists a proper defocus distance which gives a minimum main-lobe 3-db beamwidth; this defocus distance corresponds to the condition $B = 0$. The $B = 0$ points are shown by crosses in Fig. 1. Setting B in (10) equal to zero, a relation identical to (6) is obtained.

Defocus Characteristics in the Fresnel Region

The curves in Fig. 2 are useful not only because they give the proper amount of defocus in order to simulate far-zone radiation patterns at distances of $R = 2D^2/\lambda$, $1D^2/\lambda$, $\frac{1}{2}D^2/\lambda$, and $\frac{1}{4}D^2/\lambda$ for an antenna with $(1-y^2)^2$ illumination having $f/D = 0.35$, but also because they indicate the extent to which the 3-db beamwidth is increased if the primary feed is moved by a given amount on either side of the proper defocus position. The fact that for different values of n the minimum 3-db beamwidth remains unchanged when the primary feed is defocused properly is plausible inasmuch as proper defocus will simulate the same far-zone pattern. It is also clear that the initial minimum beamwidth criterion could have been made with reference to other decibel levels, instead of -3 db, without change in the outcome of the required amount of defocus.

Referring again to (9) one observes that for $u \leqq 2.405$,

$$|I(u, B)| \leqq \int_0^1 (1-y^2)^2 y J_0(uy)dy = I(u, 0). \quad (12)$$

Eq. (12) states that the condition $B = 0$ gives the least upper bound for the magnitude of $I(u)$. From this, it follows directly that the magnitude of the defocus integral is maximum with $B = 0$ (proper defocus) and, in particular, $|I(0)|$ is maximum. There is no danger of main-lobe deterioration when the criterion of minimum beamwidth is met.

The curves in Fig. 2 are symmetrical with respect to the minimum beamwidth point ($B = 0$). This can be seen from an examination of (11), the magnitude of $I(u)$ being independent of the sign of B. Numerical evaluation of theoretical radiation patterns in the Fresnel region for various defocus distances (performed on the Mark IV Computer at Harvard Computation Laboratory) checked well with the predicted results.

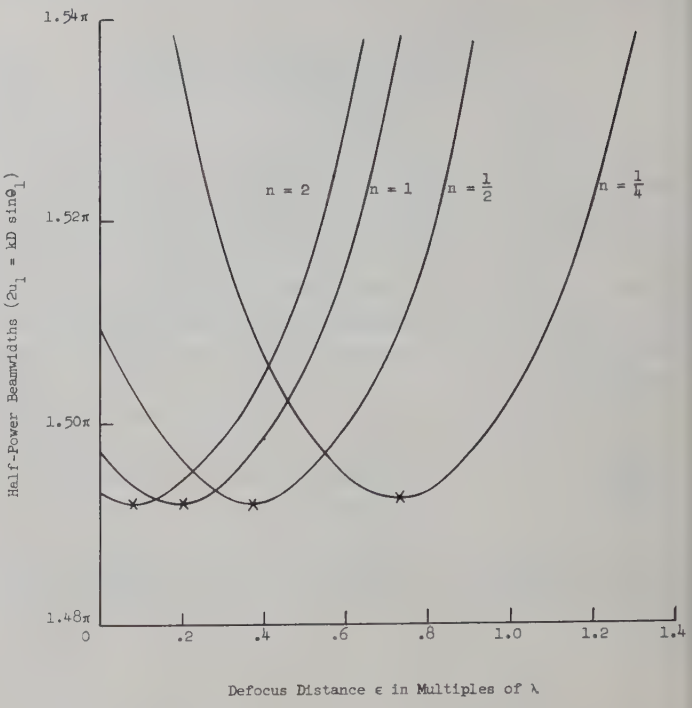

Fig. 2—Beamwidth characteristics for a defocused paraboloidal reflector, $f/D = 0.35$. $(1-y^2)^2$ illumination.

Conclusion

The defocusing practice of simulating far-zone radiation patterns in the quasi-near zone has been evaluated analytically and validated for the paraboloidal reflector. Using the minimum main-lobe beamwidth criterion, the defocus characteristics for an amplitude illumination function of the $(1-y^2)^2$ type have been obtained, which enable one to determine the proper amount of defocus as well as to predict the increase in beamwidth when the antenna system is not properly defocused. It has also been shown that the minimum beamwidth criterion coincides with the condition for maximum radiation amplitude along the reflector axis.

For a given paraboloidal reflector, the proper amount of defocus in multiples of wavelength (ϵ/λ) is approximately inversely proportional to the distance at which measurements are to be made; and for measurements at a given distance, the required amount of defocus increases with the f/D ratio of the reflector in a parabolic manner, as shown by (6) and Fig. 1.

The fundamental requirement for simulating far-zone radiation patterns in the quasi-near zone is equivalent to that for the cancellation of the effect of the additional phase term in the diffraction integral for the Fresnel region by the phase term introduced by defocusing. Neither a change in the amplitude illumination function nor a change in the integration limits would alter this condition. Actual pattern characteristics, such as beamwidth, radiation intensity, etc., would of course depend upon both the amplitude function and the integration limits.

Available Bandwidth in 200-Mile VHF Tropospheric Propagation*

L. A. AMES† AND T. F. ROGERS†

EARLY SHORT-PULSE experiments on tropospheric paths extending far beyond the radio horizon indicated that the propagation medium might support a relatively distortion-free bandwidth of several megacycles.[1] More recently, the direct transmission of television signals to distances beyond the radio horizon on both vhf[2] and shf[3] has been reported, with no evidence of degradation in signal quality due to the propagation medium. Reception of the shf signals over a 180-mile path took place well within the extra-diffraction field strength region, but measurements were confined to July and August; the year-round vhf measurements were made at 120 miles, and because of the relatively long wave-length and short path length, were influenced by diffraction propagation. In order to determine whether wide-band signal transmission is generally possible over distances far in excess of the radio horizon, measurements must be made both under cold weather propagation conditions and at such a distance that the contribution of the diffraction field—already established as capable of supporting wide-band signal transmission—is negligibly small.

During the coldest winter months extra-diffraction tropospheric signal levels are appreciably weaker than the yearly median level, and much weaker than the summer maximum.[4] This cold weather reduction in median signal level may be attributed in part, to the near absence of tropospheric refractive index gradients or layers strong enough to cause super-refraction or reflection propagation. Therefore, to the extent that scatter propagation[5] contributes to extra-diffraction field signal levels, this mode of propagation should be observable in its purest form in winter, and available bandwidth should be measured under such conditions.

In our experiments we have utilized the signals transmitted by WATV which are now radiated from the Empire State Building in New York City. These television transmissions cover the frequency range 210–216 mcps, the effective radiated peak power is 316 kw, and the horizontal radiation pattern is nearly omnidirectional. The signals are received 196 statute miles away in Scituate, Massachusetts, where the smooth earth diffraction field is calculated to be some 135 decibels below free space. A large 40′×70′ dipole receiving array 30′ above the immediate terrain is used in conjunction with a sensitive high-quality television receiver. The transmitting and receiving parameters indicate a minimum detectable signal level some 82 db below free space, thereby providing sufficient sensitivity to permit cold weather observations to be made.[4]

Photographs of the WATV test pattern were made during the entire first quarter of 1955, intermittently at first, and systematically after mid-February. An exposure was made every five minutes during the hour in which the test pattern was displayed—usually in the early morning—each day of the week. Over 600 photographs were obtained in this manner, and distinguishable test patterns can be seen in about 90 per cent of them. The median signal level for this period was close to 7 decibels above the minimum detectable signal, in excess of 20 db about 5–10 per cent of the time and maximum values exceeded 30 db.

Close examination of these test patterns indicates that, with one exception, there is no discernible distortion or loss of picture detail except that caused by poor signal-to-noise ratio; certainly no marked distortions have ever been seen. Fig. 1 presents two photographs, representative of signals approximately 36 db and 15 db, respectively, above the minimum detectable and it may be noted that, except for the deterioration caused by receiver noise in the weaker signal case, the picture quality is maintained; this is true for all the photographs taken. The conclusion may be drawn, therefore, that the propagation medium allows an effective bandwidth of some 3–4 mcps at vhf for 200 miles even during the weaker signal level periods predominantly characterized by the extra-diffraction type propagation mode. While an "effective" bandwidth, measured in this manner, cannot be compared directly with the bandwidth predictions of Rice[6] or Gordon[7] such a conclusion is in essential agreement with their calculations which are based upon the tropospheric scatter propagation theory.

* Original manuscript received, June 1, 1955.

† AF Cambridge Research Center, Cambridge, Mass.

[1] K. Bullington, "Radio propagation beyond the horizon in the 40–4000 mc band," PROC. IRE, vol. 41, pp. 132–135; January, 1953.

[2] J. C. Simon and V. Biggi, "Un nouveau type d'aérien et son application à la transmission de télévision à grande distance," *L'Onde Elect.*, vol. XXXIV, pp. 883–896; November, 1954.

[3] K. Bullington and W. H. Tidd, Panel Discussion: "Extended-range vhf and uhf propagation," PROC. IRE, vol. 43, p. 365; March, 1955.

[4] For the New England Area see, for instance, G. S. Wickizer and A. M. Braaten, "Field strengths recorded on adjacent FM channels at 93 mc over distances from 40 to 150 miles," PROC. IRE, vol. 40, pp. 1694–1699; December, 1952. Our own measurements (unpublished) on a 220 mcps 200-mile overwater path agree in this particular with these lower frequency measurements.

[5] H. G. Booker and W. E. Gordon, "A theory of radio scattering in the troposphere," PROC. IRE, vol. 38, pp. 401–412; April, 1950.

[6] S. O. Rice, "Statistical fluctuations of radio field strength far beyond the horizon," PROC. IRE, vol. 41, pp. 274–281; February, 1953.

[7] W. E. Gordon, "Radio scattering in the troposphere," PROC. IRE, vol. 43, pp. 23–28; January, 1955.

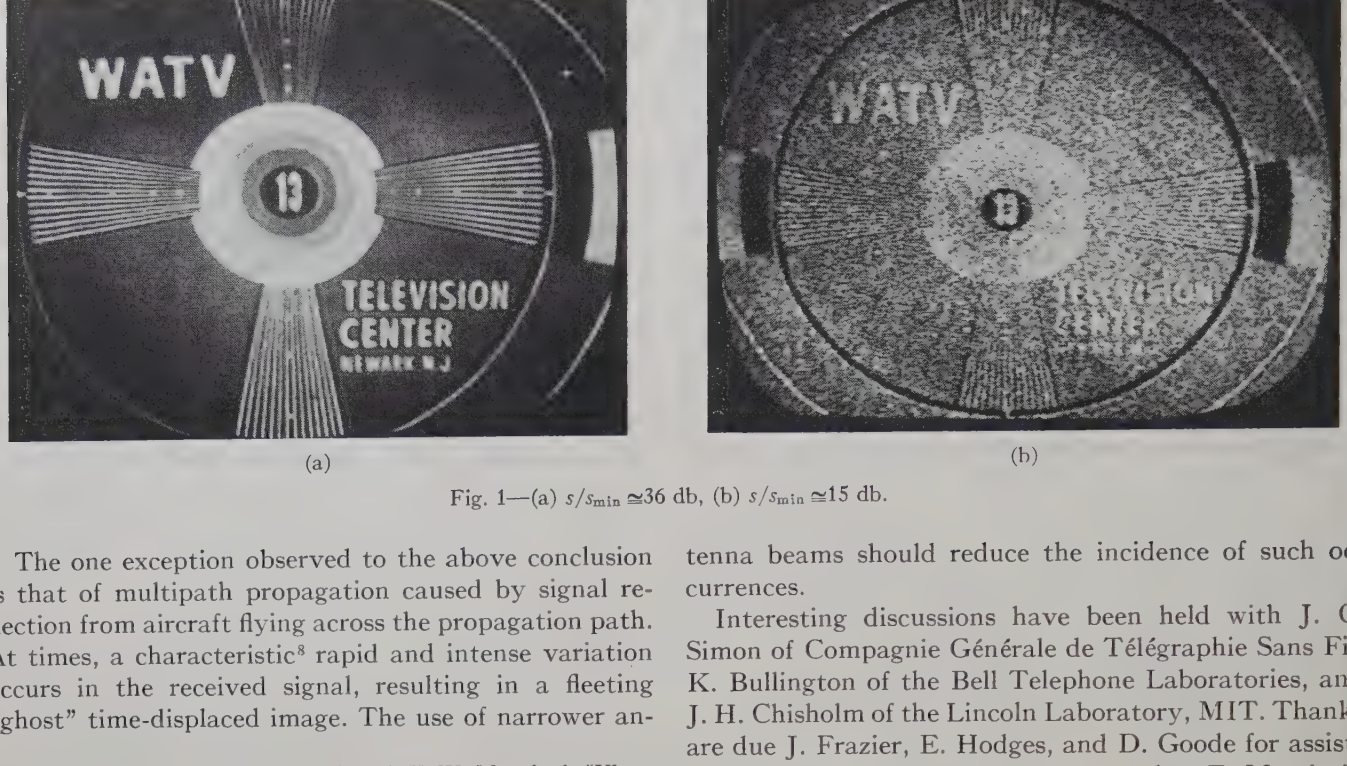

(a) (b)

Fig. 1—(a) $s/s_{min} \cong 36$ db, (b) $s/s_{min} \cong 15$ db.

The one exception observed to the above conclusion is that of multipath propagation caused by signal reflection from aircraft flying across the propagation path. At times, a characteristic[8] rapid and intense variation occurs in the received signal, resulting in a fleeting "ghost" time-displaced image. The use of narrower antenna beams should reduce the incidence of such occurrences.

Interesting discussions have been held with J. C. Simon of Compagnie Générale de Télégraphie Sans Fil, K. Bullington of the Bell Telephone Laboratories, and J. H. Chisholm of the Lincoln Laboratory, MIT. Thanks are due J. Frazier, E. Hodges, and D. Goode for assistance in making the measurements, and to E. Martin in reducing the data.

[8] C. R. Englund, A. B. Crawford, and W. W. Mumford, "Ultra-short-wave transmission and atmospheric irregularities," *Bell Sys. Tech. Jour.*, vol. 27, pp. 489–519; October, 1938. (See esp. Fig. 19.)

Bibliography of Nonuniform Transmission Lines*

H. KAUFMAN†

THE LITERATURE on nonuniform transmission lines has grown slowly but steadily since original papers by Heaviside appeared at close of the nineteenth century. (Heaviside's contributions have been almost completely overlooked by later writers.) The number of papers, although not overwhelming, is now large enough to warrant preparation of a bibliography.

References to periodicals are in Part I, to texts in Part II, and to a selected group on horn theory in Part III.

I. Periodicals

1. Arnold, J. W., and Bechberger, P. F., "Sinusoidal Currents in Linearly Tapered Loaded Transmission Lines." Proceedings of the IRE, Vol. 19 (February, 1931), pp. 304–310.
2. Arnold, J. W., and Taylor, R. C., "Linearly Tapered Loaded Transmission Lines." Proceedings of the IRE, Vol. 20 (November, 1932), pp. 1811–1817. Discussion by A. T. Starr, same journal. Vol. 21 (November, 1933), p. 1609.
3. Ballantine, S., "Non-uniform lumped electric lines." *Journal of the Franklin Institute*, Vol. 203 (April, 1927), pp. 561–582.
4. Bloom, S., and Peter, R. W., "Transmission-Line Analog of a Modulated Electron Beam." *RCA Review*, Vol. 15 (March, 1954), pp. 95–112.
5. Bolinder, F., *a.* "Fourier Transforms in the Theory of Inhomogeneous Transmission Lines." Proceedings of the IRE, Vol. 38 (November, 1950), p. 1354. *b.* "Fourier Transforms in the Theory of Inhomogeneous Transmission Lines." *Kungliga Tekniska Högskolans Handlingar*, Stockholm, no. 48, (1951), 84 pages.
6. Burkhardtsmaier, W., "Widerstandstransformation mit Leitungen." *Funk und Ton*, Vol. 3 (March, 1949), pp. 151–167; (April, 1949), pp. 202–213.
7. Burrows, C. R., *a.* "The Exponential Transmission Line." *Bell System Technical Journal*, Vol. 17 (October, 1938), pp. 555–573. *b.* "Exponential Transmission Line." *Communications*, Part I, Vol. 18 (October, 1938), pp. 7–9, 26–28; Part II, Vol. 18 (November, 1938), pp. 11–13, 17–18.
8. Carson, J. R., "Propagation of Periodic Currents over Non-Uniform Lines." *Electrician*, Vol. 86 (March 4, 1921), pp. 272–273.
9. Christiansen, W. N., "An Exponential Transmission Line Employing Straight Conductors." Proceedings of the IRE, Vol. 35 (June, 1947), pp. 576–581.
10. Clemens, G. J., "A Tapered Line Termination at Microwaves." *Quarterly of Applied Mathematics*, Vol. 7 (January, 1950), pp. 425–432.
11. Eckart, G., "Reaktanz- und Vierpoltheorie inhomogener idealer Leitungen." *Hochfrequenztechnik und Elektroakustik*, Vol. 55 (1940), pp. 173–186.
12. Federici, M. E., "Su di un nuovo tipo di cavo elettrico disuniforme." *Rendiconti della Accademia Nazionale dei Lincei*, (6) Vol. 13 (January, 1931), pp. 128–132.
13. Feldstein, A. L., "Inhomogeneous Transmission Lines as Filters." *Nachrichten Technik* (In German), Vol. 4 (June, 1954), pp. 264–266.
14. Frank, N. H., "Reflections from Sections of Tapered Transmission Lines and Wave Guides," *MIT Radiation Laboratory* Report 43–17, January 6, 1943.
15. Gazzana-Priaroggia, P., "Impedenza d'entrata di una linea disuniforme." *Alta Frequenza*, Vol. 17 (June, 1948), pp. 99–109.
16. Gent, A. W., and Wallis, P. J., "Impedance Matching by Tapered Transmission Lines," *Journal of the IEE*, Vol. 93, Part IIIA, Radiolocation (1946), pp. 559–563.
17. Graziadei, H., "Eine Lösung für einen praktisch frequenzunabhängigen Übergang zwischen einem HF-Koaxialkabel und einer erdsymmetrischen HF-Leitung." *Fernmeldetechnische Zeitschrift [FTZ]*, Vol. 6 (1953), pp. 311–319.

* Original manuscript received, June 27, 1955.
† Mathematics Dept., McGill University, Montreal, Canada.

18. Grosskopf, J., "Über den Scheinwiderstand gespreizter Doppelleitungen." *Telegraphen-, Fernsprech-, Funk-, und Fernsehtechnik*, Vol. 28 (January, 1939), pp. 8–16.
19. Gschwind, W., "Die Vierpolgleichungen von Inhomogenitäten im Zuge homogener Leitungen." *Dissertation*, T. H. München, 1952.
20. Gurley, J. G., "Impedance Matching by Means of Nonuniform Transmission Lines." *Transactions of the IRE*, Vol. AP-4 (December, 1952), pp. 107–109.
21. Heaviside, O., *a*. "Contributions to the Theory of the Propagation of Current in Wires. Paper XX in *Electrical Papers*, Vol. I (1892), pp. 141–181; see especially pp. 173–178. (Written in 1882, but first published in *Electrical Papers*.) *b*. *Electromagnetic Theory*, Vol. II, pp. 211–274; see especially pp. 211–215, 222–241. (Preface to vol. II is dated April 10, 1899.) Reissued by Benn Brothers, London, 1922, and by Dover Publications, N. Y., 1950.
22. Hershfield, S., "Tapered Coaxial Junctions." *Electronics*, Vol. 20 (December, 1947), p. 146.
23. Howe, G. W. O., "Cavity Resonator Regarded as a Transmission Line." *Wireless Engineer*, Vol. 29 (February, 1952), pp. 29–30.
24. Ilin, V. A., "Long Lines With Parameters Varying along the Line." *Elektrichestvo* (February, 1950), no. 2, pp. 54–59.
25. Ingram, W. H., *a*. "Electrical Oscillations in a Non-uniform Transmission Line." *University of Washington Publications in Mathematics*, Vol. 2 (December, 1930), pp. 17–38. *b*. "Note on the Operability of a Synchronous Motor at the End of a Transmission Line." *Proceedings of the Cambridge Philosophical Society*, Vol. 27 (1930/1931), pp. 244–249.
26. Keutner, E., "Hochfrequenzkabel mit veränderlichem Wellenwiderstand." *Europäischer Fernsprechdienst* (March, 1943), no. 62, pp. 3–9.
27. Laget, C., "Transmissioni elettriche non distorte su linee disuniformi," *Alta Frequenza*, Vol. 2 (October, 1933), pp. 500–515.
28. Lomonosov, V. Yu., "Long lines with parameters varying along the line." *Elektrichestvo* (March, 1951), no. 3, pp. 26–27.
29. Lund, C. O., "A Broadband Transition from Coaxial Line to Helix," *RCA Review*, Vol. 11 (March, 1950), pp. 133–142.
30. Meinke, H. H., "Eine abgewandelte Exponentialleitung als verbessertes Transformationsglied mit Hochpasscharakter." *Archiv der elektrischen Übertragung*, Vol. 7 (July, 1953), pp. 347–354.
31. Milnor, J. W., and Randall, G. A., "The Newfoundland-Azores High-Speed Duplex Cable," *Trans. AIEE*, Vol. 50 (June, 1931), pp. 389–396.
32. Milnor, J. W., "Tapered Transmission Lines," *Trans. AIEE*, Vol. 64 (June, 1945), pp. 345–346.
33. Neiman, M. S., "Nonuniform Lines with Distributed Constants." *Izvestiia Elektropromyshlennosti Slabogo Toka* (1938), pp. 14–25.
34. Niutta, A., "Adattamento di impedenze mediante un particolare tipo di linea esponenziale," *Poste e Telecomunicazione*, Vol. 17 (1949), 7 pages.
35. Parodi, H., and Parodi, M., "Contribution à l'étude des lignes de transmission d'énergie électrique," *Revue Générale de l'Électricité*, Vol. 53 (October, 1944), pp. 227–231.
36. Parodi, M., *a*. "Propagation des courants sinusoïdaux dans une ligne quelconque." *Comptes Rendus de l'Académie des Sciences* (Paris, Vol. 216 (June 28, 1943), pp. 876–878. *b*. "Propagation sur une câble comportant seulement de la résistance et de la capacité, ces paramètres étant fonctions de l'espace et satisfaisant à certaines relations," *Comptes Rendus de l'Académie des Sciences* (Paris), Vol. 221 (September 3, 1945), pp. 257–259. *c*. "Propagation sur une ligne électrique sans pertes dont les paramètres linéiques sont des fonctions exponentielles du carré de l'espace: Analogie avec la résolution de l'équation de Schrödinger pour l'oscillateur harmonique." *Journal de Physique et le Radium*, Vol. 6 (December, 1945), pp. 331–332. *d*. "Propagation sur une ligne quelconque dont les paramètres, fonctions de l'espace, satisfont en chaque point à une condition analogue à celle de non-déformation," *Revue Générale de l'Électricité*, Vol. 55 (October, 1946), pp. 414–415. *e*. "Remarque sur la propagation de l'électricité sur une câble hétérogène." *Revue Générale de l'Électricité*, Vol. 57 (January, 1948), pp. 37–38. *f*. "Sur la détermination de conditions d'intégration des équations de propagation de l'électricité sur une ligne hétérogène." *Comptes Rendus de l'Académie des Sciences* (Paris), Vol. 234 (April 21, 1952), pp. 1674–1676.
37. Persoz, B., "Les lignes uniformes et exponentielles de transmission." *Radio française* (December, 1947), pp. 7–13.
38. Piefke, G., *a*. "Verschiedene Lösungen der inhomogenen Leitungen mit stetig wachsendem Wellenwiderstand," *Dissertation* T. H. München, 1951. *b*. "Die 'Exponentialleitung' und ihre Wellenablösung," *Archiv der elektrischen Übertragung*, Vol. 7 (May, 1953), pp. 229–235; (June, 1953), pp. 274–280.
39. Pierce, J. R., "Note on the Transmission Line Equations in Terms of Impedance," *Bell System Technical Journal*, Vol. 22, 1943), pp. 263–265.
40. Ravut, C., "Propagation des courants sinusoïdaux sur des lignes quelconques." *Revue Générale de l'Électricité*, Vol. 7 (May 8, 1920), pp. 611–615.
41. Raymond, F. H., *a*. "Remarques sur les équations de propagation sur une ligne quelconque." *Comptes Rendus de l'Académie des Sciences* (Paris), Vol. 220 (April 4, 1945), pp. 497–500. *b*. "Remarque sur la propagation d'un signal électromagnétique sur une ligne hétérogène." *Comptes Rendus de l'Académie des Sciences* (Paris), Vol. 222 (April 24, 1946), pp. 1000–1002. *c*. "Contribution à l'étude de la propagation sur une ligne hétérogène." *Journal de Physique et le Radium*, Vol. 7 (June, 1946), pp. 171–177.
42. Rüdenberg, R., "Der Verlauf elektrischer Wellen auf Leitungen mit raümlich veränderlicher Characteristik." *Electrotechnik und Maschinenbau*, Vol. 31 (May 18, 1913), pp. 421–429. Discussion by J. Wallot, same Journal, Vol. 32 (July 12, 1914), pp. 607–608.
43. Ruhrmann, A., *a*. "Die Energieausbreitung auf Leitungen mit exponentiell veränderlichem Wellenwiderstand." *Hochfrequenztechnik und Elektroakustik*, Vol. 58 (September, 1941), pp. 61–69. *b*. "Verbesserung der Transformationseigenschaften der Exponentialleitung durch Kompensationsschaltungen." *Archiv der elektrischen Übertragung*, Vol. 4 (January, 1950), pp. 23–31. *c*. "Die Exponentialleitung bei der Genzwellenlänge und im Sperrbereich." *Archiv. elektrischen Übertragung*, Vol. 4 (October, 1950), pp. 401–412.
44. Samuelson, R. E., "Electrical Transmission Lines with Non-Uniform Parameters," Doctoral Dissertation, Northwestern University, 1949. See *Summaries of Doctoral Dissertations*, Northwestern University, Vol. 17 (1949), pp. 259–264.
45. Schatz, E. R., and Williams, E. M., "Pulse Transients in Exponential Transmission Lines." PROCEEDINGS OF THE IRE, Vol. 38 (October, 1950), pp. 1208–1212.
46. Schelkunoff, S. A., "Solution of Linear and Slightly Nonlinear Differential Equations." *Quarterly of Applied Mathematics*, Vol. 3 January, 1945), pp. 348–355.
47. Scott, H. J., "The Hyperbolic Transmission Line as a Matching Section." PROCEEDINGS OF THE IRE, Vol. 41 (November, 1953), pp. 1654–1657.
48. Seely, S., and Pollard, E. C., "Notes on Microwaves." Based upon a series of lectures by W. W. Hansen, Office of the Publication Board, Report PB 6851–6852, Chapter VI, "Tapered Lines," pp. 6–1 to 6–25. See Bibliography of Scientific and Industrial Reports, Office of the Publication Board, U. S. Department of Commerce, Vol. 1 (March 15, 1946), p. 415.
49. Siegel, E., "Strom- und Spannungsverteilung auf Turmantennen." *Hochfrequenztechnik und Elektroakustik*, Vol. 48 (November, 1936), pp. 164–170.
50. Starr, A. T., *a*. "The Nonuniform Transmission Line." PROCEEDINGS OF THE IRE, Vol. 20 (June, 1932), pp. 1052–1063. Errata, same Journal, Vol. 20 (September, 1932), pp. 1553–1554. *b*. Tapered Loaded Submarine Cable." *Philosophical Magazine*, (7) Vol. 17 (January, 1934), pp. 83–96.
51. Sternberg, R. L., and Kaufman, H., "Applications of the Theory of Systems of Differential Equations to Multiple Non-Uniform Transmission Lines." *Journal of Mathematics and Physics*, Vol. 31 (January, 1953), pp. 244–252.
52. Thomas, F., "Propagation du courant sur des lignes quelconques." *Revue Générale de l'Électricité*, Vol. 26 (October 12, 1929), pp. 567–569.
53. Volpert, A. R., "Lines with Nonuniformly Distributed Parameters." *Elektrosyvaz*, (1940), pp. 40–65.
54. Wagner, K. W., "Die Theorie ungleichförmiger Leitungen." *Archiv für Elektrotechnik*, Vol. 36 (February, 1942), pp. 69–96.
55. Walker, L. R., and Wax, N., "Nonuniform Transmission Lines and Reflection Coefficients." *Journal of Applied Physics*, Vol. 17 (December, 1946), pp. 1043–1045.
56. Wheeler, H. A., "Transmission Lines with Exponential Taper." PROCEEDINGS OF THE IRE, Vol. 27 (January, 1939), pp. 65–71.
57. Williams, E. M., and Schatz, E. R., "Design of Exponential-Line Pulse Transformers." PROCEEDINGS OF THE IRE, Vol. 39 (January, 1951), pp. 84–86.
58. Zhabotinskii, M. E., Levin, M. L., and Rytov, S. M., "The Telegraph Equation for Generalized Transmission Lines with Small Losses." *Journal of Technical Physics* (USSR), Vol. 20 (1950), pp. 257–281.
59. Zhekulin, L. A., "Influence of Nonuniformity in a Coaxial Cable on Its Parameters." *Bulletin de l'Académie des Sciences* (URSS) (September, 1947), pp. 1089–1105.
60. Zin, G., *a*. "Equazioni delle onde incidenti e riflesse nelle linee non uniformi a regime," *Alta Frequenza*, Vol. 10 (1941), pp. 149–178. *b*. "Sul comportamento delle linee non uniformi a regime." *Alta Frequenza*, Vol. 10 (1941), pp. 453–469. *c*. "I transitori nelle linee non uniformi." *Alta Frequenza*, Vol. 10 (1941), pp. 707–750. *d*. "Sulla deformazione dei segnali nei cavi irregolari." *Rendi conti di Matematica sue Appl.*, Univ. Roma Ist. naz. Alta Mat. (5) Vol. 2 (1941), pp. 33–60. [For abstract see *Atti II. Congr. Un. mat. Ital.* (1940), p. 781.]
61. Zinke, O., "Die Exponentialleitung als Transformator." *Funk und Ton*, Vol. 1 (March, 1947), pp. 119–129. *b*. "La Ligne exponentielle comme transformateur." *Radio française* (January, 1950), pp. 9–13.

II. Texts

62. Brillouin, L., *Wave Propagation in Periodic Structures* (New York, McGraw-Hill Book Co., Inc., 1946), pp. 227–236.
63. Bronwell, A. B., and Beam, R. E. *Theory and Application of Microwaves* (New York, McGraw-Hill Book Co., Inc., 1947), pp. 199–204.
64. Johnson, Walter C., *Transmission Lines and Networks* (New York, McGraw-Hill Book Co., Inc., 1950), pp. 201–208.
65. Moreno, T., *Microwave Transmission Design Data* (New York, McGraw-Hill Book Co., 1948), pp. 53–55.
66. Ragan, G. L., ed., *Microwave Transmission Circuits*, Vol. 9, Radiation Laboratory Series (New York, McGraw-Hill Book Co., Inc., 1948), pp. 305–311.
67. Schelkunoff, S. A., *Applied Mathematics for Engineers and Scientists* (New York, D. Van Nostrand Co., 1948), pp. 208–222.
68. Selgin, P. J., *Electrical Transmission in Steady State* (New York, McGraw-Hill Book Co., Inc., 1946), pp. 308–332.
69. Slater, J. C., *Microwave Transmission Lines* (New York, McGraw-Hill Book Co., 1942), pp. 61, 69–78.

III. Related Papers on Horn Theory

70. Ballantine, S., "On the Propagation of Sound in the General Bessel Horn of Infinite Length," *Journal of the Franklin Institute*, Vol. 203 (January, 1927), pp. 85–102. Discussion by C. R. Hanna, same Journal, Vol. 203 (June, 1927), pp. 849–853.
71. Crandall, I. B., *Theory of Vibrating Systems and Sound* (New York, D. Van Nostrand Co., 1927), pp. 158–174.
72. Goldsmith, A. N., and Minton, J. P., "Performance and Theory of Loud-Speaker Horns." Proceedings of the IRE, Vol. 12 (August, 1924), pp. 423–478.
73. Hanna, C. R., "The Function of the Horn as a Loud-Speaker," *Electric Journal*, Vol. 20 (November, 1923), pp. 396–397.
74. Hanna, C. R., and Slepian, J., "The Function and Design of Horns for Loud Speakers." *Transactions of the American Institute of Electrical Engineers*, Vol. 43 (1924), pp. 393–404. Discussion on pp. 405–411.
75. Kellogg, E. W., "Effect of a Horn on Pitch of a Loud-Speaking Telephone." *General Electrical Review*, Vol. 27 (August, 1924), pp. 556–562.
76. Mawardi, O. K., "Generalized Solutions of Webster's Horn Theory." *Journal of the Acoustical Society of America*, Vol. 21 (July, 1949), pp. 323–330.
77. Stewart, G. W., "The Performance of Conical Horns." *Physical Review*, (2) Vol. 16 (October, 1920), pp. 313–326.
78. Webster, A. G., "Acoustical Impedance, and the Theory of Horns and of the Phonograph," *Proceedings of the National Academy of Sciences*, Vol. 5 (1919), pp. 275–282.

Microwave Optics*

Part I—Report on Microwave Optics

R. C. SPENCER†

THE ANTENNA or propagation engineer has long been familiar with *antenna* theory and *electromagnetic* theory but of late he has been hearing the term *microwave optics*. This is a term introduced during World War II to cover those aspects of microwaves that could readily be studied by means of optical analogies. That there is no sharp demarcation between these fields can be gathered from the fact that a symposium on any one of them inevitably includes papers relating to the other two.

In its narrow sense, microwave optics makes use of analogies in geometric and physical optics. Thus defined, microwave optics is an interesting point of view, useful pedagogically for teaching either students or laymen, and useful scientifically for obtaining quick if limited answers to problems. In its broader sense, microwave optics draws on the more rigorous techniques of diffraction and electromagnetic theory. Operational or Fourier techniques are used as tools to exploit the methods of physical optics and electromagnetic theory, and also to analyze the role of the microwave optical system as a link in a communication chain. At this point certain formal aspects of communication theory or information theory can be applied.

Commission VI*c* has been concerned with the broader definition—in particular, with the inputs from Fourier transforms and information theory.

* Original manuscripts received, April 25, 1955. A report by URSI Subcommission VI*c* at the XIth General Assembly, The Hague; August 23–September 2, 1954.

† Chairman, URSI Subcommission VI*c*, Microwave Optics. Chief Antenna Lab., AF Cambridge Res. Center, Cambridge, Mass. Now with Sylvania Electric Products, Inc., Waltham, Mass.

History of Sessions on Microwave Optics

During World War II, microwave equipment was mass-produced for various radar and communication applications. In most of this equipment the antenna was designed to control the shape of the transmitted or received beam as well as to effect an impedance match. The use of microwaves stimulated studies in antenna theory and design, artificial dielectrics, diffraction, and electromagnetic theory, and interest in the new field led to a number of symposia on microwave optics. The following list of meetings held is exclusive of the various radio engineering conventions at which papers on the subject were given in the sessions on antennas.

Oct., 1947. Optical Society of America, Cincinnati, Ohio. *Symposium on Microwave Optics* (one-half day)

Apr., 1951. Joint URSI-IRE meeting, Washington, D. C. *Symposium on Microwave Optics* (one-half day)

Oct., 1951. National Bureau of Standards, Washington, D. C. *Symposium on Quality of the Optical Image* (three days). Although this symposium did not concern itself with microwave optics, it proved to be stimulating to those in attendance who were interested in this analogous field. (The *Proceedings* have recently been issued as National Bureau of Standards Circular No. 526. See papers by Zernike, Marechal, Osterberg, McDonald, and Scade; see also discussions by Spencer, pp. 38, 249; and by Grey, p. 251).

June, 1952. International Physics Union, Milan, Italy. (three days). *Symposium on Microwave Optics*. This was the first international symposium devoted entirely to the subject of microwave optics. (Proceedings have been published in *Supplemento* No. 3, *Nuovo Cimento*, vol. 9, 1952).

Aug., 1952. Tenth General Assembly of URSI, Sydney, Australia. Several papers on microwave optics were presented to Commission VI. Subcommission VI*c*, Microwave Optics, was formed particularly to study inputs from other fields such as Fourier techniques and information theory.

June, 1953. Symposium on Microwave Optics, McGill University, Montreal, P.Q., Canada. This symposium was planned to solve some of the problems of Commission VI*c*. Note reviews of the Symposium by E. Wolf in *Nature*, October 3, 1953, pp. 615–616, and by Morris Kline in *Physics Today*, March, 1954, pp. 30–32. The *Proceedings* will be published in two volumes by the Air Force Cambridge Research Center, Air Research Development Command (224 Albany Street, Cambridge 39, Massachusetts, U.S.A.), in the fall of 1955.

The following symposia were also scheduled during the summer of 1954:

Aug., 1954. Report of URSI Commission VI*c*, Microwave Optics, to 11th General Assembly, The Hague, The Netherlands.

Sept., 1954. Florence, Italy, *Meeting on Problems in Contemporary Optics, Session on Nonclassical Image-Forming Devices*. See "Preliminary Remarks on Microwave Optics," by R. C. Spencer, to appear in the PROCEEDINGS.

Interaction of Various Fields with Microwave Optics

You may be interested in a topologic diagram (Fig. 1) that illustrates the dependence of microwave optics on other fields. In the case of microwave optics shown at the bottom of the diagram, we are indeed grateful to the inputs from Physics on the left which include, in order of ascending difficulty, geometric optics, physical optics, and electromagnetic theory. On the other hand, microwaves have both drawn from and contributed to the Electronics fields of circuit theory and communication, shown on the right. At the top of the diagram are the operational methods. These usually lead to Fourier transforms for problems in physics and microwave optics, and to the Laplace transform for problems in electronics. More recently, information theory has been applied to optics and microwave optics.

Report of URSI Subcommission VI*c*

In addition to the preceding historical remarks and a short discussion of Fourier methods, the report to Commission VI included the following survey papers:

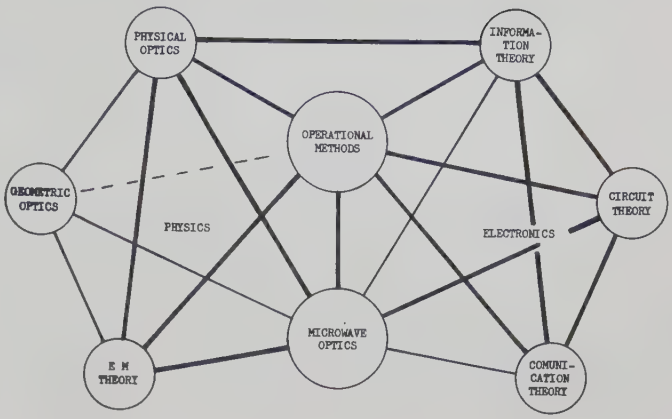

Fig. 1—Relationships between microwave optics and other fields.

1. Professor E. Wolf, "Relationship Between Geometric Optics and Diffraction Theory." This included certain energy flow relationships which hold both for geometric optics and electromagnetic theory.

2. Dr. H. Bremmer, "Diffraction Problems of Microwave Optics." This summarized recent contributions, including monograph by Bouwkamp and papers presented at *McGill Symposium on Microwave Optics*.

3. Professor A. Blanc-Lapierre, "Information Theory and Optics." This paper will be published in French in *Optica*. It is significant that although each of these three papers treated *optical* problems, they were presented by request to the International Scientific *Radio* Union because of the direct application of the ideas to *microwave optics* problems.

Current Program and Membership

The original membership of URSI Subcommission VI*c* as formed in August, 1952, included Professor G. A. Woonton of McGill University, P.Q., Canada, and P. M. Woodward of TRE, Malvern, England, but pressure of other duties forced their withdrawal. The present membership consists of A. Blanc-Lapierre, H. Bremmer, E. Wolf, and R. C. Spencer.

At the 11th General Assembly, Subcommission VI*c* was reconstituted as a "Working Group" on Microwave Optics under Commission VI and has been asked to prepare a monograph on *Microwave Optics and Its Relation to Other Fields*. This will be presented at the 12th General Assembly of URSI in Denver, Colorado, USA, in August, 1957.

In ending these preliminary remarks I would like to point out that microwaves, even more than the longer-wavelength radio waves, have stimulated the application of optical techniques to laboratory or field conditions. This is because the average laboratory experiment can both measure the phase and amplitude of points in microwave fields and yet deal with a sufficiently large number of waves so as to approximate optical conditions.

Until now the flow of ideas has been mainly from the other fields represented in the chart to microwave optics. I believe that now some of the improved techniques developed for microwave optics can contribute to these other fields.

Part II—Diffraction Problems of Microwave Optics

H. BREMMER†

Introduction

THIS STATUS report deals with methods currently applied in diffraction theories of microwaves. It is not a total summing up of the complete literature, references being restricted mainly to papers given in the *Proceedings* of the Symposium on Microwave Optics held at McGill University, Montreal, June 22–25, 1953.[1] These *Proceedings*, to be published by the Air Force Cambridge Research Center in the fall of 1955, give an excellent survey of recent theoretical and experimental results. Bouwkamp's paper "Diffraction Theory," in volume 17 of *Reports on Progress in Physics*, is also highly recommended for a study of diffraction theories in general.

Geometric optics concerns mainly ray trajectories that satisfy the reflection law and Snell's refraction law. The transportation of energy along the rays implies that the field amplitudes vary in inverse proportion to the square root of the cross section of a pencil of neighboring rays, that is, in direct proportion to the square root of the local Gaussian curvature K_g of the wavefront passing through the point of observation. The geometric optics approximations are sufficiently accurate for the design of microwave lenses even when aberration effects are taken into account (see *SM* 34, 36, 37, 39). However, geometric optics breaks down near caustic surfaces and in shadow regions, the field there becoming infinite and zero respectively. In these cases a wave treatment becomes inevitable. Diffraction describes the wave phenomena in this domain.

A. Scalar Theories

In free space the single scalar wave equation $(\Delta+k^2)u=0$ holds independently for every rectangular field component. The complications in the problems arise from the coupling of these components by the boundary conditions. The effect of this coupling is therefore significant first of all near the boundaries; where microwaves are concerned, however, the field at the boundaries can be checked experimentally since these waves admit field measurements up to a distance of one wavelength from the boundaries. The influence of the boundary conditions explains why the analogy between acoustic and electromagnetic diffraction through apertures and around disks (see Bekefi *SM* 53) holds in the far field but fails in the near field. In view of these circumstances, and discounting the fact that the field across the aperture was incorrectly assumed as equal to that of the incident wave, it is remarkable that a scalar treatment of the dominant electric field component could nevertheless account for the empirical field values observed by Andrews (*SM* 49) along the axis of a circular aperture.

The most satisfactory diffraction theories start from Maxwell's equations. Even then, a scalar treatment is not impossible in principle since the fields satisfying these equations are expressible in terms of some complex scalar quantity. Examples are: (1) a complex combination of the two scalars describing the field of moving charges in a theory of Whittaker's,[2] (2) the scalar introduced in free space by Wolf (*SM* 17) in order to arrive at expressions for the energy and momentum densities similar to those in quantum mechanics, and (3), a complex combination of two scalars describing the field in terms of multipole contributions in a recent paper by Bouwkamp and Casimir.[3] A drawback in all these scalars being the inconvenient form of the corresponding boundary conditions, an explicit vectorial treatment becomes more convenient. In problems dealing with phases (as defined in geometric optics), which are the same for all the field components, the inconvenience is slight and aberration effects of microwave lenses can therefore be investigated very simply by scalars. Dunbar (*SM* 40) thus found that the maximum tolerable spherical aberration producing a confusion equal to that caused by diffraction (Airy disk) is one-fourth as large as the one imposed by the Rayleigh criterion; in problems of astigmatism and defocusing the two corresponding tolerances proved to be of equal magnitudes.

The useful vector diffraction theories can be separated according to those dealing with corrections for the geometric optics approximation (see Section B), and those starting from very general properties of Maxwell's equations without any explicit connection with geometric optics (see Section C). In the latter case, geometric optics is recognized as the limit for $\lambda\rightarrow 0$ by applying saddlepoint approximations.

B. Vector Diffraction Theory as a Correction for Geometric Optics

The Maxwell equations for a monochromatic field (time factor e^{-ikct} in a source-free inhomogeneous medium (dielectric constant ϵ, permeability μ, refractive index $n=(\epsilon\mu)^{1/2}$ are comprised in the single vectorial equation

$$\operatorname{curl} \boldsymbol{M} + kn\boldsymbol{M} = 1/4 \operatorname{grad} \log \frac{\mu}{\epsilon} \boldsymbol{X}\boldsymbol{M}^* \qquad (1)$$

† Philips Res. Labs., N. V. Philips' Gloeilampenfabrieken, Eindhoven, Netherlands.

[1] Such references are identified by the initials *SM* after the author's name, followed by the publication number of the paper.

[2] Whittaker, *Proc. London Math. Soc.*, vol. 2, pp. 367, 1904.

[3] Bouwkamp and Casimir, *Physics*, vol. 20, pp. 539; 1954.

for the complex vector (with imaginary unit j)

$$\boldsymbol{M} = (\mu/\epsilon)^{1/4}H + i(\epsilon/\mu)^{1/4}\boldsymbol{E},$$

which was introduced by Bateman.[4] Luneburg and Kline's theory[5] amounts to the following in general asymptotic expansion

$$\boldsymbol{M} = e^{ikS}\sum_{r=0}^{\infty}\left(\frac{i}{kc}\right)^r \boldsymbol{m}_r,$$

in which the function S of the space variables should be independent of k. The two independent functions for $\boldsymbol{H}$ and $\boldsymbol{E}$ result from the real and imaginary parts with respect to j while treating $\boldsymbol{H}$, $\boldsymbol{E}$, and the other imaginary unit i as real quantities. A substitution of this expansion into (1) leads to the following relation resulting from the terms of order zero in k:

$$\text{grad } S\boldsymbol{X}\boldsymbol{m}_0 = jn\boldsymbol{m}_0,$$

whose vector components prove to be compatible only if S satisfies the conventional eikonal equation $|\text{grad } S| = n$. A further relation, however, resulting from the compatibility of the first-order terms, shows that the $\vec{m}_0$ field should vary proportionally with $n\sqrt{K_g}$ along a ray trajectory (defined as a curve perpendicular to the wavefronts $S=$constant), K_g being the local gaussian curvature of the wavefront through the point of observation. In addition, the variation in the directions of the field vectors contained in $\vec{m}_0$ is fixed by the property that these vectors suffer a parallel displacement in the Levy-Civita sense, the trajectories being geodesics in the non-Euclidean space defined by the line element

$$ds^2 = n^2(dx^2 + dy^2 + dz^2).$$

The $\boldsymbol{m}_0$ field thus obtained as the limit for $k\to\infty$ or $\lambda\to 0$ represents the geometric optics approximation. The relations resulting from the higher-order contributions in (1) determine the variation of the vectors $\boldsymbol{m}_1, \boldsymbol{m}_2, \cdots$ along the trajectories, and thus fix the corrections for the geometric optics field.

The splitting of the diffraction field as established here can be connected with pulse solutions, that is, with solutions describing the field that exists if all the sources simultaneously undergo sudden identical relative changes in intensity instead of varying oscillatorily. The resulting field discontinuities then pass in succession along the wavefronts otherwise associated with the stationary solution. The vectors $\boldsymbol{m}_r$ then prove to be proportional to the discontinuities of $\delta^r\boldsymbol{m}/t^r$ for the pulse solutions at the moment the discontinuity passes through the point of observation. In particular, the geometric optics field is linked with the discontinuity in the field described by the pulse solutions.

[4] Bateman.

[5] Luneburg and Kline, *Comm. Pure Appl. Math.*, vol. 4, pp. 225; 1951.

C. Theories Based on General Solutions of the Maxwell Equations

General solutions of the Maxwell equations may be divided into three groups according to their unique suitability in the special problems involved in: (*a*) microwave lenses; (*b*) diffracting screens and disks, reflectors, and scatterers; and (*c*) waveguides.

a. Solutions Usable for Microwave Lenses

For the case of negligible reflection losses, Luneburg[6] arrived at the following vectorial solution of Maxwell's equations in the image space ($\epsilon=\mu=1$) beyond the lens:

$$\boldsymbol{M}(P) = -\frac{ik}{2\pi}\iint dO_q\sqrt{\{K_g(Q)\}}\,\boldsymbol{m}_0(Q)e^{ik\{W(Q)+(\boldsymbol{r}\cdot\boldsymbol{u}_Q)\}}. \quad (2)$$

Ray trajectories are produced beyond the image space. The integration extends over a wavefront that cuts these at right angles, far away from the lens; K_g is the Gaussian curvature of the wavefront (with surface element dO_q); $W(Q)$ is the mixed eikonal; $\boldsymbol{r}$, the radius vector from the origin to the point of observation; and $\boldsymbol{U}_q$, the unit vector along the normal of the wavefront.

Eq. (2) includes all information about optical instruments. If the direction of polarization is constant throughout space, the field derived from a scalar F, represented by an integral similar to that of (2), can serve as a basis for the investigation of optical aberrations (see the derivation of the spherical aberration of Nijboer and Chako, *SM* 21). The case of a nonpolarized source can be treated by averaging over all polarization directions; it will be found that the propagation of energy is along curves parallel to the gradient of the phase of the complex function F. Unlike the ray trajectories, these curves may penetrate into shadow regions which would explain the establishment of small field intensities there.

b. Solutions Usable for Diffracting Screens and Disks, Reflectors, and Scatterers

The field inside the space V enclosed between the surfaces of these elements and infinity can be expressed in terms of the distribution of the electric and magnetic fields $\boldsymbol{e}$ and $\boldsymbol{h}$ across the finite parts of the boundaries. The formulas for the field inside V, in combined form, read:

$$\boldsymbol{e},\boldsymbol{h}(P) = \boldsymbol{e}_{pr},\boldsymbol{h}_{pr}(P) + \frac{1}{4\pi}\text{curl}\iint_{\Sigma} dO_q(\boldsymbol{e},\boldsymbol{h}\boldsymbol{X}\boldsymbol{u})_q e^{ikPQ}/PQ$$

$$\pm\frac{i}{4\pi k}\text{curl curl}\iint_{\Sigma} dO_q(\boldsymbol{h},\boldsymbol{e}\boldsymbol{X}\boldsymbol{u})_q e^{ikPQ}/PQ, \quad (3)$$

the first term of which represents the primary field that would be produced by the sources inside V if the enclosing walls constituting Σ were absent, while $\boldsymbol{u}$ is the unit vector along the outward normal of Σ.

[6] Luneburg, "The Mathematical Theory of Optics," Brown University Press, Section 47; 1944.

The expression in (3) can be interpreted as the linear superposition of contributions produced by infinitesimal electric and magnetic dipoles on Σ, the electric dipoles depending on the tangential components of the magnetic field on Σ, and the magnetic dipoles depending on those of the electric field on Σ. The actual field results from the radiation from these dipoles in accordance with Huygens' principle (see Possel, *SM* 50). The field of the elementary dipoles can be represented conveniently by Green tensors, whose elements connect the vector for a dipole of unit moment, located somewhere on Σ, with its field observed at a point P, taking into account the influence of Σ. Such a Green tensor appears to have been evaluated for the cases of free space and of a half-space limited by a plane (see Severin, *SM* 54).

The difficulties encountered in diffraction problems are due to the interdependence of the electric and magnetic fields tangential on Σ. Eq. (3) constitutes the basis for the deduction of integral equations fixing one of these quantities. In the usually considered case of perfectly conducting boundaries, such an equation can be expressed in terms of the vectorial density j of the currents induced on Σ. One of these equations, derived by Maue, reads:

$$\frac{k}{c}\boldsymbol{u}(P) \times \iint_{\Sigma} dO_q \boldsymbol{j}(Q) \frac{e^{ikPQ}}{PQ} + \frac{1}{kc}\boldsymbol{u}(P) \times \operatorname{grad} \iint_{\Sigma} dO_q \operatorname{div} \boldsymbol{j}(Q) \frac{e^{ikPQ}}{PQ} = i\boldsymbol{u}(P) \times \boldsymbol{e}_{pr}(P),$$

and can even be applied to the boundaries of the infinitely thin screens considered in the simplest diffraction problems. Unfortunately, a straightforward attack through integral equations of this type or its equivalent has been successful in exceptional cases only, for instance, in Bouwkamp's treatment of the diffraction through a small circular aperture, in which the additional edge conditions along the rim play an important role.[7] But these equations may be the starting point for successive approximations (see Sections G and H).

c. Solutions Usable for Waveguide Problems

An example of a solution of this type is the so-called "configuration lens," which consists of two cylindrical curved parallel metallic plates between which *TE* waves can be propagated. The principle can be described with the aid of curvilinear orthogonal co-ordinates. The corresponding solution of Maxwell's equations works out to a two-dimensional wave propagation along the geodesics of the mean surfaces parallel to the metallic faces. The design of microwave configuration lenses thus depends on differential geometry. The theoretical and experimental aspects have been reviewed by Myers.[8]

[7] *Philips Res. Reps.*, vol. 5, pp. 401; December, 1950.
[8] Myers, *Jour. Appl. Phys.*, vol. 8, pp. 220; 1947.

D. Approximative Methods Depending on Kirchhoff Integrals

When the boundary values of one single parameter over the diffracting or scattering surfaces are unknown, it is necessary to resort to approximative scalar methods, these being particularly suitable for discussing experimental results. The material boundaries of the problem in question are then replaced by a surface S that consists partly of these boundaries and partly of imaginary sheets filling up the open space between them.

Unfortunately, the boundary conditions used for the material surfaces of S must obviously be different from those used for the open parts of S. In the case of apertures in a plane, for instance, conditions of symmetry, originally applied by Bethe, make it apparent that the normal derivatives of the tangential electric field and of the magnetic field normal to it must be identical with those of the primary field on the open parts of S, whereas the field components themselves should of course vanish on the perfectly conducting metal parts of S. For the rest, these rigorous boundary conditions lead to the vectorial form of Babinet's principle, which connects the two complementary diffraction problems in which the apertures and metal parts have been interchanged.[9] To obtain a simple approximative boundary condition for one and the same quantity throughout S (assumed to be a plane), the exact boundary condition for a quantity nonvanishing in the diffracting apertures or disks might be combined with a reasonable assumption for the same quantity in the remaining part of S (see Severin, *SM* 54). The quantity in question could then be evaluated for any field from a Kirchhoff integral over the aperture plane, provided it satisfies the ordinary wave equation.

Among others who have discussed the possible imperfections of this method is Neugebauer (*SM* 51), who has considered such limiting cases as vanishing or infinite apertures. The results derived by means of these methods nevertheless prove to agree with many experimental data, as has been emphasized by Andrews (*SM* 49) with respect to measurements up to the aperture plane. By a related approximation method, Severin (*SM* 66) has determined diffraction field from a Kirchhoff integral over conic limit of shadow cast by a point source behind an aperture, using geometric optics approximation for the field on the shadow limit.

Another approximative method interprets the secondary field as originating from wavelets radiated from the points of the aperture rim. This concept is not inconsistent with representation by a Kirchhoff integral over the aperture since, as shown by Rubinowicz, such an integral can be split into a geometric optic part and a contour integral along the rim (see also *SM* 64). An empirical formula based on this idea has been suc-

[9] Bouwkamp, "Diffraction Theory," *Reps. Prog. Phys.*, vol. 17, p. 46.

cessfully applied by Andrews (*SM* 49). According to the saddlepoint method, contributions from the rim arrive mainly from special points on latter (see Section E).

All the boundary conditions considered so far have reference to a single field parameter. Further complications arise when the finite conductivity of diffracting or reflecting screens has to be taken into account. Approximations valid for high conductivities lead to mixed boundary conditions, depending on both the parameter in question and its normal derivative. Little work has been done so far in this field (see Felsen, *SM* 6).

E. Saddlepoint Approximations

Exponential factor of diffraction integrals enables application of saddlepoint approximations. These are useful in working with wavelengths that are short compared with dimensions of diffracting or scattering body, and in evaluating radiation field (see Section F).

This particular exponent represents phase of contribution from a special point on surface of integration, whereas extreme values at saddlepoints correspond to optical path lengths of ray trajectories that connect source of field with point of observation (Fermat's principle). Geometric optics constitutes the limit of wave optics inasmuch as the smaller the wavelength the more the contributions of the surface integral are restricted to the immediate vicinity of the saddlepoints.

The problem presented by diffraction integrals over smoothly curved surfaces is not the same as that presented by diffraction integrals over surfaces bounded by sharp edges such as apertures. On the one hand, with smoothly curved surfaces, the contributions due to the two-dimensional saddlepoints can be approximated by cutting off the Taylor expansion of the exponent, taken around the saddlepoint, after the second-order terms while extending the integration at both sides up to infinite values of the two co-ordinates. The second-order approximation thus obtained proves to be identical with the geometric optics approximation.

On the other hand, diffraction integrals that extend to an edge involve one-dimensional saddlepoints connected with positions on the rim. A corresponding ray trajectory with a turning point at such a position is characterized by an extreme path length. The trajectories through these so-called "critical points of the second kind"[10] can be included in geometric optics considerations by extending Fermat's principle. This extension worked out on a formal basis by Keller (*SM* 20).

The second-order saddlepoint approximations of ordinary diffraction integrals over unbounded surfaces break down if the Gaussian curvature of the wavefront of the corresponding rays becomes infinite, that is, on caustic surfaces. The simplest approximation then takes into account the smallest number of high-order terms of the mentioned Taylor expansion, which leads to a finite expression even on the caustic. In the vicinity of ordinary points on caustics, this procedure results in an Airy integral, whose value involves a maximum of the field near the caustic, and an exponential decrease at one side (shadow region impenetrable to rays). The field on the caustic increases as $k^{1/6}$ as $\lambda \to 0$, with a phase shift of $\pi/4$ relative to the geometric-optics value. At foci, that is at cusps of the caustic surface, the field increases as $k^{1/4}$, the phase shift being $\pi/2$. Other singularities may lead to different phase shifts and powers of k. Further, since the diffraction fields associated with the critical points of the second kind are proportional to $k^{-1/2}$, they become negligible with respect to the ordinary geometric optics fields as $k \to \infty$.

The field distributions near caustic surfaces have, in particular, been investigated for rotationally symmetric systems (in connection with spherical aberration) and for systems with cylindrical symmetry (see Kay, *SM* 42, for rays reflected by a cylindrical wall). Derivation of geometric properties, and of position of caustic surfaces is a matter of differential geometry (Parke, *SM* 38).

F. Radiation Pattern

The limiting field distribution existing at distances that are large by comparison with both the wavelength and dimensions of diffracting and scattering bodies can be obtained, for example, by substituting asymptotic expansions for the integrals or series representing the field throughout space. Distance beyond which such an expression may be used for checking experimental results can be derived from the condition that remainder of expansion should represent contributions beyond accuracy of measurements (see Siegel, *SM* 8).

Although the radiation field can be expressed in terms of the current distributions on the conducting surfaces, for microwave applications it is more important to express it in terms of its dependence on the field distribution in an aperture. For a plane aperture, the far field proves to be proportional to the amplitude of a single Fourier component of the two-dimensional aperture distribution. This Fourier component concerns periodic repetitions of the field along intersections of the aperture with planes normal to the direction of observation, occurring one wavelength apart. The radiation pattern of the aperture distribution is not affected by details that are finer than one wavelength; the part of the field that corresponds to the Fourier spectrum of these finer details does not radiate (evanescent waves). These results can be derived from a saddlepoint approximation for the rigorous integral representing any quantity that satisfies the wave equation.

These illustrations of the relationship between the distant field and the near field show that from any known expansion of the near field it is possible to derive corresponding terms for the far field (Stevenson, *SM* 53).

[10] Van Kampen, *Physica*, vol. 14, pp. 575; 1948–1949.

The relationship between these terms is simplest if the terms of a rigorous expansion have well-defined limiting values at great distances. This is true, for example, of the expansion in Mathieu functions of the field for an infinite slit in a plane aperture (Leonard, *SM* 19).

Knowledge of the far field is not only important for antenna design, but also for study of scattered fields that are far fields produced by reflection. Investigation of these fields by Crispin (*SM* 10) shows that radar cross sections can in special circumstances be increased by moving receiver away from the transmitter. The reciprocity theorem makes it possible to replace determination of radiation patterns by that of currents induced by a plane incident wave on a receiving system; this may be useful in study of slot antennas (see Sinclair, *SM* 58).

G. Integral Equations as a Basis for Further Computations

Integral equations such as Maue's (see Section C) are suitable not only for numerical approach to diffraction problems in general but for a proper physical understanding of scattering phenomena. Successive terms of the Liouville-Neumann expansion of such an equation, whose right-hand side depends on primary field, can be interpreted as contributions that are due to repeated scatterings. This is particularly clear if current distributions to be derived from the equation belong to two or more spatially separated bodies, for instance, an antenna feed and a reflector opposite it. Iterative kernels then contain contributions that depend on integrations over different bodies; interaction through scattering is expressed in a mathematical form. Scattering produced by a set of identical cylindrical reflectors has been investigated by Twersky and by Karp (*SM* 63).

The wave theory of microwave reflectors is connected with the first two terms of the Liouville expansion. For reflectors with radii of curvature that are large as compared with the wavelength, the second term proves to be approximately equal to the first term; and the first term itself corresponds to the primary current distribution, defined here as the distribution induced directly by the primary field in the absence of any interaction with the other parts of the scatterer. The far field can thus be derived approximately by assuming a current distribution equal to twice the primary distribution. The field derived by geometric optics from the reflection against the scatterer proves to be identical with this far field. In other words, the corrections in the geometric optics theory correspond to the amounts that the induced currents deviate from twice the value of the primary distribution. An example of an integral equation for another parameter is the equation starting from a scalar Green's formula, derived by Franz (*SM* 61) for the field on an infinite circular diffracting cylinder. The evaluation of the integral term by the saddlepoint method enables the investigation of a creeping wave, that is, a wave propagated along the surface of the cylinder in the part not illuminated by the incident wave (see also Imai's paper[11] mentioned in Section G*b*).

G. Various Methods Applied in Microwave Diffraction Problems

In addition to the general principles discussed before, the following special techniques have been applied and may also be useful for future work.

a. Expansion in Modes

Mode solutions of the proper differential equations satisfy the necessary boundary conditions, including the radiation condition at infinity, but their amplitudes have to be derived from data concerning the primary field. For a point source this amounts to the construction of a linear combination having the required singularity at the source. The method has been applied to the theory of wave propagation around the earth, and has been used by Jasik in the wave theory of the inhomogeneous Luneburg lens (*SM* 32).

For extended sources, such as the aperture of a slot antenna, the amplitudes can be derived through the aid of the Lorentz relation

$$\int\int (E_1 \times H_2)_n dO = \int\int (E_2 \times H_1)_n dO$$

for the integral over a closed surface of the indicated normal components which refer to two solutions of Maxwell's equations. This identity replaces Green's theorem for scalar wave problems. If we identify the two fields with the actual field and with that of a single mode, respectively, and integrate over the perfectly conducting screen and over an aperture in it, this relation yields the amplitude of the mode in question in the expansion of the actual field. A possible complication is that the analytic form of the radial factor of the mode often has to be taken differently in the near field and in the far field (see Bailin and Silver, *SM* 1; and Tilston, *SM* 11).

b. Watson Transformations

These transformations concern reduction of mode and other expansions into an integral in the complex plane. This integral may be the basis for a suitable saddlepoint approximation or for derivation of a new mode series converging more rapidly than the original one. Originally introduced by Watson for the wave propagation around the earth, the method has been successfully applied by Row (*SM* 57), by Felsen (*SM* 56) to the diffraction problem of a wedge, and by Riblet (*SM* 62) and by Imai,[11] to that of a cylinder. The method can often be interpreted as a transformation from an expansion in azimuthal modes into one in radial modes.

[11] Imai, *Z. Phys.*, vol. 137, pp. 31; 1954.

c. Variational Principles

Numerical solution of integral equations, such as for current distributions on conducting parts of the system, can be facilitated by deducting a quantity that, relative to actual distribution, remains stationary with respect to fictitious changes in it. According to Rayleigh-Ritz's principle, approximations can then be derived by starting from a reasonably assumed analytic expression for the unknown distribution and choosing its parameters so as to minimize the quantity that has to remain stationary (for an example, see Levine, *SM* 66). General stationary quantities derived by Levine and Schwinger are complicated but stationary expression deducted by Kouyoumjian (*SM* 14) for radar cross sections in terms of current distribution on a scatterer hit by a plane-polarized wave is rather simple. The variational method has enabled Huang (*SM* 13) to verify a satisfactory agreement between theory and experimental results for transmission coefficient of plane waves diffracted through apertures of various shapes.

d. Wiener-Hopf Technique

The two-dimensional integral equations of diffraction problems generally depend on, among others, the distance of an integration point to a fixed point, that is, on the differences of three-dimensional co-ordinates. Owing to special conditions of symmetry the general equations may occasionally be reduced to one or more one-dimensional equations depending on a difference kernel only, at least for a limited range of the main variable. Explicit analytic solutions can then be derived by means of the well-known Wiener-Hopf technique. Three examples are: (1) the determination by Heins[12] of the current distribution in an infinite set of parallel plates hit by a plane-incident wave; (2) the investigation by Kay and Kotik (*SM* 16) of the field of a surface wave guided by a thin dielectric panel of limited width in one direction, but semi-infinite in the other; (3) the reduction by Blass (*SM* 22) of the scalar wave propagation through a semi-infinite cylinder with elliptic cross section to an infinite number of Wiener-Hopf equations.

e. Applications of the Rules of the Operational Calculus to the Fourier Transforms Involved in the Connection between the Radiation Pattern and Field Distributions across an Aperture

(See Spencer, *SM* 43.) For instance, coefficients of expansions of the radiation pattern can be expressed in terms of higher-order moments of the aperture distribution by applying such rules. Further, the influence of phase errors represented by a factor exp $[i\phi(x, y)]$ amounts to the multiplication of the undisturbed transform $f(\omega_1, \omega_2)$ by a symbolic factor

$$\exp\left[i\phi(-i\delta/\delta\omega_1, -i\delta/\delta\omega_2)\right].$$

f. Procedures for Improving the Convergence of Special Series

As an example we refer to Schensted's (*SM* 9) transformation of a known expansion for the backscattering by a half-infinite cone into a more rapidly converging series by means of the formula

$$\sum_{n=1}^{\infty} a_b = \frac{1}{(1-x)}\left[a_1 + \sum_{n=1}^{\infty}(a_{n+1} - xa_n)\right].$$

g. Procedures for the Solution of Integral Equations Depending on a Small Parameter (Usually the Product of the Wave Number and Some Characteristic Distance)

Yen (*SM* 7) pointed out that the method worked out by Bouwkamp for the rigorous vectorial solution of the diffraction by a circular aperture can also be applied to the other problems. If the kernel of the equation

$$f(s)\int I(s')K(s, s')ds'$$

admits an expansion

$$K(s, s') = \Sigma\epsilon^n K_n(s, s'),$$

then the coefficients of

$$I(s) = \Sigma\epsilon^n I_n(s)$$

are to be derived from the equation:

$$\sum_{r=0}^{n}\int I_r(s')K_{n-r}(s, s')ds' = \delta_n{}^0 f(s),$$

with $\delta n^0 = 0$ for $n \neq 0$, and $\delta 0^0 = 1$. All these relations reduce in succession to inhomogeneous integral equations, with different known right-hand members but with the same kernel $K_0(s, s')$. Expansions of this type have been derived by Stevenson[13] in connection with (3), Σ being a scattering boundary.

H. The Parameter Observable in Field-Strength Measurements

The well-known difficulty in such measurements is that the quantity being measured is disturbed by the measuring equipment. An application of the reciprocity theorem, as given by Burgess,[14] shows that the voltage measured across the input terminals of a linear receiving antenna becomes proportional to the integral

$$\int E_{\text{inc,II}}(s)\cdot I_{tr}(s)\cdot ds,$$

where ds is a line element of the receiver, $E_{\text{inc,II}}$ is the local value of the component parallel to it of the undisturbed incident field we want to measure and I_{tr} is the

[12] Heins, *Quart. Appl. Math.*, vol. 8, pp. 281; 1950.

[13] Stevenson, *Jour. Appl. Phys.*, vol. 24, pp. 1134, 1143; 1953.

[14] Burgess, *Wireless Engr.*, vol. 21, pp. 154; 1944.

current that would exist if the receiver were used as a transmitter energized at its input terminals.

The evaluation by Woonton (*SM* 56) of this integral, in the case of a received field depending on a Kirchhoff integral, shows that the contributions arriving from the different parts of an aperture are modified by a weighting factor depending directly on the amplitude and phase of the radiation pattern in the direction of arrival. This plausible result is particularly important in measurements near and in the aperture, such as those possible only for microwaves. The directions of arrival from the different parts of the aperture vary greatly; this influences a significant effect on the voltage induced in the receiver, which Borts and Woonton were able to verify by empirical experiments.

The preceding integral has to be replaced by the corresponding three-dimensional integral

$$\iiint (E_{\text{inc}} \cdot I_{tr}) d\tau$$

in the general case of nonlinear receiving antennas. On the basis of the reciprocity theorem, this expression equals the equivalent one over the conducting parts of the source if the roles of transmitter and receiver have been interchanged. The integral has been termed "reaction" by Rumsey (*SM* 2), who was able to derive a variational principle for its numerical evaluation. The previously mentioned determination of radar cross sections is an example of such a variational principle.

Part III—Recent Researches on the Foundations of Geometric Optics and Related Investigations in Electro-magnetic Theory

E. WOLF†

Introduction

THIS report surveys the researches carried out in recent years on the foundations of geometric optics and discusses some of their implications in rigorous electromagnetic theory.

Geometric optics has as a rule been presented independently of Maxwell's theory, as a system based on *Fermat's principle of a stationary path*. According to this principle, light is propagated along certain curves (the light rays), which are the solution of the variational problem

$$\delta \int n ds = 0, \tag{1}$$

n being the refractive index of the medium. The surfaces orthogonal to these curves are the *geometric wavefronts* (say $S(\boldsymbol{r}) = \text{constant}$) and satisfy the eikonal equation

$$(\nabla S)^2 = n^2. \tag{2}$$

Although an approach based on (1) or (2) may be completely satisfactory for some problems, for example, in estimating the approximate performance of a light-optical or microwave-optical system, it is well known to be unsatisfactory in others, and the knowledge of the range of validity of the geometric optics approximation is therefore of utmost importance.

† Formerly, Dept. of Mathematical Physics, Edinburgh University, Edinburgh, U. K. Now at the Physical Labs., University of Manchester, Manchester, England.

It is clear that to determine this range, the connection between geometric optics and electromagnetic theory must be investigated.

Although the basic laws concerning rays and wavefronts were known for a very long time, it was not until 1911 that Sommerfeld and Runge,[1] following a suggestion of P. Debye, derived the eikonal equation from the wave equation, in the limit of infinitely high frequency (negligible wavelength). More precisely, what they showed was this, that if

$$f(\boldsymbol{r}) = a(\boldsymbol{r}) e^{ikS(\boldsymbol{r})} \tag{3}$$

is a solution of the time-independent scalar wave equation

$$\nabla^2 f + n^2 k^2 f = 0, \tag{4}$$

then as $k = 2\pi/\lambda = \omega/c \to \infty$, (4) goes over into the eikonal equation, (2). This confirmed Kirchhoff's well-known theorem that geometric optics is the limit of physical optics for negligibly small wavelengths.

The Sommerfeld-Runge paper was an important step toward the understanding of the connection between geometrical optics and Maxwell's theory. But it was only a first step, for their analysis was based on the scalar wave equation as opposed to the vector equations that govern the behavior of an electromagnetic field. It was not until the last ten years or so that the analysis of

[1] A. Sommerfeld and J. Runge, "Anwendung der Vectorrechnung auf die Grundlagen der geometrischen Optik," *Ann. Phys.*, vol. 35, pp. 277–298; 1911.

Sommerfeld and Runge was extended to take the vectorial aspect into account. These investigations, which led to a number of interesting new results, will now be surveyed.

Researches on the Foundations of Geometric Optics

Friedlander, in 1947,[2] suggested that when the wavelength is sufficiently small, a time-harmonic electromagnetic field may be approximated in the form

$$\boldsymbol{E} = \boldsymbol{e}(\boldsymbol{r})e^{i[kS(\boldsymbol{r})-\omega t]}, \qquad \boldsymbol{H} = \boldsymbol{h}(\boldsymbol{r})e^{i[kS(\boldsymbol{r})-\omega t]}, \tag{5}$$

where S is the eikonal, and he showed that the intensity law of geometric optics then follows from Maxwell's equations in the limit as $k\to\infty$. Moreover, Friedlander found that the amplitude vectors $\boldsymbol{e}$ and $\boldsymbol{h}$ obey a simple propagation law along each ray. In a somewhat different notation, Friedlander's equation may be written as

$$\frac{\partial \boldsymbol{e}}{\partial \tau} + \frac{1}{2}\mu\nabla\cdot\left(\frac{1}{\mu}\nabla S\right)\boldsymbol{e} + (\boldsymbol{e}\cdot\nabla\log n)\nabla S = 0;$$

$$\frac{\partial \boldsymbol{h}}{\partial \tau} + \frac{1}{2}\epsilon\nabla\cdot\left(\frac{1}{\epsilon}\nabla S\right)\boldsymbol{h} + (\boldsymbol{h}\cdot\nabla\log n)\nabla S = 0. \tag{6}$$

Here τ denotes a certain parameter that specifies the position along each ray:

$$\frac{\partial}{\partial \tau} = \nabla S\cdot\nabla, \tag{7}$$

ϵ is the dielectric constant and μ is the magnetic permeability. Thus, if $\boldsymbol{e}$ and $\boldsymbol{h}$ are known at one point of a ray, their values at any other point on the ray may be determined by integrating (6). Eq. (6) is thus a *transport equation* for the vector amplitudes $\boldsymbol{e}$ and $\boldsymbol{h}$ and gives information about the change in the state of polarization along each ray.

Friedlander also suggested that (5) should perhaps be regarded as first terms in the asymptotic expansion of the field vectors, in the form (omitting as usual the time harmonic factor)

$$\boldsymbol{u} \sim e^{ikS}\sum_{\nu=0}^{\infty}\frac{1}{(ik)^{\nu}}\boldsymbol{e}_{\nu}, \qquad \boldsymbol{v} \sim e^{ikS}\sum_{\nu=0}^{\infty}\frac{1}{(ik)^{\nu}}\boldsymbol{h}_{\nu}, \tag{8}$$

a suggestion confirmed for a wide class of fields by other investigations about which more will be said later.

The relations in (6) have an interesting implication in terms of non-Euclidian geometry. With a medium specified by the refractive index function $n(\boldsymbol{r}) = \sqrt{\epsilon\mu}$ one may associate a non-Euclidian space whose line element ds' is given by

$$ds' = nds = n\sqrt{dx^2 + dy^2 + dz^2}. \tag{9}$$

From (1) and (9) it follows that the geometric rays in ordinary space correspond to the geodesics in the non-Euclidian space, and it may be shown that (6) implies that each of the directions of polarization remains parallel to itself along each geodesic in the sense of Levi-Civita. This implication of (6) was pointed out by Luneburg,[3] although the result was stated much earlier in a somewhat different form by Bortolotti.[4]

The following authors studied the connection between Maxwell's theory and geometric optics in anisotropic and, in some cases, nonconducting media: Arley,[5] Suchy,[6] Mandl,[7] and Cap and Röver.[8]

The paper by Arley is concerned with the derivation of Huygens' principle and Fermat's principle. This paper, as well as that of Suchy and Mandl, considers also the limits of validity of geometric optics. Cap and Röver were concerned mainly with the formulation of Fermat's principle for an absorbing medium.

Some of the results obtained in these papers are not entirely satisfactory. For example, Arley and Mandl overlooked the fact that in a time-harmonic vector field it is necessary to introduce, not *one*, but *three* phase functions, one for each Cartesian component. Also, the conditions obtained by Arley and Suchy for the validity of geometric optics do not appear to be all independent of each other, and are probably too strong in some cases. According to their results, geometric optics can be a good approximation only if the fractional changes of the refractive index over a linear domain of the order of a wavelength is small compared to unity. If this result is true, it is difficult to understand how the law of refraction can be valid, because across a refracting surface the refractive index changes discontinuously by an appreciable amount. Actually, no satisfactory derivation of the geometric optics law of refraction from Maxwell's theory appears to have been given so far.

Luneburg[3] and Born and Wolf[9] derived explicit expressions, in terms of the eikonal, for the variation of the intensity along each ray. If I_1 and I_2 are the intensities at two points of the ray, and n_1 and n_2 are the corresponding values of the refractive index, then

$$\frac{I_2}{I_1} = \frac{n^2}{n_1}\exp\left(-\int_{s_1}^{s_2}\frac{\nabla^2 S}{n^2}\,dS\right) = \frac{n_1}{n_2}\exp\left(-\int_{s_1}^{s_2}\frac{\nabla^2 S}{n}\,ds\right), \tag{10}$$

[2] F. G. Friedlander, "Geometrical optics and Maxwell's equations," *Proc. Camb. Phys. Soc.*, vol. 43, pp. 284–286; 1947.

[3] R. K. Luneburg, "Propagation of Electromagnetic Waves," Notes of lectures delivered at New York University, 1947–1948.

[4] E. Bortolotti, "Sulle rappresentazioni conformi, e su di una interpretazione fisica del parallelismo di Levi-Civita," *Rend. Acc. Linc.*, vol. 4, pp. 552–556; 1926.

[5] N. Arley, "A note on the foundations of geometrical optics," *Det. Kgl. Danske Vidensk. Selsk.*, vol. 22; pp. 1–21; 1945.

[6] K. Suchy, "Schrittweiser übergang von der wellenoptik zur strahlenoptik in inhomogenen anisotropen absorbierenden medien," *Ann. Phys.*, vol. 11, pp. 113–130; 1952; vol. 12, p. 423; 1953; vol. 13, pp. 178–197; 1953.

[7] G. Mandl, "Zur begründung der strahlenoptik aus der Maxwellschen feldtheorie," *Acta Phys. Aus.*, vol. 7, pp. 365–389; 1953.

[8] F. Cap and W. Röver, "Lichtwege in inhomogenen, absorbierenden, isotropen medien," *Acta Phys. Aus.*, vol. 8, pp. 346–355; 1954.

[9] M. Born and E. Wolf, "Principles of Optics," Pergamon Press, London, England. In press.

the integral being taken along the ray. Similar relations also hold for the variation of the squared amplitudes of electric and magnetic vectors. In the special case when wavefronts are concentric spheres, in a homogeneous medium, (10), of course, reduces to inverse-square law.

A fuller account of results of these researches will appear in a forthcoming book by Born and Wolf.[9]

Pulse Solutions of Maxwell's Equations and Asymptotic Expansions of Steady-State Fields

It is well known that the eikonal equation, (2) may also be regarded as the equation of the characteristics of the wave equation and describes rigorously the propagation of discontinuities in the solutions of these equations. Physically, the discontinuous solutions represent the following situation:

A source begins to radiate at a particular instant $t=t_0$. The field then spreads into the surrounding space, and at any later time $t>t_0$, the disturbance reaches a well-defined region. Let

$$F(\boldsymbol{r}) = ct, \tag{11}$$

be the equation of the boundary surface of this region. Across this surface the field changes discontinuously from a finite value in the interior to zero value outside it. The statement that the eikonal equation is the characteristic equation of the wave equation is physically equivalent to the statement that the surfaces $F(\boldsymbol{p})=$ constant obey the eikonal equation

$$(\nabla F)^2 = n^2. \tag{12}$$

Hence, there exists a formal analogy between the steady-state field at small wavelengths and the field of discontinuities (representing a so-called *pulse solution*), latter being a rigorous solution of Maxwell's equations.

In important investigations carried out by Luneburg[3,10] and extended by Kline,[11] it was found that in some cases it is possible to derive formally the whole asymptotic expansion for a steady-state field from the knowledge of the associated pulse solution. We shall briefly indicate the main results of these investigations.

Let the sources of the field be specified by a function $\boldsymbol{Q}(r, t)$ in terms of which the charge density ρ and the enforced current density j are given by

$$\rho = -\frac{1}{4\pi}\nabla\cdot\boldsymbol{Q}, \qquad j = \frac{1}{4\pi c}\dot{\boldsymbol{Q}}. \tag{13}$$

If the charges remain at a fixed location in space but vary in strength with the time, as is usually the case, $\boldsymbol{Q}$ will be of the form

$$\boldsymbol{Q}(\boldsymbol{r}, t) = \boldsymbol{K}(\boldsymbol{r})T(t). \tag{14}$$

In particular, for a *pulse solution*, $\boldsymbol{Q}=\boldsymbol{Q}_0$, where

$$\left.\begin{aligned} \boldsymbol{Q}_0(\boldsymbol{r}, t) &= 0 \qquad \text{when } t<0,\\ &= \boldsymbol{K}(\boldsymbol{r}) \quad \text{when } t>0. \end{aligned}\right\} \tag{15}$$

In terms of the pulse solution $\boldsymbol{E}_0$, $\boldsymbol{H}_0$, the field $\boldsymbol{E}$, $\boldsymbol{H}$ that arises from a $\boldsymbol{Q}$ distribution with any prescribed time dependence $T(t)$, may be derived from the *Duhamel principle:*

$$\left.\begin{aligned} \boldsymbol{E} &= \frac{\partial}{\partial t}\int_0^t \boldsymbol{E}_0(t-t')T(t')dt';\\ \boldsymbol{H} &= \frac{\partial}{\partial t}\int_0^t \boldsymbol{H}_0(t-t')T(t')dt'. \end{aligned}\right\} \tag{16}$$

Using this result, Luneburg and Kline showed that when there is a time-harmonic dependence $T(t)=e^{-i\omega t}$, with increasing time $\boldsymbol{E}$ and $\boldsymbol{H}$ approach the form

$$\boldsymbol{E} = \boldsymbol{u}(\boldsymbol{r})e^{-i\omega t}, \qquad \boldsymbol{H} = \boldsymbol{v}(\boldsymbol{r})e^{-i\omega t}, \tag{17}$$

where $\boldsymbol{u}$ and $\boldsymbol{v}$ may be developed into the following asymptotic series[12]

$$\boldsymbol{u} = -\boldsymbol{K}/\epsilon + e^{ikF}\left\{\boldsymbol{e}_0 - \frac{1}{i\omega}\boldsymbol{e}_1 + \frac{1}{(i\omega)^2}\boldsymbol{e}_2 - \cdots\right\};$$

$$\boldsymbol{v} = e^{ikF}\left\{\boldsymbol{h}_0 - \frac{1}{i\omega}\boldsymbol{h}_1 + \frac{1}{(i\omega)^2}\boldsymbol{h}_2 - \cdots\right\}; \tag{18}$$

where

$$\boldsymbol{e}_\nu = \left[\frac{\partial^\nu \boldsymbol{E}_0}{\partial t^\nu}\right] \quad \text{and} \quad \boldsymbol{h}_\nu \quad \left[\frac{\partial^\nu \boldsymbol{H}_0}{\partial t^\nu}\right] \tag{19}$$

are the changes in the successive derivatives of $\boldsymbol{E}_0$ and $\boldsymbol{H}_0$ across the discontinuity surface and

$$\frac{\omega}{c} = \frac{2\pi}{\lambda} = k. \tag{20}$$

Hence, *each coefficient in the asymptotic expansion of a steady-state field is given by the discontinuous change in a derivative of a field that represents a certain pulse solution of Maxwell's equations.*

For sufficiently large values of ω, in the region where $\boldsymbol{K}=0$,

$$\boldsymbol{E} \sim [\boldsymbol{E}_0]e^{i[kF-\omega t]}; \qquad \boldsymbol{H} \sim [\boldsymbol{H}_0]e^{i[kF-\omega t]}. \tag{21}$$

This confirms the assumption of Friedlander about the form of $\boldsymbol{E}$ and $\boldsymbol{H}$. See (5).

Luneburg and Kline also found that each term in the expansion of (18) satisfies the following transport equations:

[10] R. K. Luneburg, "Mathematical Theory of Optics," Notes of lectures delivered at Brown University; 1944. Also "Asymptotic Developments of Steady-State Electromagnetic Fields," New York University Math. Res. Group. Rep. No. EN. 14; 1949.

[11] M. Kline, "An asymptotic solution of Maxwell's equations," *Comm. Pure and Appl. Math.*, vol. 4, 225–262; 1951. Also "Symposium on Theory of Electromagnetic Waves," Interscience Publishers, New York, N. Y., pp. 225–262; 1951.

[12] It is assumed here that only one discontinuity surface passes through each point. In some cases, such as when reflection takes place at bodies embedded in the medium, several such surfaces may pass through some points. Eq. (18) must then be modified, each term replaced by the sum of such terms, each of which arises from one of the partial fields.

$$\frac{\partial \mathbf{e}_\nu}{\partial \tau} + \frac{1}{2}\mu\nabla\cdot\left(\frac{1}{\mu}\nabla F\right)\mathbf{e}_\nu + [\mathbf{e}_\nu\cdot\nabla\log n]\nabla F = -\mathbf{C}_\nu$$

$$\frac{\partial \mathbf{h}_\nu}{\partial \tau} + \frac{1}{2}\epsilon\nabla\cdot\left(\frac{1}{\epsilon}\nabla F\right)\mathbf{h}_\nu + [\mathbf{h}_\nu\cdot\nabla\log n]\nabla F = -\mathbf{D}_\nu, \quad (22)$$

where

$$\mathbf{C}_0 = \mathbf{D}_0 = 0$$

and for $\nu > 0$,

$$\mathbf{C}_\nu = \frac{1}{2}c\left\{\mu\nabla\times\left(\frac{1}{\mu}\nabla\times\mathbf{e}_{\nu-1}\right) - \nabla\left[\frac{1}{\epsilon}\nabla\cdot(\epsilon\mathbf{e}_{\nu-1})\right]\right\};$$

$$\mathbf{D}_\nu = \frac{1}{2}c\left\{\epsilon\nabla\times\left(\frac{1}{\epsilon}\nabla\times\mathbf{h}_{\nu-1}\right) - \nabla\left[\frac{1}{\mu}\nabla\cdot(\mu\mathbf{h}_{\nu-1})\right]\right\}, \quad (23)$$

τ being as before a parameter that specifies the position on each "ray":

$$\frac{\partial}{\partial\tau} = \nabla F\cdot\nabla. \quad (24)$$

In the special case $\nu = 0$, (22) is identical with (6).

In addition to the work of Luneburg and Kline, in which the transport equations for the pulse solutions were derived by using the full Maxwell's equations, two related investigations must be mentioned. Copson[13] showed that the transport equations for $\mathbf{e}_0$ and $\mathbf{h}_0$ can be derived from the second-order wave equations for the electric and magnetic vectors. Bremmer,[14] in a very elegant analysis, further demonstrated the mathematical equivalence of the geometric optics solution and the pulse solution by using the delta function techniques.

The connection between the discontinuous solutions and the geometric optics field was also studied by Mandl[7] in the paper already referred to.

Since there is a tendency in the literature to identify the pulse solution with the geometric optics solution, it should be stressed that this identity is a purely formal one, based on the *mathematical* equivalence of the corresponding equations. From the point of view of *physics*, the two solutions are of course quite distinct. The steady-state field, where geometric optics is a high-frequency limit, represents a wave that exists for an infinite length of time. On the other hand, the discontinuity surface of the pulse solution passes through each point in an infinitesimal instant of time—and is in a sense somewhat fictitious, for one can never measure the field on such a moving surface. Nevertheless, the mathematical analogy demonstrated by the work of Luneburg and Kline gives us a much clearer insight than was hitherto possible into the nature of the geometric optics approximation. It is also likely to prove of value in other problems concerned with high-frequency electromagnetic fields.

[13] E. T. Copson, "The transport of discontinuities in an electromagnetic field," *Comm. Pure and Appl. Math.*, vol. 4; pp. 427–433; 1951.

[14] H. Bremmer, "The jumps of discontinuous solutions of the wave equation," *Comm. Pure and Appl. Math.*, vol. 4; pp. 419–426; 1951.

Some Analogies between Geometric Optics and Rigorous Electromagnetic Theory

Unlike the geometric optics approximation, the pulse solution represents a rigorous solution of Maxwell's equations. The question naturally arises whether some of the geometric optics laws do not also hold, with appropriate modifications, in time-harmonic fields of an arbitrary frequency.

An essential property of the geometrical optics approximation is the orthogonality between the energy flow and a family of cophasal surfaces, and one must therefore consider whether such a relationship of orthogonality is found in any of the known rigorous solutions of Maxwell's equations.

It was first pointed out by Braunbec[15] and illustrated in beautiful diagrams by him and Laukien[16] that orthogonality of this type exists in the classic half-plane problem of Sommerfeld (see Fig. 1). If we bear in mind the complexity of the field near the diffracting edge the relationship of orthogonality seems to be a rather surprising feature.

Braunbek[15] investigated whether such a relationship exists in more general fields and came to the conclusion that only in a limited class of fields (two-dimensional, or those with rotational symmetry) are the lines of the energy flow orthogonal to a family of cophasal surfaces.

Somewhat more general results in this direction were recently obtained by Nisbet and Wolf[17] in studies of electromagnetic fields where the waves are of arbitrary shape but where at least one of the field vectors is *linearly polarized*.[18] They found that such fields show a close resemblance to the field in geometric optics. For example, if the linearly polarized vector is the electric vector $\boldsymbol{E}$ and we write

$$\boldsymbol{E} = \mathbf{e}\, e^{i(kS-\omega t)}, \quad (25)$$

where $\mathbf{e}$ is a real vector function of position, the energy flow is at each point found to be along the normal to the cophasal surfaces $S(\boldsymbol{r}) = \text{constant}$, and the "electromagnetic rays" (lines of energy flow) so defined satisfy the *generalized Fermat's principle*

$$\delta\int N ds = 0, \quad (26)$$

[15] W. Braunbek, "Zur darstellung von wellenfeldern," *Zeit. Naturf.*, vol. 6a, pp. 12–15; 1951.

[16] W. Braunbek and G. Laukien, "Einzelheiten zur halbenen-Beugung," *Optik*, vol. 9, pp. 174–179; 1952.

[17] A. Nisbet and E. Wolf, "On linearly polarized electromagnetic waves of arbitrary form," *Proc. Camb. Phil. Soc.*, vol. 50, pp. 614–622; 1954.

[18] This is to say that with varying time, the field vector at any particular point remains always in the same direction; unlike in the case of a homogeneous plane wave, however, this direction may be different at different points of the field. It has been shown by Nisbet and Wolf that many fields of practical interest are of this type.

where

$$N^2 = n^2 - \frac{\mu}{e^2 k^2} e \cdot \left[\nabla \times \left(\frac{1}{\mu} \nabla \times e \right) \right]. \tag{27}$$

As $k \to \infty$, $N \to n$, and (26) then correctly reduces to the ordinary Fermat's principle. Nisbet and Wolf also showed that along the "electromagnetic rays" the vector amplitude e rigorously obeys a transport equation of the form of (6).

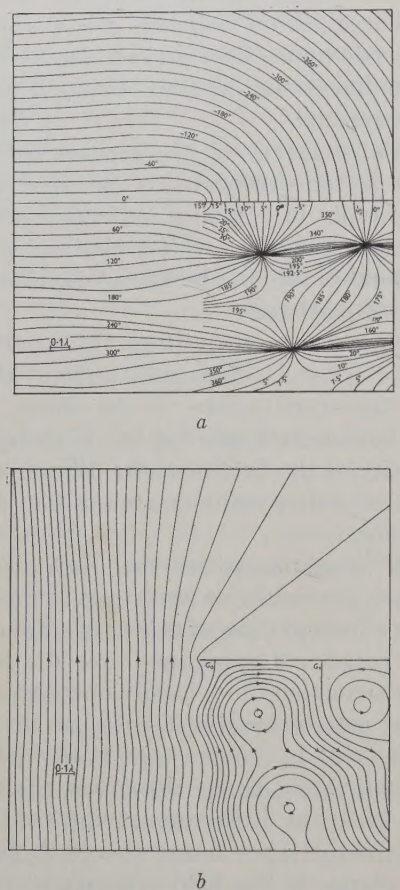

a

b

Fig. 1—The classic Sommerfeld half-plane diffraction problem (*H*-polarization). (*a*) Curves of constant phase of the *H*-vector; (*b*) Lines of the average energy flow (Poynting vector). (*After Braunbek and Laukien.*[16])

Another approach to the question of finding a simple model for the transport of energy arises from the fact that the field vectors do not uniquely define the flow. The usual definition is in terms of the Poynting vector

$$S = \frac{c}{4\pi} E \times H, \tag{28}$$

which obeys the conservation law

$$\frac{dw}{dt} + \nabla . S + Q = 0 \tag{29}$$

where

$$w = \frac{1}{8\pi} (E \cdot D + H \cdot B) \tag{30}$$

is the energy density and

$$Q = \sigma E^2 \tag{31}$$

is the Joule heat, σ being the conductivity. From (29) it is evident that the flow could also be defined by

$$S' = S + \nabla \times A, \tag{32}$$

where A is any arbitrary vector, since on account of the identity $\nabla \cdot (\nabla \times A) = 0$, the A vector contributes nothing to the total outward flux from any closed domain.

According to modern field theories, freedom in defining the flow density and the energy density is still greater; any definition consistent with the addition of a four-divergence to the Lagrangian density L of the field

$$L = \frac{1}{8\pi} (E \cdot D - H \cdot B) \tag{33}$$

is permissible. As long ago as 1902, definitions of w and S which differ from the usual ones in this way were proposed by McDonald.[19] Recently, Hines[20] asserted that McDonald's definition of the flow shows definite advantages over that of Poynting's.

Green and Wolf[21] recently showed that in vacuum, in regions free of currents and charges, the field may be derived from a single complex scalar wave function $V(r, t)$, and that in terms of this function the energy density and the flux density may be defined by means of expressions analogous to the quantum-mechanical expressions for the probability density and the probability current.

The class of transformations introduced by Green and Wolf was studied in detail by Bremmer,[22] who also investigated the relationship between the V function and other potential functions previously considered by E. T. Whittaker and R. K. Luneburg. Nisbet recently showed that the real and imaginary parts of the V function are closely related to certain Hertz vectors. A paper by Nisbet[23] fully clarifies the old question relating to the number of components of a Hertz vector needed in the solution of different types of electromagnetic problems.

From the very brief account of the researches discussed in this report, it will be apparent that the subject has attracted a good deal of attention in recent years and that these investigations have considerably clarified our understanding of some general properties of electromagnetic fields.

[19] H. M. MacDonald, "Electric Waves," Cambridge University Press, Cambridge, p. 72; 1902. See also "Electromagnetism," Bell & Sons, Ltd., p. 137; 1934.

[20] C. O. Hines, "Electromagnetic energy density and flux," *Canad. Jour. Phys.*, vol. 30, pp. 123–129; 1952.

[21] H. S. Green and E. Wolf, "A scalar representation of electromagnetic fields," *Proc. Phys. Soc.*, vol. 66, pp. 1129–1137; 1953.

[22] H. Bremmer, "Remarks on the complex scalar function introduced by H. S. Green and E. Wolf in the theory of electromagnetic fields," Philips Res. Reps. In Press.

[23] A. Nisbet, "Hertzian electromagnetic potentials and associated gauge transformations," *Proc. Roy. Soc. A*, vol. 231, pp. 250–263; 1955.

INSTITUTIONAL LISTINGS

The IRE Professional Group on Antennas and Propagation is grateful for the assistance given by the firms listed below, and invites application for Institutional Listing from other firms interested in the field of Antennas and Propagation.

COLLINS RADIO COMPANY, Cedar Rapids, Iowa
Fundamental Antenna Design and Propagation Research Related to Development of Airborne and Ground Communication Systems.

DORNE AND MARGOLIN, INC., 30 Sylvester Street, Westbury, L. I., New York
Antenna Research and Development—Radiation Pattern Measuring Services.

D. S. KENNEDY & CO., Cohasset, Mass.
Microwave Antennas, Reflectors, Lenses, Radomes and Accessories. Design, Development and Production.

THE GABRIEL LABORATORIES, Div. of the Gabriel Co., 135 Crescent Road, Needham Heights 94, Mass.
Research and Development of Antenna Equipment for Government and Industry.

HUGHES AIRCRAFT COMPANY, Culver City, California
Research, Development, Manufacture: Radar Systems, Guided Missiles, Antennas, Radomes, Tubes, Solid State Physics, Computers.

I-T-E CIRCUIT BREAKER CO., Special Products Div., 601 E. Erie Ave., Philadelphia 34, Pa.
Design, Development and Manufacture of Antennas, and Related Equipment.

JANSKY & BAILEY, INC., 1339 Wisconsin Ave. N.W., Washington 7, D.C.
Radio & Electronic Engineering; Antenna Research & Propagation Measurements; Systems Design & Evaluation.

MARYLAND ELECTRONIC MANUFACTURING CORPORATION, College Park, Md.
Antenna and System Development and Production for Civil and Military Requirements.

RADIO ENGINEERING LABS., INC., 36-40 37th St., Long Island City 1, N. Y.
Complete equipment for communication and propagation test purposes for beyond the horizon UHF communications systems.

WEINSCHEL ENGINEERING CO., INC., Kensington, Md.
Attenuation Standards, Coaxial Attenuators and Insertion Loss Test Sets.

WHEELER LABORATORIES, INC., 122 Cutter Mill Road, Great Neck, New York
Consulting Services, Research and Development, Microwave Antennas and Waveguide Components.

The charge for an Institutional Listing is $25.00 per issue or $75.00 for four consecutive issues. Application may be made to the Technical Secretary, The Institute of Radio Engineers, 1 East 79th Street, New York 21, N.Y.